PHYSICAL CHARACTERISTICS OF LT SHIFT CATALYSTS

A Thesis
submitted for the degree of Doctor of Philosophy
of the University of London

by
Sukhendu Bikash Bhowmik, B.Sc., M.Phil.

February 1991

Ramsay Memorial Laboratories
Department of Chemical and
Biochemical Engineering
University College London
Torrington Place
London WC1E 7JE

ProQuest LLC.
789 East Eisenhower Parkway
P.O. Box 1346
Ann Arbor, MI 48106 – 1346

ACKNOWLEDGEMENTS

I would like to express my gratitude to Dr. Simon Waldram for his encouragement, guidance and advice throughout the research and for obtaining for me the studentship from ICI Chemicals and Polymers Group which supported me during this research.

I would also like to extend my gratitude to Dr. G.C. Chinchen of ICI's Billingham Catalysis Research Centre through whom this grant was arranged and who provided for me the facilities to prepare all the necessary catalyst samples.

My sincere thanks to Prof. J.M.Newton of the School of Pharmacy of University of London for allowing me to use some of his departmental apparatus and software as well as his valuable help relating to the research.

Thanks to all departmental technicians for their sincere co-operation and help throughout the research and also to Professor Mullin and Professor Cornish for providing me with the departmental facilities which allowed me to carry out the research.

I gratefully acknowledge the help from Dr. Usman Ullah, Mr. P.G.Williams of UCL Mathematics Department, Dr. Minaz Punzani of the University of London Computer Centre and Dr. Sashi Kanboor and Mr. Keith Robinson of the UCL Computer Centre for helping me in solving the mathematical models.

Finally, I would like to thank Miss Sandra Couch and Mr. Aaron Sheldrick for preparing tables and typing equations for this thesis.

ABSTRACT

Literature on diffusion and permeability are reviewed with the conclusion that measurements of diffusion under both reacting and non-reacting conditions are invaluable in a reactor design context. When a large number of experiments must be conducted, a factorial design can reduce the overall total number of experiments.

The physical structure of industrially produced porous solid catalysts can be partially characterised in terms of BET surface area, porosity, pore size distribution, permeability, effective diffusivity and tensile strength. Various standard techniques and methods of measuring these properties along with advantages and disadvantages are discussed in Chapter 2.

The co-precipitation method of catalyst preparation is described in Chapter 3. A total of 85 "green" and "reduced" catalyst samples were produced from a dried powder of co-precipitated copper oxide, zinc oxide and alumina. These were prepared under carefully controlled conditions at ICI's Billingham Catalysis Research Centre varying five key physical production parameters at their low, normal, high and extra high levels. These five production parameters are:

(1) the amount of lubricant added
(2) the pre-compaction load
(3) the calcination temperature
(4) the primary particle cut size
(5) the pelleting density

A non-isobaric, isothermal model of combined diffusion and flow within a single catalyst pellet is developed for a binary gas system. Numerical solutions of this model are presented. An agreement within 20% was found when compared with the experimental results. Under certain limiting conditions, the model became essentially

isobaric. Solution of this model confirmed that large pore diameter systems can adequately be described by such a model.

The pellet permeabilities and effective diffusivities are determined using a purpose built Wicke-Kallenbach type single pellet test apparatus. These tests are discussed in detail in Chapter 5.

Experimental results on the ICI $Cu/Zn/Al_2O_3$ LT shift catalyst are presented in Chapter 6 and from these several conclusions are drawn:

(i) The amount of lubricant added and magnitude of the pre-compaction load do not significantly affect the properties of the final catalyst pellet.

(ii) Alterations in calcination temperature, particle cut size and pellet density cause large changes in pellet permeability, effective diffusivity and tensile strength. These were much greater than the variations in the values of surface area and porosity. For quality control it is vitally important to characterize catalysts in terms of those properties which vary significantly with alterations in pellet production conditions.

(iii) Chemical reduction increased diffusivity by a factor more than 3 and, in some catalysts, permeabilities were increased by a factor in excess of 400. This latter result is attributed to the development of microscopic cracks which can be clearly observed on the Scanning Electron Microscope. Pellet tensile strength following reduction was decreased by a factor more than 3.

In Chapter 7, experimental results on porous carbon systems are presented and discussed.

Finally overall discussion, conclusions and recommendations for future work are discussed in Chapter 8.

CONTENTS

NOMENCLATURE

A	Cross sectional area	m^2
A_1, A_2, A_3	As defined in Appendix 3	
A_4, A_5, A_6	" " "	
A_9, A_{10}	As defined in Appendix 4	
A_{11}, A_{12}	" " "	
B_o	Permeability coefficient	m^2
B_{12}, B_{13}, B_{14}	As defined in Appendix 4	
c_A	Concentration of A	$molm^{-3}$
c_{A1in}, c_{A2in}	Inlet concentration, left and right end chamber	$molm^{-3}$
c_{A1out}, c_{A2out}	Outlet concentration, left and right end chamber	$molm^{-3}$
c_{in}	Inlet concentration, left hand chamber	$molm^{-3}$
c_L	Outlet concentration, left hand chamber	$molm^{-3}$
c_R	Outlet concentration, right hand chamber	$molm^{-3}$
c_1, c_2	As defined in Appendix 4	
c_{1i}, c_{1o}	As defined in Appendix 5	
c_{2i}, c_{2o}	" " "	
D_{AB}	Free gas diffusivity of gas A in B	m^2s^{-1}
D_{ABe}	Effective bulk diffusivity of gas A in B	m^2s^{-1}
D_{Ae}	Effective diffusivity of A	m^2s^{-1}
D_{Ao}, D_{Ai-1}	As defined in Appendix 4	
D_{Ai}, D_{Ai+1}	" " " "	
D_{An}, D^*_{Ao}	" " " "	
D^*_{Ai-1}, D^*_{Ai}	" " " "	
D^*_{Ai+1}, D^*_{An}	" " " "	
D_{Be}	Effective diffusivity of B	m^2s^{-1}
D_e	Effective diffusivity	m^2s^{-1}
D_{KAe}	Effective Knudsen diffusivity of gas A	m^2s^{-1}
D_{KBe}	Effective Knudsen diffusivity of gas B	m^2s^{-1}

D_{Kie}	effective Knudsen diffusivity of component i	m^2s^{-1}
D_L, D_R	Steady state diffusivity, left and right end chamber	m^2s^{-1}
D_s	Diameter of the pellet	m
K_1, K_2, K_3	As defined in Appendix 2	
L	Length of the pellet	m
M_A	Relative molecular mass of A	-
M_B	Relative molecular mass of B	-
M_i	Relative molecular mass of i	-
m	Weibull modulus	-
P	Pressure	Nm^{-2}
P_f	Weibull distribution function	-
P_L	Applied load	kg
P_T	Total pressure	Nm^{-2}
P_1	Left hand chamber pressure	Nm^{-2}
P_2	Right hand chamber pressure	Nm^{-2}
ΔP	Pressure differential	Nm-2
q_{1in}, q_{2in}	Inlet flowrate,left and right end chamber	m^3s^{-1}
q_{1out}, q_{2out}	Outlet flowrate,left and right end chamber	m^3s^{-1}
q_1, q_L	Outlet flowrate,left hand chamber	m^3s^{-1}
q_2, q_R	Outlet flowrate,right hand chamber	m^3s^{-1}
q_p	Permeation flow rate	m^3s^{-1}
R	Ideal gas constant	$Jmol^{-1}K$
R	Radius of pellet (eqn. 5.3 & 5.4)	m
r	Radius of capillary	nm
S_{gm}	Total micro pore surface area	m^2g^{-1}
T	Absolute temperature	K
T_s	Thickness of the pellet	m
T_s	Normalised tensile strength in plots	-
T_1, T_2	As defined in Appendix 2	
t	Time	s
V_g	Pore volume of the pellet	cm^3g^{-1}
V_1, V_L	Left hand chamber volume	m^3
V_2, V_R	Right hand chamber volume	m^3
W_p	Weight of the pellet	g
x	Length variable in pellet	m

x_A	Mole fraction of A	-
x_{A1in}	Inlet mole fraction, left end chamber	-
x_{A1out}, x_{A2out}	Outlet mole fraction, left and right end chamber	-
u_{-1}, u_o, u_1	As defined in Appendices 3 and 4	
u_{i-1}, u_i, u_{i+1}	" " " "	
u_{n-1}, u_n, u_{n+1}	" " " "	
u^*_{-1}, u^*_o, u^*_1	" " " "	
u^*_{i-1}, u^*_i	" " " "	
u^*_{i+1}, u^*_{n-1}	" " " "	
u^*_n, u^*_{n+1}	" " " "	
v_{-1}, v_o, v_1	As defined in Appendix 4	
v_{i-1}, v_i, v_{i+1}	" " "	
v_{n-1}, v_n, v_{n+1}	" " "	
v^*_{-1}, v^*_o, v^*_1	" " "	
v^*_{i-1}, v^*_i	" " "	
v^*_{i+1}, v^*_{n-1}	" " "	
v^*_n, v^*_{n+1}	" " "	
z	Length variable	m

Greek

ε	Porosity of the pellet	-
ε_{micro}	Microporosity of the pellet	-
γ	Surface tension	Nm-1
ϕ	Wetting angle	
μ	Viscosity of gas	Nsm-2
μ_m	Viscosity of the gas mixture	Nsm-2
ρ	Density of gas	gcm-3
ρ_p	Apparent density of pellet	gcm-3
ρ_s	Absolute solid density	gcm-3
τ	Tortuosity factor	-
τ_m	Tortuosity factor based on microporosity of the pellet	-
σ_{AB}	Force constant in the Lennard Jones potential function	nm
σ_x, σ_f	Tensile stress	MNm-2
$\bar{\sigma}_f$	Mean tensile stress	MNm-2
Ω_D	Collision integral	-

LIST OF FIGURES

LIST OF TABLES

CHAPTER - 1

INTRODUCTION AND LITERATURE SURVEY

1.1. Introduction to diffusion and permeability in porous catalysts

The civilised nations of the world, are largely dependent for an abundant supply of their basic survival needs (such as foods, clothing, shelter, pharmaceuticals, fuels, energy etc.), on the chemical process industries. At the heart of these process industries lies the actual reactor where one or more substances react, transform or decompose to yield the desired products. A key question is how efficiently and economically this synthesis or decomposition can be carried out in order to obtain an acceptable return on capital?

Numerous analyses and investigations by chemists and chemical engineers have lead to the conclusion that conversion from reactants to products can often be profitably enhanced if the reaction is carried out in the presence of some selected foreign material which virtually remains unchanged at the end of reaction and is thus readily available for reuse. This foreign material is called the catalyst. If the reactants exist in the same phase as that of the catalyst, the system is called homogeneous; otherwise the system is heterogeneous. Most heterogeneous catalytic systems involve porous catalyst particles and the physical characterization of these with respect to their key physical preparation variables is the main focus of this thesis. The solid catalysts are randomly dumped into reactors of fixed bed, fluidised bed or trickle bed form but can also include monoliths and slurry systems. The fluid reactants are directed to pass through these reactors. One of the advantages of the solid catalyst is that it can often be used for many years in a reactor depending of course on the level of poison either in the inlet stream (e.g., sulphur) or that builds up within the

reactor in the form, for instance, of coke. For example, irregular shaped multi promoted iron catalyst for ammonia synthesis can be used for as many as 10 years, whereas, zinc oxide catalyst which is employed to reduce the sulphur content from the feed raw materials (e.g., natural gas) loses activity over 1 to 2 years. Low temperature $Cu/Zn/Al_2O_3$ shift catalyst displays a typical life time of 1 to 3 years. However, other catalysts, e.g., cracking catalysts have a short life time and therefore need regular regeneration to regain activity.

According to a survey in 1984 it has been observed that about 90% of the chemical process industries including refineries are catalytic in nature (Hegedus, 1987). About 43% of total sales of catalysts are used for the manufacture of chemicals, 35% are used for petroleum refining and the rest, 22% of the total, are utilised for exhaust emission control purposes.

Chemists have known about catalytic agents for more than one hundred and fifty five years but it was J. Berzelius (Berzelius, 1836) who in 1836 first used the word catalyst to define these agents. Since then hundreds of catalysts have been developed and used in commercial plant operations and many others are now being developed. An economic analysis shows that for each dollar of investment in a catalyst, manufactured goods to the value of one hundred and ninety five dollars can be made (Hegedus, 1987). Since catalysts are sold based primarily on their performance, catalyst manufacturers often spend over 10% of total sales on research (Stone, 1985).

The main roles that catalysts play in a reaction are:

1. A catalyst reduces the energy of activation for the overall reaction. For example, for the bimolecular homogeneous decomposition of nitrous oxide, the energy of activation has been found to be 245 kJ/mol

whereas over a platinum catalyst, assuming a unimolecular reaction, this is reduced to approximately 136.1 kJ/mol or about 121.4 kJ/mol on a gold catalyst (Maxted, 1933). For most reactions the activation energy lies in the range of 40 to 250 kJ/mol resulting in an increase of rate coefficient by a factor of between 2 to 50 for a temperature rise of 10 ^{o}C at room temperature and by a factor of 1.1 to 1.6 at a reaction temperature of 600 ^{o}C (Westerterp, 1984). A catalyst speeds up the rate of both forward and reverse reactions without affecting the equilibrium constant which is defined by the thermodynamic properties and the specification of an operating temperature.

2. Catalysts can be prepared according to the surface area requirements of the specific process. Fine powders are often compacted into pellets with large surface areas per gram of catalysts. For example, measurements of surface areas of "green" copper/zinc/alumina shift catalysts studied in this thesis have been observed to be of the order of 115 m^2/g.

3. A catalyst can reduce the overall cost of production thereby increasing the return on investment. As catalysts increase reaction rates, so for a given duty the equipment can be of smaller size, and hence cheaper, but on the other hand the system is usually more complex.

Based on the above discussion and the fact that many present large scale chemical productions utilize catalysts in key processes (Mukhlyonov, 1974), it is therefore imperative to know more about catalysts; particularly about the nature of the interaction between catalysts, reactants and the products. The pore structure of catalysts can, to some extent, be characterised in terms of physical properties such as porosity, surface area, pore size distribution, effective diffusivity, permeability and tensile strength. Each of these physical properties can change significantly with alterations to key physical processing steps during catalyst preparation. To produce and market good quality

catalysts with appropriate combinations of effective diffusivity, permeability and tensile strength, the effects of all preparation steps must be considered. Investigations of this type have not appeared in the open literature previously.

One facet of solid catalysts created during their preparation and reduction is their pore structure. It is this pore structure which can significantly change the rate of formation of a product or the selectivity achieved in the case of multiple reactions (Cresswell, 1985). If this is the case, one must pay careful attention to this subject matter. Pores within a pellet are not of uniform length or diameter and are highly irregular in shape forming cross-linked channels or channels of only one end open called dead-end channels. Because of these complexities and the wide variation in pore structure in terms of the above mentioned sizes, shapes and interconnections (McGreavy, 1980), pore models such as the parallel path pore model (Johnson, 1965; Smith 1970; Youngquist, 1970) or the pseudocapillary or random pore model (Pollard, 1948; Rothfeld 1963; Scott, 1962; Wakao, 1962) are only crude approximations of reality. For uniformly distributed regular pores, they can provide relatively accurate and reliable predictions of properties whereas for a real commercial catalyst the descriptions of these pore models are unable to mirror the real overall complexity of the porous network. This has made the study of catalysts, and its allied subjects, (catalytic stripping, cracking, reforming, etc.) particularly complicated.

Generally in a catalytic reactor the reactant flows as a result of a gradient in total pressure. Reactant then reaches the catalyst external and internal surface area following mass transfer and diffusion steps resulting from a gradient in mole fraction. The reaction takes place and the products diffuse back to the main stream of the fluid. If the reaction is potentially

faster than the diffusion process, which is true for many cases in practice, the overall rate of the catalytic process tends to be governed by diffusion alone and vice versa. This coupling of diffusion with reaction again makes the process complicated and is the concern of heterogeneous reactor designers.

Furthermore, the process of diffusion in industrial catalysts proceeds not solely by a bulk mode or Knudsen mode but rather by the combination of the two (see section 1.1.1). This creates an additional problem of choosing the right model of diffusion which can provide equations applicable to a combination of bulk and Knudsen diffusion as well as permeation.

Thus in summary we have three problems. The first concerning the description of the geometry of the porous structure; the second involving the specification of the rate of a diffusion limited reaction and the third concerning what equation or equations can be used to characterise transitional diffusion and flow in combination. The third problem can be resolved using the dusty gas model which was developed by Mason and co-workers (Evans, 1961; Mason 1967; Mason 1969) through the 1960s. This model provides equations which do cover the entire ranges of diffusion. In this model if a binary system consisting of gases A and B are counter diffusing through a porous medium, the medium is considered as a third "dummy" component of this binary system thus forming as a whole a ternary system. Multicomponent diffusion equations obtained from the classical kinetic theory of gases can then be written for this ternary system. Making the molecular weight of the "dummy" component infinitely large so that there is no net flux of it, the equations then become applicable to the binary system within a porous structure. The model neither talks about the detailed form of porous structure nor provides an "a priori" means of evaluating effective diffusion coefficients. At present these have to be found by

experimentation alone. This value of the diffusion coefficient can then be used to treat the second problem, that of predicting the rate of a diffusion limited reaction. More information about the dusty gas model is available in a number of references, Cunningham, 1980; Waldram, 1976; Jackson, 1977 and Mason, 1983.

Part of this project is to measure binary gas effective diffusivities in single catalyst pellets using both steady and unsteady state techniques and permeabilities using steady state flow measurements. Other physical properties measured are surface area, porosity, pore size distribution and tensile strength. Establishing the dependencies of all these on processing variables used in the course of catalyst preparation (e.g., precompaction load, particle cut size, amount of lubricant, calcination temperature, pelleting density and reduction) is the main objective of this research. A summary of such processing variables along with the properties to be investigated is presented in figure 1. ICI $Cu/Zn/Al_2O_3$ LT shift catalyst has been chosen as a model catalyst sample for all measurements and correlations. This catalyst is used, for instance, in ammonia synthesis for converting CO into CO_2 at a low temperature of approximately 200 ^oC. It's physical properties are poorly understood compared to its chemical properties such as structure, reaction rate, reaction intermediates, bonding etc. which are relatively well established.

This project has been financially supported by ICI Chemicals and Polymers Group and additional objectives are:

(1) Assessing the variability of the physical properties between nominally identical individual pellets of a given product. This information should be vital for good quality control.

(2) Observing the variation of properties between "green" and "reduced" catalysts. This is important because

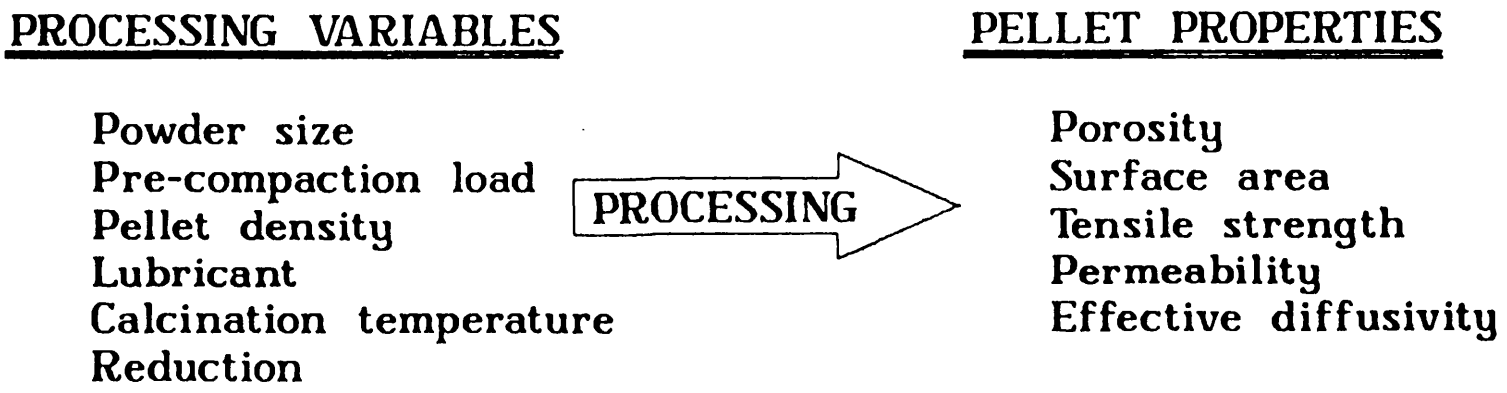

Figure 1. Summary of the variations of catalyst production parameters and the properties to be measured.

catalysts are used finally in "reduced" form.

There is no standard equipment used by any catalyst manufacturer for effective diffusion measurements: this is in contrast to the measurements of surface area, by the BET method, or pore size distribution by mercury porosimetry. Therefore the project also focuses on the design and development of a relatively simple technique for making such measurements. A theoretical model for combined diffusion and flow has also been developed and solved for the case of nonisobaric nonequimolar counter diffusion.

1.1.1 Diffusion

For potential exploitation of the whole surface area of a catalyst, both external and internal, the reactant molecules must reach the active sites of the porous structure for the selected reaction. This transport of reactant which is caused by a gradient in mole fraction of components is called diffusion. The term effective diffusivity is often used instead of free gas diffusivity or Knudsen diffusivity to characterize diffusion through porous media. It is usually a function of both effective bulk and Knudsen diffusivities as defined by Bosanquet. Arithmetically the effective diffusivity can be considered to be directly proportional to the porosity of the porous structure and inversely proportional to the tortuosity of the passage through which a gradient in mole fraction is established. Tortuosity can not be measured directly. The proportionality constant is either the Knudsen or the free gas diffusivity which is always by definition greater than the effective diffusion coefficient. The tortuosity factor for isotropic porous media has been defined by Waldram et al (Foscolo, 1983) as

$$\tau = \frac{1}{\varepsilon} \qquad (1.1)$$

It was Thomas Graham (Graham, 1829) who first studied the phenomena of diffusion and flow using a porous plug. However, from the late 1930s to the mid 1940s there were several publications, for example, Damkohler, 1937; Thiele, 1939; Zel'dowitsch, 1934 and Wagner, 1943 especially, concerning the influence of diffusion on chemical reaction in porous catalysts. These publications have largely motivated reaction engineers to study diffusion through porous media (Cunningham, 1980).

Diffusion is purely a mass transfer phenomena and the higher the value of the coefficient, the more gradual is the fall in mole fraction. In porous catalysts diffusion proceeds principally by three mechanisms and these are bulk, Knudsen and surface diffusion.

1.1.1.1 Bulk diffusion

If the pores are much larger than the mean free path of the gas molecules, there are frequent collisions between the individual molecules and hence their movement can be adequately described by the kinetic theory. For a binary mixture consisting of gases A and B, the effective bulk diffusion coefficient can be defined, (Satterfield, 1970), as:

$$D_{ABe} = D_{AB} \frac{\varepsilon}{\tau} \qquad (1.2)$$

But the problem is that τ can not be predicted other than by experimental measurements of D_{ABe} so the value of equation (1.2) is limited. The free gas diffusivity can be obtained from the following theoretical expression which is based on the classical kinetic theory and the Lennard-Jones expression for intermolecular forces (Hirschfelder, 1954),

$$D_{AB} = \frac{0.01858\ T^{1.5}\ (M_A + M_B)/(M_A M_B)^{0.5}}{P\sigma^2_{AB}\ \Omega_D} \qquad (1.3)$$

It is evident from equation (1.3) that ordinary diffusivities are proportional to absolute temperature to the 1.5 power and inversely proportional to pressure.

Pores are classified as macro, meso and micro pores (see Chapter 2, section 2.3) and bulk diffusion occurs in macropores only. To identify whether bulk or Knudsen diffusion occurs within a porous medium, measurement of the pore size distribution for that medium is necessary.

1.1.1.2 Knudsen diffusion

If the mean free path is much larger than the pore dimensions, the molecule will in general strike the wall more frequently than other molecules and predictions from the kinetic theory are no longer valid. In this case Knudsen diffusion, or Knudsen flow, results. Knudsen diffusion is independent of pressure but dependent on temperature and relative molecular mass. The effective Knudsen diffusion of component i can be obtained from (Satterfield, 1970),

$$D_{Kie} = 19400 \frac{\varepsilon^2_{micro}}{\tau_m S_{gm} \rho_p} (T/ M_i)^{0.5} \qquad (1.4)$$

From the above definition of bulk and Knudsen diffusion, it is quite clear that there exists a region in between these two extremes of diffusion processes which is intermediate in nature: this is called transition diffusion. As a rule of thumb, in the Knudsen extreme of this region the mean free path is some 10 times larger than the pore dimensions and in the bulk extreme the mean free path is at least 10 times smaller than the pore dimensions (Scott, 1962). For many gases at near ambient conditions, pore radii or diameters between 5 nm and 500 nm will span these diffusion regimes (Scott, 1962). A large number of commercial catalysts contain pores in just this size range and therefore these transitional or intermediate diffusion cases are of

paramount practical importance.

1.1.1.3 Surface diffusion

When molecules adsorb on surfaces, and if the adsorption process is physical in character, i.e. if the bond of adsorption is not too strong, the molecules may move from place to place along the surface in the direction of decreasing surface concentration; this phenomena is called surface diffusion. For helium at ambient temperature and pressure surface diffusion is assumed negligible because of very little adsorption (Satterfield, 1970; Smith, 1970). Surface diffusion may be important for a vapour phase reaction at temperatures close to the boiling points of the reactants and products (Wheeler, 1951). This diffusion is however unimportant when the reaction is carried out well above the boiling points of the reactants and products (Hoogschagen, 1955) or for a liquid phase reaction (Wheeler, 1951). Surface diffusion has not been considered in this research.

1.1.2 Permeability

In a porous catalyst, as well as diffusion, there may be a flow phenomena due to the total pressure gradient across the pellet and this is called permeation. Permeation usually occurs at low Reynold's numbers and is a viscous flow phenomenon and simply indicates how easily a gas, or a mixture of gases, can pass through a given porous medium. For a small differential pressure across the pellet the permeation flux is given by (Perry, 1986; Jackson, 1977)

$$q_p = - \frac{B_0 P}{\mu RT} \frac{A}{\rho} \frac{dP}{dz} \qquad (1.5)$$

1.2 Importance of studying diffusion and permeability in porous catalysts

Diffusion in porous particles is largely dealt within the subject of chemical reaction engineering one part of which deals with solid-fluid (heterogeneous)

reactor design. This requires a knowledge of fluid mechanics, chemical kinetics, thermodynamics, transport process and economics (Waldram, 1983). However the design approach of such a reactor is not as simple as one can nakedly imagine because of the coupling of diffusion with chemical reaction (as already mentioned in section 1.1), a potential problem which is yet unresolved. For this reason the design of a heterogeneous reactor is often still based on empiricism (Satterfield, 1970). Two important parameters based on which heterogeneous reactors are at present designed are the Thiele modulus and the effectiveness factor. The expressions for these and the theories which led to their definitions were developed independently by Damkohler (Damkohler, 1937); Zeldowitsch (Zeldowitsch, 1934) and Wagner (Wagner, 1943) and subsequently extended by Thiele (Thiele, 1939). From a plot of effectiveness factor versus Thiele modulus one can immediately define the influence of diffusion on the chemical reaction. Effectiveness factors can be obtained experimentally or predicted theoretically. In the latter case a value of the effective diffusivity is needed to calculate the Thiele modulus. An effective diffusivity is required to solve an isobaric model of diffusion. Thus, concentration gradients along the length of a catalyst pellet can be established and simulated. A good review on this is given in Gibilaro, 1985.

From the measurements of single pellet permeabilities much useful information about the pore structure can be obtained. For example if the pores are interconnected i.e. continuous or increase in size during chemical reduction one should naturally expect to have a relatively large permeation flux and vice versa. Structural variations between nominally identical individual pellets can also be investigated. That is the presence of macro, meso and micro pores can immediately be detected from permeability experiments (Wheeler, 1951). From permeability data it is possible to estimate the tortuosity factor of the catalyst particles (Asaeda,

1979). More of the importance of measuring single pellet permeabilities is available in Wheeler, 1951.

An experimental value of effective diffusivity (see equation 1.2) and permeability coefficient (see equation 1.5) is necessary to solve a nonisobaric model of diffusion.

The study of diffusion and flow can potentially be applied to many other areas such as oil field modelling, hydrology, geology etc.

1.3. Study of diffusion in porous catalysts

Following Graham's work on diffusion and flow in porous media and using an analogy with Ohm's law (Cunningham, 1980; Cussler, 1984), Adolf Fick published his first and second laws of diffusion in 1855 (Fick, 1855). These are now universally used to describe free gas diffusion as well as diffusion through porous media. The development of an axial diffusion test in a cylindrical pellet housed in a cell by Wicke and Kallenbach (Wicke, 1941) was later modified by Weisz and Prater (Weisz, 1954). This type of cell is now loosely referred to as a Wicke and Kallenbach type diffusion cell (see chapter 2), and is used for both steady and unsteady state single pellet diffusion and permeation measurements. Other measurement techniques such as chromatographic techniques (Davis, 1965; Schneider, 1968; Eberly, 1969) are also available with respective advantages and disadvantages (chapter 2). It is beyond the scope of this work to discuss all possible experiments and results of diffusion that have been conducted so far and hence a selection from recent studies i.e. from 1973 onward only will be considered. For more information and references it is suggested that the interested reader should consult the following references: Satterfield, 1970, 1980; Jackson, 1977; Waldram, 1976; Cunningham, 1980.

1.3.1 Recent studies on diffusion

From 1974 to 1981 Asaeda et al published a series of papers (Asaeda, 1974a; Asaeda, 1974b; Asaeda, 1979 and Asaeda, 1981) on flow, isobaric and non-isobaric diffusion through porous media. In the first paper they derived an analytical expression for the permeability of gases through a packed bed of spherical granules from the rigorous kinetic theory of gases. The expression was valid for the Knudsen flow regime only. The results were in good agreement with the experiments for beds packed with non-porous glass spheres of 5.7 and 9.3 microns diameter. In the second paper they studied isobaric diffusion of gases with special attention to the solid parts of the porous media, that is, through packed beds of fine spherical particles of glass using again the rigorous kinetic theory of gases with a two sided Maxwellian velocity distribution function and Maxwell's transport equation. They proposed a method for the measurement of effective diffusivities of gases through porous media to obtain experimental confirmation of the dependency of mean effective diffusivities on composition. The apparatus as they used for diffusion measurement was a glass bulb of volume about 55 cm^3 with a main gas inlet. The porous sample was mounted at the top of this glass bulb with a second gas inlet. A movable oil piston was placed into a 3 mm diameter glass tube and this was the outlet from the glass bulb. The piston sealed the apparatus. Another glass bulb with a similar piston arrangement was attached to the main glass bulb for the reference. A pure gas (gas A) of known composition was introduced through the main gas inlet. Another gas (gas B) was then introduced through the second inlet at a relatively high speed and thus diffusion occured as confirmed by the movement of the oil piston. After the piston had travelled some distance, gas B was switched to gas A and the oil piston returned to its original position. The experimental results obtained by this method were in relatively good agreement with the analytical results. In the third paper, they proposed a

new method of determining the tortuosity factor of monodispersed unconsolidated and consolidated packed beds, consisting of fine non-porous glass beads, crushed ceramics or crushed sand from flow permeability data using a packed column. The apparatus was the same as that described in the second paper. All samples had diameters between 6.3 to 13 microns. The tortuosity factor obtained from this new method coincided well with that obtained from the usual diffusion method. However the route of calculating the tortuosity factor from the experimental data was tedious compared to obtaining the tortuosity factor directly from the measurement of D_{ABe} by the diffusion cell method. Finally, they studied the effect of total pressure gradient on unsteady state diffusivities using a Fick type isobaric diffusion equation (Asaeda, 1981). The porous sample used was a packed bed of fine glass powder of 6 microns diameter with a porosity of 0.297. Using a step change in concentration of He in N_2 and He in Ar, a relatively large pressure change was observed within few seconds. The numerical solution of the non-isobaric equations showed good agreement with the experimental results for the above two binary systems.

Hashimoto and Smith (Hashimoto, 1973) used a chromatographic technique to determine macropore diffusivities in commercial pellets containing a clay binder and 5Å molecular sieve. Nitrogen and n-butane pulses were introduced into a column packed with crushed pellets and the moments of the effluent peak were evaluated. Analysis of results indicated that significant internal diffusion resistance would be encountered with pellets of a size practical for commercial adsorption equipment.

Cresswell and Orr (Cresswell, 1982) measured effective diffusion coefficients in silica/alumina isomerization catalyst under nonsteady state conditions using both the single pellet diffusion cell method and

the packed bed chromatographic approach. The cylindrical sample (3.18 mm in diameter and 3.3 to 4.26 mm in length) for the former method was prepared from the original silica/alumina spheres of 3.3 mm diameter which were used for experimentation in the packed bed. For the single pellet experiment, the cylindrical pellet was sealed into a metal ring using silicone rubber. The packed bed study was carried out in a single pellet string reactor (SPSR). The SPSR is a small vertical cylindrical column packed with few hundreds of spherical catalyst particles. The column diameter is between 1.1 and 1.4 times the particle diameter. The mean pore radius determined by mercury porosimetry was about 3.5 nm. This confirmed that diffusion was in the Knudsen region. Pellet porosity was o.5. The single pellet cell experiment was conducted at 50 ^{o}C. In both cases helium was used as a pulse gas and nitrogen as the carrier gas. The effective Knudsen diffusivity using the single pellet diffusion cell method averaged over five pellets was 3.81×10^{-3} cm^2/s and $(3.62 \pm 0.16) \times 10^{-3}$ cm^2/s for the SPSR (averaged over five runs). Thus good agreement was found between two completely different approaches to diffusion measurement. However, in case of the diffusion cell method, the observed pellet to pellet variations of effective diffusivities were considerably larger than the uncertainty limits associated with the measurements on a single pellet. Cresswell and Orr therefore recommended, when using a single pellet diffusion cell technique, to examine several pellets in order to obtain a true measure of the mean effective diffusivity to be used in reactor modelling.

Gibilaro and Waldram (Gibilaro, 1985) measured effective diffusion coefficients of argon in nitrogen within Hydronyl 356 GA 4C alumina pellets. They housed five pellets in a purpose built cell and showed that effective diffusivities calculated from system moments were generally reproducible to within +/- 12% and average values for diffusivities in radial and axial directions

within the pellets agreed to within +/- 25%. In another study Waldram et al (Bower, 1984) measured steady and unsteady state diffusion coefficients in a single sphere of commercially produced catalyst support housed also in a purpose built cell. Using a step change of 20 mole% of helium in nitrogen they found that steady and unsteady state diffusivities agreed within 25%.

McGreavy and Asaeda developed a non-isobaric diffusion model for a binary gas system allowing for nonequimolal fluxes in porous solids (McGreavy, Personal communication). The porous samples used were plugs made up from compressed non-porous fine glass powder of a few microns in diameter and were monodispersed in character. Using a Wicke Kallenbach type diffusion cell and introducing a helium pulse in nitrogen, they determined that the unsteady state diffusion coefficients were in good agreement with theoretical results obtained from the solution of the nonisobaric model. Unfortunately these porous media had no microporosity and were produced from narrow cut sizes of glass powder. As a consequence the results are of very limited value or applicability to porous systems of more complex form. Petrini and Schneider (Petrini, 1984) proposed a method for "a priori" prediction of the intraparticle diffusion effects in the low temperature water gas shift reaction catalyst. Use was made of transport characteristics of the $Cu/Zn/Al_2O_3$ pelleted catalyst determined independently by a combination of diffusion and permeation experiments made under nonreacting conditions. The porous medium was described by the mean transport pore model and diffusional behaviour of the multicomponent reaction mixture by a modified Stefan-Maxwell equation. Using kinetic data obtained at 200 ^{o}C, it was possible to predict the performance of a batch scale reactor packed with pelleted catalysts at 200 ^{o}C and 220 ^{o}C.

Allawi and Gunn (Allawi, 1987) studied combined flow and diffusion through four porous catalyst

substrates in the range of 1 to 3 bar absolute pressure. The differential equations in the form of Chapman Enskog first order approximations obtained from assumptions of simultaneous diffusion and flow were solved analytically considering the variation of viscosity with composition. The parameters for the diffusion and flow processes were found from separate experiments on isobaric flow and diffusion, on nonisobaric flow and diffusion and from composition transients in fixed beds. There was good agreement between theory and experiment except with the permeability experiments at low pressures where significant differences were found. Finally, Al-Rqobah et al (Al-Rqobah, 1988) studied diffusion of gases through porous pellets under constant total pressure introducing hydrogen and helium pulses in nitrogen. Moments and numerical methods were used to analyse the response curves. The results were found to be in good agreement when compared with the results obtained from the random and the parallel path pore models.

1.3.2 Which diffusion coefficient should be used for reactor modelling?

One vital question which has been discussed in the literature is what value of a diffusion coefficient is it sensible to use to predict the actual rate of a heterogeneous reaction? Is it appropriate to choose a D_e value obtained from measurements made under non-reacting conditions (physical effective diffusion coefficient) or to choose one that was obtained under reacting conditions (kinetic effective diffusion coefficient). A review of this question has been given in Park, 1984a and Park, 1984b, and suggests using kinetic diffusion coefficients in order to arrive at a valid effectiveness factor. Another review has been also given in Wakao, 1974 and this suggests using the physical diffusion coefficients. Several other authors have also put forward their individual comments: Rothfeld, 1963; Wakao, 1964, 1969, 1974; Weisz, 1954; Otani, 1966; Balder, 1968a, 1968b; Toei 1973; Hawtin, 1964a, 1964b, 1966, Steisel, 1967 etc.

For example, Rothfeld suggests measuring D_e under non-reacting conditions and using this value to solve the differential equation with chemical reaction under the same conditions of temperature, pressure and chemical composition (Rothfeld, 1963). However this is not easy to achieve and most diffusivity measurements are made at conditions not far removed from ambient. In Wakao and Smith's view, the prediction of D_e made by different investigators, e.g., Wicke, 1941; Hoogschagen, 1955; Scott, 1960; Masamune, 1962; Henry, 1961 etc. always has been considered from the standpoint of diffusion in the absence of chemical reaction which in most instances is not equivalent to diffusion measured under reaction conditions (Wakao, 1964). Weisz and Prater (Weisz, 1954) have made observations of the obvious limitation of measuring D_e at room temperature and pressure and then extrapolating this measurement to widely different conditions of pressure, temperature and molecular species. Otani and Smith reported that the effective diffusivity under non-reacting conditions was some four or five times greater than that actually measured under reacting conditions (Otani, 1966). This was due to the skin effect created during pellet moulding which displayed a much lower diffusivity than the inner materials. Wakao et al found that the physical diffusion coefficients were larger than kinetic diffusion coefficients by a factor between 3 and 4 in the para-ortho hydrogen conversion (Wakao, 1969).

Using a two dimensional network model of macro and micropores (see chapter 2 for definition), Wakao and Nardse estimated the values of effective diffusivity for both reacting and non-reacting systems with and without dead ended pore effects. With no dead end pores, D_e under reacting conditions was smaller than under non-reacting conditions. The cause was due to the fact that diffusion under reacting conditions was contributed to largely by micropaths while under non-reacting conditions it was largely by macropaths (Wakao, 1974). With 8% macro and

micro dead ended pores, the computation showed that D_e for non-reacting conditions decreased more rapidly than the D_e for reacting conditions ultimately the ratio of D_e for both the measurements approaching to unity. The sharp decrease in the former case was due to the formation of detours through the micro pores. Balder and Petersen, using a single pellet reactor (SPR) at steady state found that the effective diffusivities under reacting conditions were about 25% below those from under non-reacting conditions for alumina supported platinum catalyst. This was attributed to the nonuniformity of catalyst activity, but identical diffusivities were obtained in the catalyst pellet made from a mechanical mixture of platinum black and alumina (Balder, 1968a, 1968b).

Toei et al (Toei, 1973) studied the hydrogenation of ethylene on nickel catalysts and showed that the value of the effective diffusivity obtained using a single pellet diffusion cell under non-reacting conditions coincided with that obtained using a SPR, but the values obtained using a fixed bed reactor showed a large discrepancy between the two. Hawtin et al measured effective diffusion coefficients of oxygen through nitrogen in graphite and in ungraphitised highly reactive porous carbon under both non-reacting and reacting conditions and in all cases they observed similar diffusion coefficients (Hawtin, 1966; Hawtin, 1964a and Hawtin, 1964b). Steisel and Butt used their convergent divergent pore model to show that both physical and kinetic diffusion coefficients for the oxidation of carbon monoxide were the same (Steisel, 1967). Whitaker et al derived the effective diffusivity tensor under reaction conditions using a spatially periodic pore model to show that the effective diffusivity should be independent of the chemical reaction rate (Ryan, 1980).

So far the measurements of effective diffusion coefficients under reacting and non-reacting conditions

from several individual points of view have been discussed; it is evident that most researchers, largely for reasons of simplicity, have favoured making the measurements under non-reacting conditions. Let us look at this whole problem in a more philosophical way.

There are several reasons for the differences between effective diffusivities determined under reacting and non-reacting conditions. First, the problem of diffusion is often different. This means, no matter whether the diffusion is in the bulk mode, the Knudsen mode or the transition mode, when a reaction occurs the pore structure may change significantly due to sintering and the formation of hot spots inside the catalyst particles. Therefore diffusion characteristics will alter. Moreover Knudsen diffusion often dominates under reacting conditions. Second, under steady state conditions reaction fluxes are dictated by the stoichiometry of the reaction. That is, when diffusion under reacting conditions is considered, any additional flux due to the chemical reaction has to be included in the mass balance equations. Finally in most cases actual reaction conditions (for pressure, temperature and composition) do differ from typical experimental conditions. Most diffusion experiments are carried out at near ambient conditions using a binary gas mixture. But in real practice multicomponent gas diffusion occurs within the catalyst particle and also depending upon the process the pressure and temperature of the reaction are considerably higher. Hence the methods and conditions adopted for measuring D_e do not reflect a true industrial situation. All these factors can mislead one and it is important to pick the correct experimental technique and conditions for diffusion measurements. Now at this critical stage if we consider the coefficient itself, it will be observed that the diffusion coefficient is only one of several extremely important physical parameters of catalysts or other porous media. Its dependency on pressure and temperature (see section 1.1.1) is

reasonably well understood: however the absolute dependency on the inner physical pore structure, which in turn is affected by key production variables such as pellet density, calcination temperature, cut size etc., has not been investigated in the open literature. For example, in this thesis, with ICI $Cu/Zn/Al_2O_3$ LT shift catalyst, a three fold increase in diffusivity has been experimentally observed within pellets produced at a low pressing density. Similarly, for those pellets produced at a high pellet density, the diffusivity is lowered by a factor of 2 compared to the base sample. It has also been experimentally demonstrated that upon chemical reduction the permeability in some cases has increased by a factor in excess of 400 while the diffusivity for the same catalyst sample has increased by a factor of only 2. These two examples strongly reconfirm the crucial dependency of transport parameters such as diffusion coefficients upon the processes and conditions used to make the porous structure. Experimental D_e values determined under any conditions are always valuable in a comparative context. That is, we can pick up changes in pore structure even if the diffusivity we are measuring may not strictly apply at process conditions.

1.4 Factorial experimentation

In much technological, academic and industrial research, the effects of several factors need to be considered and these are varied individually or simultaneously over ranges of specified interest. Varying one factor at a time whilst keeping the others constant increases the number of experiments and hence the experimental time; moreover designing experiments in this way does not provide all the information needed. This is because in reality factors do interact and this interaction must be taken into account. That is, more than one factor must be varied at each level of interest to arrive at a reasonable conclusion. For example, to observe the effects of use of two kinds of fertilizers on a particular crop at two different application levels,

one needs to carry out only four experiments. These four experiments can be designated as AlBl, AlBh, AhBl and AhBh where A and B represent two fertilizers and l and h represent their low and high levels of application. From these the effect of the variation of A when B is at its low level can be obtained as AhBl - AlBl or the effect of the variation of A when B at its high level can be obtained as AhBh - AlBh and so on (Cox, 1958). Experiments designed in this way are referred to as factorial experiments.

If three factors are to be varied at two levels, 2^3 i.e. 8 experiments need to be carried out and the general formula for n factors to be varied at m levels is m^n (Das, 1979).

Factorial experiments therefore provide an opportunity to investigate not only the individual effects of each factor but also their interactions. The factorial approach reduces the overall number of experiments to a manageable level (Das, 1979).

The main drawback with factorial experimentation is that the total number of treatments goes up sharply as the number of factors or the number of levels are increased. Thus with a seven factor experiment at two levels, there are 7 main effects, 21 first order interactions, 35 second order interactions, 35 third order interactions, 21 fourth order interactions, 7 fifth order interactions and one sixth order interaction making 127 effects in all. That is including the base experiment a total of 128 experiments need to be investigated. But by designing the experiments factorially all necessary information can be extracted by conducting only 28 experiments (Duckworth, 1968). Experiments on second or higher order interactions are only valuable when a search for optimum condition is required (Duckworth, 1968).

When treatments are considered at three levels,

the number of experiments increases but at the same time more information can be recovered. A linear or quadratic variation of properties can be investigated when the factors are considered at three levels (Das, 1979). This means, if the effect of a level of two factors is the same, the overall effect on a particular property will then be additive.

In summary, the design of a factorial experiment depends primarily on the type of information needed. A quick overall picture of the effects of factors which are independent of each other can be obtained by considering all factors simultaneously within a factorial experiment. Even if the factors are dependent then also the effect of a single factor for every other combination of levels can be examined by a factorial approach (Cochren, 1957). However, the number of levels selected should be such that the total number of experiments fall to a manageable level (Das, 1979).

If there are several treatment combinations, a large group of experiments has to be conducted: in this case the interpretation of data becomes difficult (Cochren, 1957). Nonetheless, if some previous knowledge about the factors and their interactions are available, then a factorial design will considerably reduce the overall total experimentation (Davies, 1954). As a result time will be saved as well as the money if cost per experiment is high.

CHAPTER - 2

PHYSICAL CHARACTERISATION OF CATALYSTS

2.1 Introduction

In order to understand the behaviour of a single catalyst, or a mass of catalyst particles when in contact with reactants and products, the first and foremost thing is to measure and quantify all the catalyst's properties. Unfortunately, unlike surface chemical properties (bonding, oxidation state, reaction intermediates, heat of adsorption etc.), relatively few well established techniques are available for measuring the physical properties (Twigg, 1989). In a review over five years from 1935 to 1940 on the development of catalysis, Taylor (Emmett, 1948), commented that "this five year period gave catalytic science a tool of which it had long been in sore need." This comment by Taylor was due to the development of a surface area measurement technique by Brunauer, Emmett and Teller: this is now universally known as the BET method. This development formed the foundation of a whole area of surface chemistry research concerned with surface area measurement, surface adsorption studies and evaluation of pore size distributions in the micro pore range.

A single porous solid catalyst can physically be partially characterised by means of its surface area, porosity, pore size distribution, mechanical strength and in particular by permeability and effective diffusivity measurements within it. All of these are of fundamental importance when studying any porous catalyst. Without these basic pieces of information, catalyst performance specification in terms of an effectiveness factor is not possible even at the most elementary level. Catalyst tensile strength (see section 2.7) is another property which must be determined in order to minimise particle fracture within the reactor. This chapter will deal briefly with the importance of, and various measurement

techniques for, these parameters.

2.2 Surface area

One fundamentally important property of a catalyst particle is its surface area. Knowledge of this surface area can lead one not only to estimate the variation of activities between individual pellets but it also immediately implies general information about the permeability, effective diffusivity and pore volume of the catalyst.

Catalysts possess both external and internal surfaces. An external surface can be formed of cracks or fissures which are wider than deep; the internal surface is comprised of cracks, pores and cavities which are deeper than wide (Gregg, 1967). Very fine powders have large external surface and negligible internal surface area. When such powders are pelleted by compaction, part of the external surface becomes internal and a pore system is developed. A variety of porous materials have an internal surface area greater than the external surface area by several orders of magnitude (Gregg, 1967). This is usual for many pelleted catalysts and it is this internal surface where the potential for most chemical reaction is present.

The highest surface areas that can be reliably measured are of the order of 1000 to 1200 m^2/g of catalyst (Satterfield, 1980). To obtain high surface areas, the catalyst is made enormously porous with a pore structure of very small dimensions. However, too much porosity can cause an unacceptable reduction in pellet strength. Expensive catalysts such as platinum, nickel etc. are often dispersed on highly porous supports, such as alumina, to create large surface areas for adsorption and reaction. Surface areas as low as 0.01 m^2/g can also be used and these may be measured using a chromatographic technique (Mukhlyonov, 1974).

The most widely used technique for surface area measurements is the BET method. The method is based on the fact that at a constant low temperature, molecules from a liquid or a gas are physically adsorbed on to the surface of a solid eventually forming a complete layer of approximately one molecule thick i.e. a monolayer. If the area covered by each molecule is known, the quantity of adsorbed material will then directly provide the total surface area of the sample. For such adsorption the gas or liquid chosen, would be such that the molecule can penetrate the smallest pore of the sample. Nitrogen is usually used.

The BET method measures the total surface area of the catalyst sample. In practice, not all of the surfaces are active for chemical reaction nor are all surfaces exposed to reactants at a significant concentration. These are prominant limitations of this method.

2.3 Pore volume or porosity

By pore volume within a catalyst pellet, we simply mean the sum of the accessible empty or void volumes to which gas molecules can permeate. The knowledge of this pore volume is necessary for evaluating the void fraction or porosity of the pellet. According to Sing et al (Sing, 1985) "porosity is a concept related to texture and refers to the pore space in a material." Pore volumes can be visualised as macro, meso and micro pore volumes and accordingly one can determine macroporosity, mesoporosity and microporosity independently. The total porosity of the pellet can be obtained by simple addition.

A convenient classification of pores according to their average width has been proposed by Dubinin (Dubinin, 1960). Pores of widths below 2 nm are described as micropores; those with above 20 nm are macropores and those with widths in between these two extremes as

mesopores. Satterfield (Satterfield, 1980) and Sing et al (Sing, 1985) classified pores larger than 50 nm in diameter as macropores; those less than about 2 nm in diameter micropores and pores of intermediate size as mesopores. Unfortunately none of these classifications coincides exactly with a division of pores into those in which Knudsen or bulk diffusion occurs (see chapter 6 section 6.2.4). Nonetheless, the significance of determining these porosities centres on the fact that without their values effective diffusion coefficients can not be predicted.

Three well known methods for determining the pore volume or porosity are (1) the imbibition method (2) the pycnometric method and (3) the helium-mercury method.

2.3.1 Imbibition method

In this method the mass of a porous pellet is measured. The sample is then soaked in a suitable solvent, say carbon tetrachloride, so that the air in the pores is replaced by the solvent. When all the air is displaced, the sample is taken out of the solvent, surface dried and the weight is again taken. The increase in weight divided by the density of the solvent will provide the pore volume of the sample.

The porosity or void fraction can then be obtained by dividing this pore volume by the envelope volume of the porous pellet.

2.3.2 Pycnometric method

This method is more commonly used but, unlike the imbibition method, this can not determine the single pellet porosity unless the pellet is relatively large. Therefore pellet to pellet variations of porosity can not be investigated conveniently by this method.

A helium pycnometer determines the average solid volume of a batch of catalyst. From this the density can

be found if the weight is known. In this method the chamber containing the sample is pressurized with helium which is allowed to expand isothermally into a second chamber thereby causing a reduction in pressure. From a mass balance around these two chambers, each of known calibrated volume, a relationship can be derived which enables one to obtain the solid volume within the porous sample. More information on this method is available for instance in the Operator's Manual, for the Micromeritics 1330 Autopycnometer, 1989.

2.3.3 Helium-mercury method

In this method the volumes of helium and mercury displaced by the sample are noted separately. Since mercury will not penetrate pores smaller than 15 μm diameter at pressures near to atmospheric, the difference in these two volumes will give the pore volume of the catalyst sample less than this size. The porosity of the pellet can then be obtained either from the density of the solid contained in the sample or alternatively by knowing the density of the porous pellet. The weight of the sample divided by the helium displacement volume will give the solid density and the apparent density of the porous pellet can be obtained from the weight of the sample divided by its mercury displacement volume.

If W_p represents the weight of the pellet in grammes, V_g the pore volume in cm3/g, ρ_p and ρ_s, the apparent density and the absolute solid density of the porous pellet in g/cm^3, then the porosity can be obtained from the following two expressions as quoted from Smith, 1970,

$$\varepsilon = \frac{\text{Pore volume of the porous pellet}}{\text{Total volume of the porous pellet}} = \frac{W_p V_g}{W_p V_g + W_p (1/\rho_s)} = \frac{V_g \rho_s}{V_g \rho_s + 1} \qquad (2.1)$$

$$\text{or,} \quad \varepsilon = \frac{\text{Pore volume}}{\text{Total volume}} = \frac{V_g}{1/\rho_p} = V_g \rho_p \qquad (2.2)$$

2.4 Pore size distribution

The distribution of pores according to sizes within the porous matrix of a catalyst is also an extremely important property. Without this information being known no prediction can be made of effective diffusion coefficients unless the diffusion process is entirely in the bulk mode which is unlikely for a commercial catalyst. Pores vary randomly in size and orientation throughout the cross section of the pellet. Hence with a pore size distribution, whether a particular diffusing species displays diffusion in bulk, Knudsen or transition mode can be defined and thus the diffusivity for that species can be predicted.

A catalyst is said to be monodispersed, or unimodal, if all the pores fall in a narrow band of sizes and bidispersed, or bimodal, if two peaks in the pore size distribution are observed (see figure 6.18 of Chapter 6). There are two established methods of determining pore size distribution.

2.4.1 Mercury penetration method

This method consists of measuring the pressure and the corresponding volume of mercury that is intruded or penetrated into a porous sample. This measurement provides the cumulative pore size distribution from which the differential distribution of the pores can be obtained (Dullien, 1969). The pore radius that can be studied by this method ranges from 200000 nm to 1.5 nm.

Irrespective of the angle of contact between a liquid and a solid, the pressure will be greater on the convex than on the concave side of the meniscus. An excess pressure will be required to force the liquid into a capillary within the solid. By a simple adaptation of the Young and Laplace equation (Gregg, 1967) one arrives at the following expression:

$$P = \frac{-2\gamma\cos\phi}{r} \qquad (2.3)$$

where r is the radius of the capillary and γ is the surface tension of mercury. Assuming the surface tension of mercury as 0.48 N/m and an average value of the wetting angle for mercury against typical solids as 140^{o}, the above expression will reduce to

$$r = \frac{7500}{P} \qquad (2.4)$$

where r is in nm and P is in atmospheres. Although the value r x P in the above expression is 7500, however, this varies from 6000 to 7500, depending on the choice of the contact angle (Satterfield, 1970).

It is obvious from the above expression that the lower the radius, the higher will be the pressure required for mercury intrusion. This trend can best be observed from the following table as obtained from a Micromeritics pore size distribution measurement (the contact angle used was 141.3^{o}):

Pressure, MN/m^2	Pore radius, nm
0.0345	2188.0
0.1013	7397.8
0.2040	3674.0
0.4205	1781.3
1.1304	662.6

2.4.2 Nitrogen desorption method

The BET surface area of a catalyst can be calculated from an adsorption isotherm obtained from a constant low temperature adsorption experiment. This experiment can be continued at higher pressures until the entire void region is filled with liquid nitrogen due to capillary condensation within the pores (Smith, 1970). Starting from this point the pressure can be decreased incrementally such that the evaporation of nitrogen begins. Proceeding in this manner, a desorption isotherm can be obtained. This can then be used to determine the pore size distribution of the porous material. An

Omnisorp size analyser can be used for both surface area and the pore size analysis measurements. By this method pore radii of between 0.4nm and 40 nm can be determined. Detailed descriptions of surface area, pore volume and pore size distribution measurements are available in Operator's manual, 1987, 1989; Satterfield, 1980; Smith, 1970; Gregg, 1967; Mukhlyonov, 1976 and Satterfield, 1970.

2.5 Measurements of the effective diffusion coefficients

Two well known methods for measuring the effective diffusion coefficients are (1) the diffusion cell method and (2) the dynamic pulse or chromatographic method. Vuuren, 1980; Cresswell, 1982 and Weisz, 1954 discuss the methods with their relative merits and drawbacks.

2.5.1 Diffusion cell method

This method was originally developed by Wicke and Kallenbach for steady state gas phase single pellet diffusion measurements and is the only true steady state method available (Vuuren, 1980). At present both steady and the unsteady state diffusivities can be measured by this method using a single pellet technique. A typical diffusion cell is shown in figure 2.1.

Constructing a diffusion cell as in the figure 2.1 is simple. Usually the cylindrical pellets are forced into a small piece of slightly under-sized silicone rubber tubing to ensure that there are no leaks around the curved surfaces of the pellet. Connecting the two ends of the tube to two purpose built gas distributors constructs the complete diffusion test cell.

This method offers the following advantages and disadvantages:-

Advantages

(1) Relatively simple to construct and

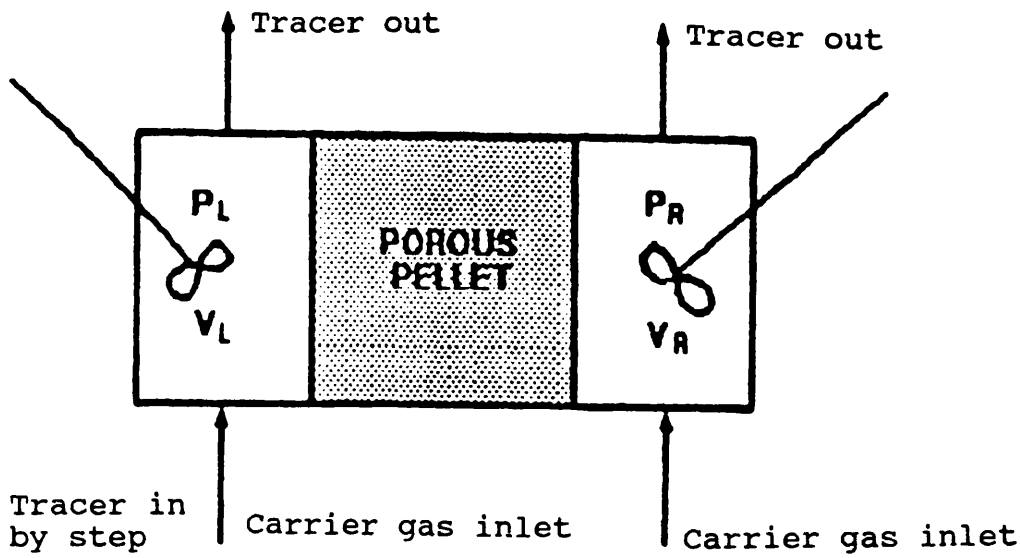

Figure 2.1. Wicke-Kallenbach type diffusion test cell.

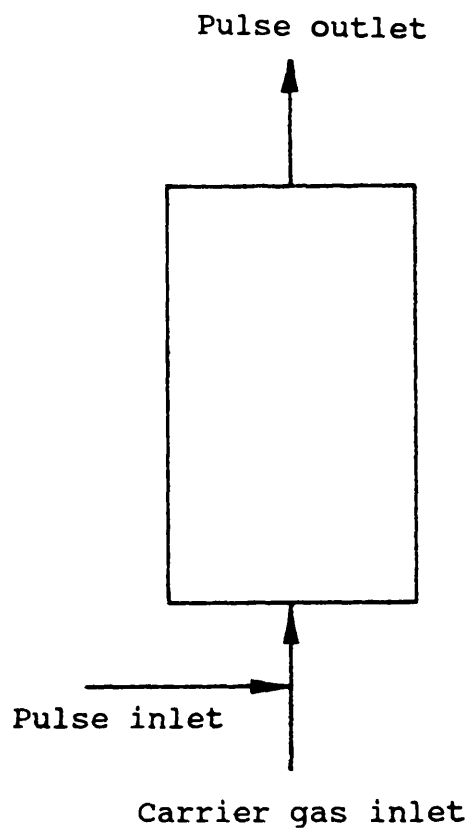

Figure 2.2. Dynamic pulse or chromatographic test apparatus.

measurement is quick.

(2) No dispersion effects.

(3) Both steady and unsteady state measurements can be performed from a single experimental run.

(4) Pellet anisotropy can be investigated (Vuuren, 1980) by reversing the arrangement of the diffusion test cell.

(5) Unsteady state diffusivities can be obtained from the first moment of the system impulse response.

(6) Using an appropriate correction factor, geometries other than the cylindrical can also be investigated (Waldram, 1985b).

(7) Variability between individual pellets can be studied.

Disadvantages

(1) Measures only axial diffusion coefficients.

(2) Sensitive to leakage because cracks may develop during forcing the pellet into the rubber tubing.

(3) Dead ended pores do not participate when the measurements are conducted at steady state.

(4) Limited to regular geometries.

2.5.2 The pulse or chromatographic method

A fixed bed consisting of many catalyst pellets or granules constitutes the pulse or chromatographic column as shown in figure 2.2. Initially a carrier gas is allowed to flow through the column at steady state and then a pulse of the diffusing gas is suddenly introduced into the carrier and both inlet and outlet responses are recorded as a function of time. The effective diffusion coefficient is obtained by analysing these response curves.

This method has gained popularity because of the following obvious reasons. First, any arbitrary shaped

particle can be investigated; second, the effect of dead ended pores, if present, can be investigated; and third, the experiments can be carried out at temperatures and pressures of the reacting vessel at which the actual catalyst is to be used.

Several disadvantages of this method are:-

(1) Axial dispersion effects within the void spaces of the chromatographic column are very significant.
(2) External mass transfer resistances can be present, i.e. the concentration is different between the bulk and external surfaces of catalyst.
(3) Interpretation of data is relatively difficult because the second moment i.e. the variance has to be determined. The model required to do this contains many unknown, or at best inaccurately known parameters.
(4) Pellet anisotropy as well as pellet to pellet variations of properties can not be investigated.

2.6 Determination of permeability

Permeabilities of porous material can be obtained using the Wicke Kallenbach diffusion apparatus and the test cell. Two methods, viz. the differential and the integral, may be adopted to evaluate the permeability constant B_o. A flow of a gas, say nitrogen, is passed through one gas distributor and this flow is balanced by an opposing flow through the other gas distributor so as to make the two chamber pressures equal (see figure 2.1 and also figure 5.3 of Chapter 5). Then keeping one flow constant and varying the other, the volumetric flow rate that permeates through the porous pellet can be obtained from the calibrated rotameters. When the catalyst is relatively impermeable or when the system pressure is low, not much gas will penetrate through the sample and a gas bubble meter rather than a rotameter may be used

to measure the volumetric flow through the pellet.

Either of the following methods can then be used to evaluate the permeability constant B_o.

2.6.1 Differential method

The volumetric flux due to a pressure gradient across the porous medium is given by

$$q_p = - \frac{B_o P \ A \ dP}{\mu RT \ \rho \ dz} \qquad (2.5)$$

$$= - \frac{B_o P \ A \ \Delta P}{\mu RT \ \rho \ L} \qquad (2.6)$$

A plot of q_p versus ΔP will have a

$$\text{Slope} = - \frac{B_o PA}{\mu RT \rho L}$$

$$\text{or, } B_o = \frac{(- \text{ slope}) \times \mu RT \rho L}{PA} \qquad (2.7)$$

Hence B_o can be calculated from equation (2.7). The slope is obtained from a least squares best fit line through a selection of data. In general this line displays gentle curvature but the slope at $\Delta P = 0$ may be evaluated directly from the equation of the least squares fit. This method is suitable for highly permeable catalysts and only one permeability constant is obtained.

2.6.2 Integral method

In equation (2.5), the terms B_o, RT and A are constants. The density, ρ, is not constant but $q_p \times \rho$ which represents a mass flux, is constant. The remaining term, μ, that is, the viscosity is only a weak function of P (Bird et al, 1960). Under this circumstance,

equation (2.5) can be integrated directly to obtain the following expression for B_o

$$B_o = \frac{2\mu RT\ \rho L q_p}{A(P_1^2 - P_2^2)} \qquad (2.8)$$

Since a value of B_o is obtained from each set of data, the overall pellet permeability will be the average of each value determined for a given applied pressures P_1 and P_2. This method can be adopted for both low and high permeability catalysts.

2.7 Introduction to mechanical strength of catalysts

The mechanical strength of materials such as pelleted catalysts, like diffusion and other physical parameters, is an important characteristic which must be considered at some stages of catalyst production for quality control, durability and life while in use in reactors. Pellet porosity, length to diameter ratio (Leach, 1983) and the variables involved during processing for production can each have a profound effect on the strength of the pellet. For example, too high a porosity, extra high calcination temperature, chemical reduction and high length to diameter ratio significantly reduce the crushing and/or tensile strength of the pellet. Optimal choice of those parameters is always necessary in order to retain substantial strength of the pellet.

Catalysts do crush and break during shipment and while loading into reactors. Moreover, chemical attack (catalyst deactivation) and thermal shock (Satterfield, 1980) can also lead to substantial reduction in pellet strength. As a result fracturing may occur and fines accumulate thereby creating excessive pressure drops across the reactors. Thus it is necessary to determine

the pellet strength required to reduce catalyst breakage to such a low level that excessive pressure drops can not develop during the catalyst life time.

Mechanical strength tests can be grouped into static and dynamic tests (Mukhlyonov, 1976). Static tests are used for tension, compression, shear etc. while dynamic tests are conducted for resilience, durability, creep etc. Materials can also be tested for hardness, wear and abrasion.

During static tests loads are gradually applied to the specimen until its destruction and during dynamic tests shock loads are applied to the specimen and only the overall work of deformation of the specimen is determined. Wear and abrasion tests are made to ascertain the behaviour of surface layers of materials after long action of friction (Mukhlyonov, 1976). As the details of these tests are beyond the scope of this work, only static tensile tests will be described.

2.7.1 Determination of pellet tensile strength

To date, catalyst tensile strength has not been studied in great detail by any potential catalyst manufacturer. The present need for this determination is due largely to commercial reasons. A good quality catalyst produced by any manufacturer must be robust i.e. resistant to breakage and attrition and able to withstand sharp thermal shock and high pressures. To ascertain whether these characteristics are indeed present in a sample is difficult and tedious but the quantitative determination of the catalyst's tensile strength is a good indicator of these properties and is relatively straight forward.

When a cylindrical catalyst particle is loaded across its diameter it will fail in a tensile mode and ideally will split into two halves along its centre line. This type of failure usually occurs at loads well

below those which would cause crushing failure and is a better indicator of catalyst "robustness" than the pure compressive strength. It is then vital to quantify this tensile strength rather than the crush strength. If this information was quoted during marketing of catalysts by any manufacturer, then this would enable a potential catalyst buyer to discriminate between rival products (Waldram et al, 1990).

The magnitude of this tensile strength can be determined by a static tensile load test as already outlined. This test for a porous compact is accomplished by compressing the test specimen gradually and smoothly across its diameter (diametrical compression). Under the condition of ideal line loading the pellet will break in tensile mode across its diameter, figure, 2.4. Perfect line loading can never be achieved in practice but a good approximation to it is possible. The test was devised originally by two Brazilian civil engineers, F.L.L.B Carneiro and A. Barcellos, during their investigation with concrete (Carneiro, 1953) and is widely known as the "Brazilian test" or "indirect tensile test" because it obtains a tensile fracture stress from a pure compressive loading. The important characteristic of this method is that a uniform tensile stress is developed normal to and along the load diameter (the diameter joining the point of application of the two loads). This uniform tensile stress (Fell, 1970; Pitt, 1988), σ_x, is given by

$$\sigma_x = \frac{2P_L}{\pi D_s T_s} \qquad (2.9)$$

where P_L is the applied load, D_s is the diameter of the specimen and T_s is the thickness. Using equation (2.9), the tensile strength of the pellet can readily be determined (Pitt, 1988): this is reported in MN/m^2.

The mechanism of failure of material when

subjected to load is dependent on testing conditions, e.g., temperature, strain rate etc. Materials subjected to low strain rate may fail in a ductile manner because of excessive deformation while the same material subjected to a high strain rate may fail in a brittle manner with less deformation (Newton, 1970).

Rudnick et al (Rudnick, 1963) reported three types of specimen failure for crystalline lactose and spray dried lactose from experimental observations. The first is the failure due to compression and/or shear where the specimen fractures irregularly into several fragments; normal tensile failure where the specimen splits into two portions along its diameter and triple cleft failure where the specimen breaks symmetrically about the loaded diameter into six pieces. These three types of failure are illustrated in figure 2.3 for tablets subjected to diametral compression (Rudnick, 1963).

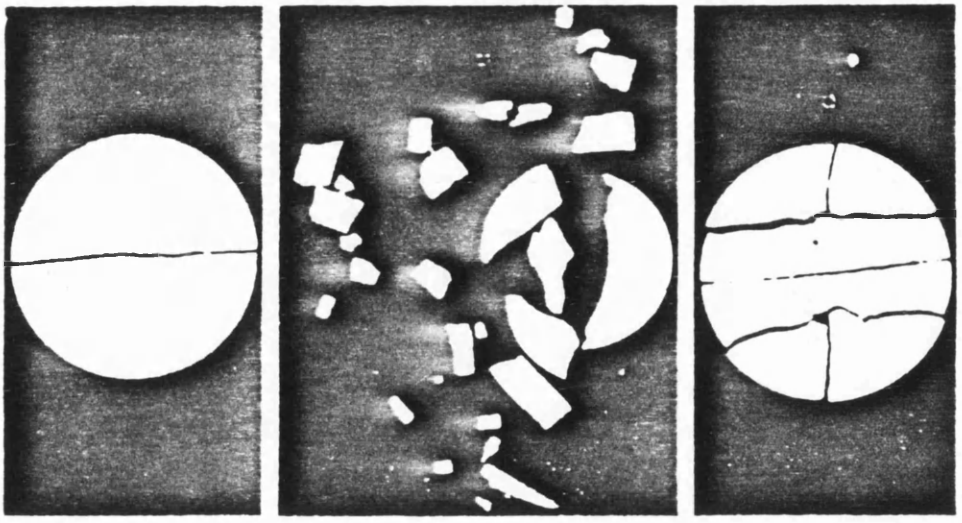

(A) (B) (C)

Figure 2.3. Three types of failure for crystalline and spray dried lactose: (A) Normal tensile failure; (B) Shear and compression failure; and (C) Tensile failure using padding material (quoted from Fell and Newton,1970).

All tensile experiments for ICI $Cu/Zn/Al_2O_3$ pellets have been carried out at the School of Pharmacy of the University of London using a CT 40 machine designed by Systems Engineering Nottingham. A maximum of 40 kg load can be applied by this machine. The procedure of the test is rather simple and involves placing the pellet diametrically on the platten under the condition of ideal line loading as shown in figure 2.4. The load is then applied at a constant rate of 1 mm/min until the failure occurs. The failure load is then recorded either from the digital readout of the machine, which retains the reading of the load at the time of failure, or from the chart recorder.

For each sample a minimum of 15 tensile tests have been performed and the mean and standard deviation at the 95% confidence level have been calculated.

2.7.2 Variability in the strength of powder compacts

The mechanical strength of a single catalyst pellet is not only dependent on the pellet porosity, length to diameter ratio and pellet processing conditions as mentioned earlier but is dependent also on the component materials from which it is made and on the pouring characteristics of powders or granules into the die of the final pelleting machine. For example, some materials may possess an adhesive nature while some may display a lower friction between primary particles (e.g., the lubricants that are added: graphite, stearic acid etc.). Due to this inherent variability in properties, pellets produced with a given machine setting will to some extent vary in size and density and thus exhibit different properties including tensile strength. In studying pellet strength and strength variability it is therefore necessary to consider the factors which determine these characteristics (Kennerley, 1979).

These variations in tensile strength can

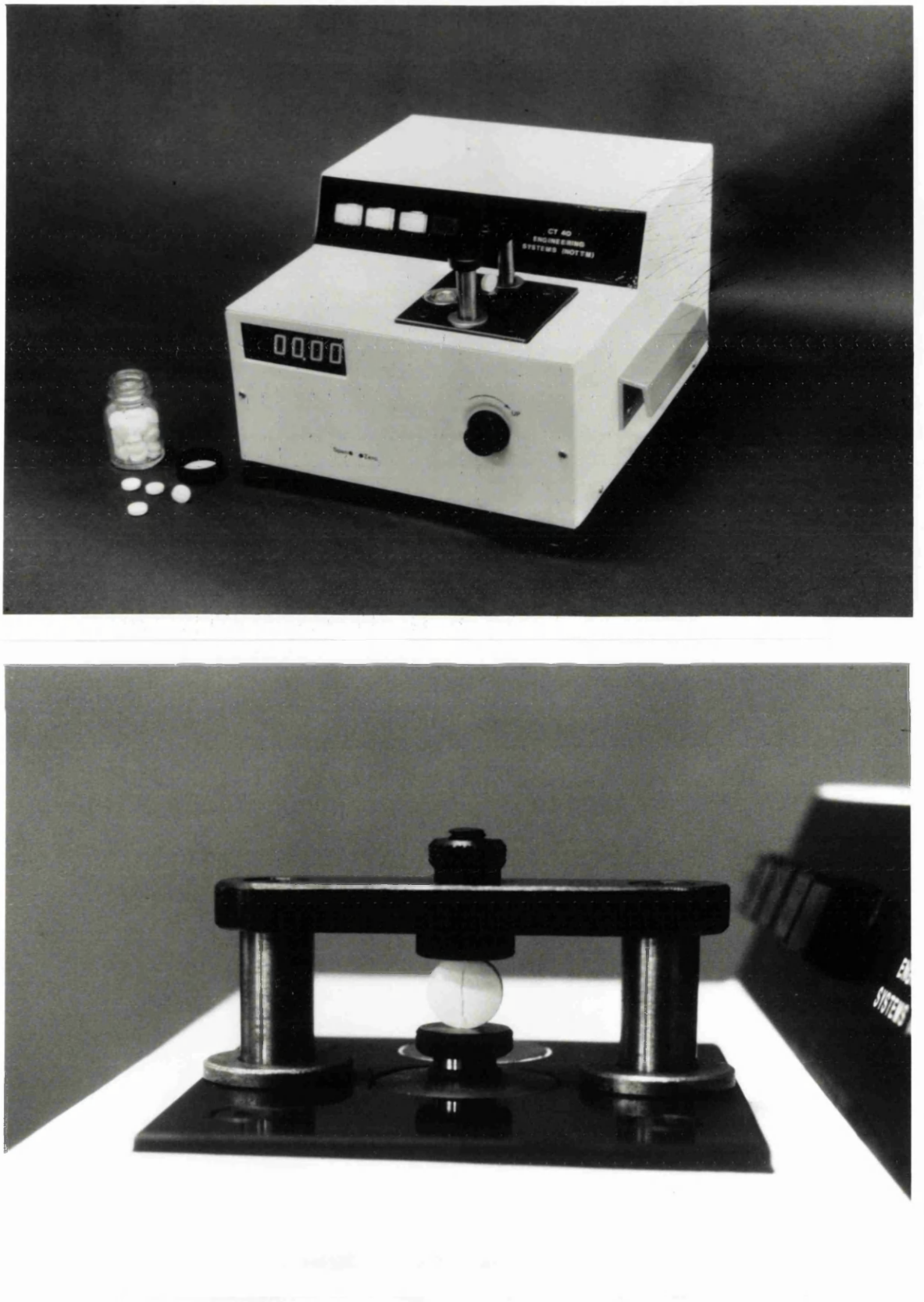

Figure 2.4. Photograph of CT 40 load tester showing tensile failure by diametral compression.

satisfactorily be represented in terms of the two parameter Weibull distribution (Kennerley, 1979; Stanley, 1977) as given below:-

$$P_f = 1 - \exp \{ - (\frac{1}{m}!)^m (\frac{\sigma_f}{\bar{\sigma}_f})^m \} \quad (2.10)$$

The two parameters are (i) the mean tensile fracture stress of the specimen tested ($\bar{\sigma}_f$) and (ii) the Weibull modulus (m), which is a reciprocal measure of the variability of the fracture stresses about the mean value and (1/m!) is the factorial function of (1/m) which is available in Abramowitz, 1970.

The quantity m is in fact a measure of brittleness. This brittleness in fractured materials is governed by the flaw distribution within those materials and variability in the tensile strengths of a set of nominally identical test specimens is a direct consequence of the random nature of this distribution. The Weibull modulus, m, should be constant for different selections of samples of a given material provided a statistically significant sample size has been selected. For materials produced under different processing conditions one would anticipate potential variations in brittleness, and hence in the value of m (Stanley, 1977).

CHAPTER - 3

CATALYST PRODUCTION AND PREPARATION OF SAMPLES

3.1 Introduction

There are two broad methods for producing commercial pelleted catalysts, viz. the co-precipitation method and the impregnation method. The method adopted for a particular catalyst to be prepared, depends upon the type of reaction (diffusion or reaction rate limited), the principal constituents of the catalyst mass and their comparative costs, and finally the requirements of surface area, porosity and activity. For example, a reaction which is likely to be diffusion limited requires permeable catalysts to facilitate easy movement of molecules within the pores of the catalyst. Again if the cost of the principal active component is high, as in the case of platinum group metals, nickel and silver, the active component is often dispersed on a carrier and the usual choice is the impregnation method of preparation. One advantage of this impregnation method is that a suitable pore size can be defined by producing the support material in a defined form. Also the impregnation route requires fewer unit operations than that of the precipitation method. However, in the case of preformed carriers, such as pellets, spheres or granules, attention must be paid to the distribution of the active ingredient achieved during impregnation. For example, a diffusion limited reaction may require the active phase to be on the outer surface of the catalyst alone. If the active component of the catalyst is inexpensive and whenever a high surface area catalyst is required (as in the case of LT shift catalyst) the co-precipitation method is usually employed. Other methods of preparation are specific for a particular type of catalyst production. For example, multipromoted iron catalyst for ammonia synthesis is prepared by the method of fusion and in this case it is the subsequent activation process which creates the porous network.

As $Cu/Zn/Al_2O_3$ LT shift catalyst is prepared by the co-precipitation route, the details of this method will be considered here.

3.2 Co-precipitation method

The method is based on separate dissolution of solid parent compounds into appropriate solutions which are then mixed so as to undergo a double decomposition reaction to produce a precipitated mass.

The main variables that influence the precipitation and size of particles of the precipitate are temperature, stirring and micromixing rate and order of addition of any precipitating agents, ionic concentration of parent solutions, pH, aging time and conditions. For high surface area fine particles are necessary although filtration of these may be difficult. If this is the case then lower temperature, higher stirring rate and shorter aging times should be adopted (Leach, 1984).

One great problem is that if two or more metal compounds are present as in the case of the LT shift catalyst, they may precipitate at different rates or in sequence rather than simultaneously thus affecting the final structure of the solid (Satterfield, 1980); homogeneity, in the case of two or more mixed metals, is very important.

The preparation of $Cu/Zn/Al_2O_3$ co-precipitated catalysts requires a series combination of simple unit operations. The entire batch preparation can best be represented by a simple flow diagram as shown in figure 3.1.

The starting point is the dissolution of Cu and Zn metals in concentrated nitric acid in separate tanks to form copper nitrate and zinc nitrate solutions. Alumina is dissolved with sodium hydroxide solution in

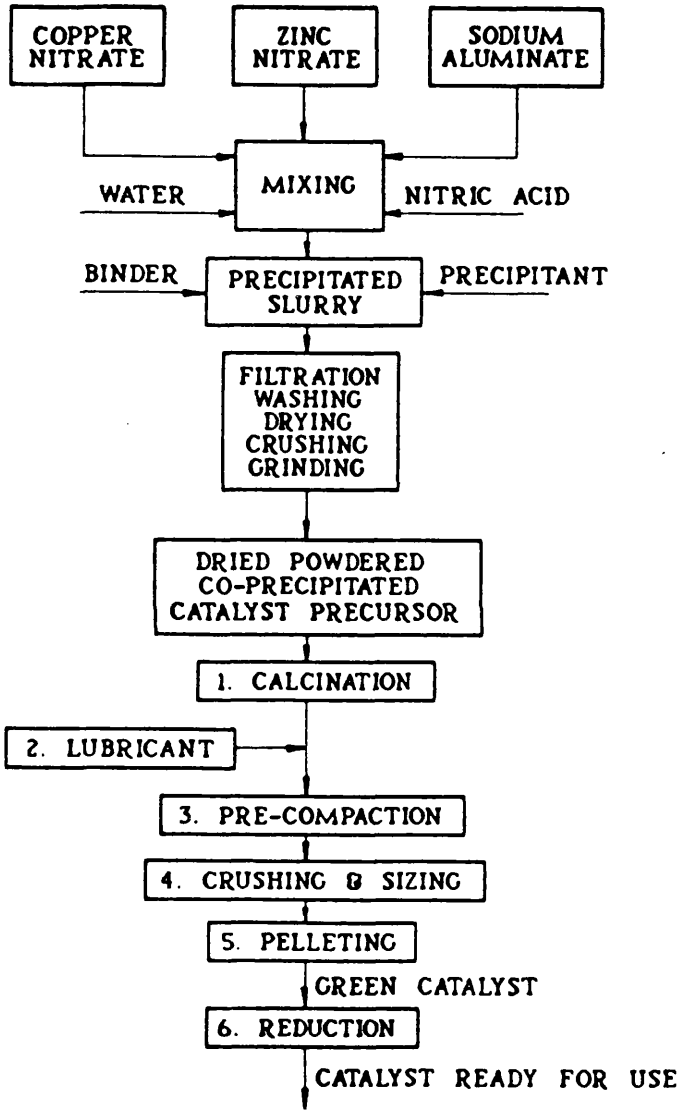

Figure 3.1. Production route for ICI 52-8 LT shift catalyst.

another tank to form sodium aluminate. These three solutions are mixed together in a tank to which a constant flow of hot water is maintained. A precipitant is added to obtain the slurry precipitate. After aging and/or conditioning, this slurry is then passed to a rotary drum filter to form the filter cake of the mixed metals. Successive washing, drying, crushing and grinding convert the filter cake into a powder which is then dried.

The dried powder is calcined and precompacted. The compacted mass is then broken down and sieved into a specific size range and graphite is added as a lubricant and admixed thoroughly for uniformity of distribution. This material is then sent for pelletizing. This is carried out using Manesty pelleting machines at ICI. The density of each pellet, i.e. the volume of powdered catalyst flowing to each die on the machine, is adjusted so that when compacted into a defined final volume a pellet of defined specification results. The product then is drummed and packed.

3.3 Preparation of Samples

All samples for this research have been prepared at ICI's Billingham Catalysis Research Centre under carefully controlled conditions using dried powder taken from a normal production run at the Clitheroe catalyst factory as the starting material. During preparation five production parameters have been varied each at their low, normal, high and, in some cases, extra high level. These five are: pre-compaction load, calcination temperature, particle cut size, amount of lubricant and the final pelleting density respectively. The specification of these production parameters at their low, normal, high and extra high level is represented in table 3.1.

In the first instance 41 batches of catalyst were prepared of which 28 were "green" and 13 were

	Low	Normal	High	Extra High
	L	N	H	EH
Calcination temperature (°C)	250	350	450	700
Addition of lubricant (wt%)	1	2	3	4
Pre-compaction load (tons)	8	10	12	16
Primary particle cut size (micron)	T: 295 B: 120	T: 1003 B: 251	T: 1500 B: 295	T: 2057 B: 355
Pelleting density (g/cm^3)	1.5	2	2.5	3

Note: T = top sieve; B = bottom sieve

Table 3.1. Specification of five production parameters at their low, normal, high and extra high levels considered during preparation of test samples.

"prereduced." Green catalysts are finished pelleted products obtained from a catalyst manufacturing plant which have not been employed for any production purposes. When such green catalysts are activated by reduction these are then called reduced or prereduced catalysts. These are shown in table 3.2.

During the second and final phases of work 44 further batches of samples were made. 22 of these were green and the remaining 22 were the corresponding product after reduction and stabilization. These are specified in table 3.3.

3.4 Reduction and stabilization of green catalyst

$Cu/Zn/Al_2O_3$ catalyst must be activated by reduction before being put into operation. This can be

Table 3.2. Specification of first batch of catalyst samples. Samples S-1 to S-28 are "green" and samples S-29 to S-41 are "reduced".

Sample No:	Addition of lubricant (wt%)	Precompaction load (tons)	Calcination temperature (°C)	Cut Size (microns)	Pelleting density (g/cm^3)
S-1	N	N	N	N	N
S-2	L	N	N	N	N
S-3	H	N	N	N	N
S-4	N	L	N	N	N
S-5	L	L	N	N	N
S-6	H	L	N	N	N
S-7	N	H	N	N	N
S-8	L	H	N	N	N
S-9	H	H	N	N	N
S-10	N	N	H	N	N
S-11	L	N	H	N	N
S-12	H	N	H	N	N
S-13	N	H	H	N	N
S-14	L	H	H	N	N
S-15	H	H	H	N	N

Table 3.2 continued

Sample No:	Addition of lubricant (wt%)	Precompaction load (tons)	Calcination temperature (°C)	Cut Size (microns)	Pelleting density (g/cm^3)
S-16	N	L	H	N	N
S-17	L	L	H	N	N
S-18	H	L	H	N	N
S-19	N	N	L	N	N
S-20	N	N	N	L	N
S-21	N	N	N	H	N
S-22	N	N	N	N	L
S-23	N	N	N	N	H
S-24	N	N	EH	N	N
S-25	EH	N	N	N	N
S-26	N	EH	N	N	N
S-27	N	N	N	EH	N
S-28	N	N	N	N	EH

NOTE:

S-29	is	the	reduction	of	S-1	S-35	"	"	"	"	S-16
S-30	"	"	"	"	S-4	S-36	"	"	"	"	S-21
S-31	"	"	"	"	S-9	S-37	"	"	"	"	S-22
S-32	"	"	"	"	S-11	S-38	"	"	"	"	S-23
S-33	"	"	"	"	S-12	S-39	"	"	"	"	S-26
S-34	"	"	"	"	S-13	S-40	"	"	"	"	S-27
						S-41	"	"	"	"	S-28

Table 3.3. Specification of second and final batch of catalyst samples. Samples S-42 to S-63 are "green" and samples S-64 to S-85 are "reduced".

Sample No:	Addition of lubricant (wt%)	Precompaction load (tons)	Calcination Temperature (°C)	Cut Size (microns)	Pelleting density (g/cm^3)
S-42	N	N	N	L	L
S-43	N	N	N	H	L
S-44	N	N	N	EH	L
S-45	N	N	N	L	H
S-46	N	N	N	H	H
S-47	N	N	N	EH	H
S-48	N	N	N	L	EH
S-49	N	N	N	H	EH
S-50	N	N	N	EH	EH
S-51	N	N	200°C	N	N
S-52	N	N	L	N	L
S-53	N	N	L	N	H
S-54	N	N	L	L	N
S-55	N	N	L	H	N
S-56	N	N	L	EH	N
S-57	N	N	H	N	H
S-58	N	N	H	L	N
S-59	N	N	H	H	N
S-60	N	N	H	EH	N
S-61	N	N	H	N	L
S-62	N	N	500°C	N	N
S-63	N	N	600°C	N	N

Samples S-64 to S-85 are the reduction of samples S-42 to S-63 in the same order, e.g., S-64 is the reduction of S-42; S-65 is the reduction of S-43 and so on.

done on a once through or recycle basis (ICI Catalyst Manual) either after loading into the reactors or before delivery by the manufacturer. At Billingham Catalysis Research Centre the following procedure was adopted for sample reduction. The sample to be reduced was placed into a glass cylindrical, vertical, reactor column of approximately 15 cm diameter. A flow of a mixture containing 95 volume% N_2 and 5 volume% H_2 was then passed through the reactor. The reactor temperature was gradually increased to 250 ^{o}C. The completion of the reduction process was confirmed from the inlet and the outlet gas concentration analysis which eventually became essentially identical.

About 20 pellets from each sample were taken for the reduction. The equipment was capable of reducing about 15 different samples at a time. Normally 10 to 12 hours are required for reduction.

The question of stabilization of the reduced catalyst arises when the catalyst is shipped to other places. This involves forming a monolayer of oxide on the outer surface of the catalyst particle. Again at Billingham this was performed in the following manner. On completion of reduction the reactor was cooled to the ambient temperature keeping the previous N_2 and H_2 flow. A flow of compressed gas containing 0.5 volume% O_2 was introduced. When the outlet O_2 concentration was observed to reach the inlet value, the flow of compressed O_2 was increased to give a level of 1 volume% O_2. This procedure was continued for 1.5 volume%, 2 volume% and 2.5 volume% inlet $\%O_2$ concentrations respectively. The N_2 flow was then decreased to 50% of its initial value and after 30 minutes it was stopped completely. After waiting for another 30 minutes the catalyst was finally taken out from the stabilizer.

CHAPTER - 4

MATHEMATICAL MODELLING OF DIFFUSION AND PERMEABILITY

4.1 Introduction to mathematical modelling

Mathematical modelling is one of the most complex parts of any research. The reason is that it is fairly difficult to describe a real process in mathematic terms without a thorough understanding of the process. Even with a thorough understanding of the physics of a process, simplifying assumptions often have to be made so as to generate a mathematically tractible model.

Depending on the degree of complexity of the process, the final form of a model can be of steady state (independent of time) ordinary differential type or it can be of unsteady state (dependent on time) partial (more than one independent variable) differential type. The resultant model can then be solved using an appropriate set of boundary and initial conditions either numerically (Smith,1985; Jenson, 1977; Finlayson, 1980) or analytically (Crank, 1975; Burghardt, 1979). The degree of complexity of the solution of the model depends upon the type, order and the extent of nonlinearity within the model.

In this thesis, a dynamic, non-isobaric, isothermal model describing combined diffusion and flow within a single cylindrical catalyst pellet has been developed for a binary gas system subject to particular assumptions. Of these, one of the most important is that the diffusive flux and the viscous or convective flux are additive. The expression for the diffusive flux takes into account the composition dependency of both bulk and Knudsen diffusion coefficients (Evans, 1961; Smith 1970) and has been described with a Fickian type expression. The viscous flux has been expressed with a D'arcy type equation (Jackson, 1977). The model is flexible in the

sense that the viscous flux term can be included into it or it can be excluded from the model to treat it as either an isobaric or a non-isobaric model. At low gas concentrations, the viscosity term appearing in the D'arcy term of the model equations is dependent on composition (Bird, 1960). An expression showing this dependency is provided in section 4.2.

The non-isobaric model which has been developed was solved numerically using the Crank-Nicolson finite difference technique. For large pores, the model predictions become essentially identical to those of an isobaric model. Model equations of this type were solved using both a numerical method and the moments method. This chapter thus concentrates on the development and solution of both isobaric and non-isobaric models of diffusion.

4.2 One dimensional model of diffusion and permeability

The following one dimensional, non-isobaric isothermal model of diffusion has been developed for gases A and B with diffusion taking place in a porous pellet housed in Wicke-Kallenbach type single pellet diffusion test cell (see Appendix 1). Two assumptions considered during its development were:

(1) The porous medium was isotropic;

(2) There was no adsorption of species A on the porous structure.

The mass balance equation for species A within the porous pellet (see Appendix 1 for detailed derivation) i.e. within the bound $0<x<L$ is:

$$\frac{\partial}{\partial x}\left(D_{Ae}\frac{\partial}{\partial x}\left(P_T x_A\right)\right) + B_0\frac{\partial}{\partial x}\left(\frac{P_T x_A}{\mu_m}\frac{\partial P_T}{\partial x}\right) = \varepsilon\frac{\partial}{\partial x}\left(P_T x_A\right) \qquad (4.1)$$

The overall mass balance equation (for species A and B) within the porous pellet over the same bounds is given by equation (4.2).

$$\frac{\partial}{\partial x}\left[\left(D_{Ae} - D_{Be}\right)\frac{\partial}{\partial x}\left(P_T x_A\right)\right] + \frac{\partial}{\partial x}\left(D_{Be}\frac{\partial P_T}{\partial x}\right) + B_0\frac{\partial}{\partial x}\left(\frac{P_T}{\mu_m}\frac{\partial P_T}{\partial x}\right) = \varepsilon\frac{\partial P_T}{\partial t} \qquad (4.2)$$

Two end chamber balance equations were written: these also involved assumptions:

(1) There was no mass transfer resistance at the gas solid interface; and

(2) Chamber volumes V_1 and V_2 were perfectly mixed.

The left hand side chamber mass balance equation is:

$$q_{1in}x_{A1in}P_T - q_{1out}x_{A1out}P_T + AD_{Ae}\frac{\partial}{\partial x}\left(P_T x_A\right)\Big|_{x=0} + A\frac{B_0}{\mu_m}\left(P_T x_A\frac{\partial P_T}{\partial x}\right)\Big|_{x=0} = V_1\frac{d}{dt}\left(P_T x_{A1out}\right) \qquad (4.3)$$

whilst the corresponding equation for the right hand chamber is:

$$q_{2in}x_{A2in}P_T - q_{2out}x_{A2out}P_T - AD_{Ae}\frac{\partial}{\partial x}\left(P_T x_A\right)\Big|_{x=L} - A\frac{B_0}{\mu_m}\left(P_T x_A\frac{\partial P_T}{\partial x}\right)\Big|_{x=L} = V_2\frac{d}{dt}\left(P_T x_{A2out}\right) \qquad (4.4)$$

where

D_{Ae} = Effective diffusivity of A, m^2/s and defined by

$$= \frac{1}{\frac{1 - \alpha_{AB}x_A}{D_{ABe}} + \frac{1}{D_{KAe}}} = \frac{D_{ABe}D_{KAe}}{\left(1 - \alpha_{AB}x_A\right)D_{KAe} + D_{ABe}}$$

D_{Be} = Effective diffusivity of B, m^2/s and defined by

$$= \frac{1}{\frac{1 - \alpha_{BA} x_B}{D_{ABe}} + \frac{1}{D_{KBe}}} = \frac{D_{ABe} D_{KBe}}{(1 - \alpha_{BA} x_B) D_{KBe} + D_{ABe}}$$

$$\alpha_{AB} = 1 - \sqrt{\frac{M_A}{M_B}} \qquad \alpha_{BA} = 1 - \sqrt{\frac{M_B}{M_A}}$$

and

$$\mu_m = (1.78 + 0.46\ x_A) \times 10^{-5}\ Ns/m^2$$

The following four boundary conditions have been used in conjunction with equations (4.1) and (4.2). In addition, the initial condition was that at t=0, the mole fraction of tracer (gas A, e.g., helium) at all points within the pellet is 0.

(1) The mole fraction of the tracer species at both the left hand side and right hand side chamber outlet is equal to the mole fraction of the tracer at the gas solid-interface, i.e. $x_{A1out} = x_A\big|_{x=0}$ and $x_{A2out} = x_A\big|_{x=L}$ for all values of t.

(2) The left hand side chamber pressure P_1 and the right hand side chamber pressure P_2 are constant and equal, i.e. $P_1 = P_2 = P_T$ for all time t.

(3) Equation (4.3) may be rearranged to make $\frac{\partial P_T}{\partial x}$ and $\frac{\partial}{\partial x}(P_T x_A)$ the subject of the equation.

(4) Equation (4.4) can be rearranged in an analogous manner.

(5) The mole fraction, x_A, of the tracer within the pellet from x=0 to x=L, is 0, for time t=0.

4.3 Solution for the isobaric case

If the system is isobaric there would be no pressure gradient within the porous particle i.e. $P_1 = P_2 = P_T$. This also implies that the relative molecular masses of species A and B must be equal so that D_{Ae} and D_{Be} are equal. Applying these two conditions to equations (4.1) and (4.2) of section 4.2, the following isobaric equation was obtained:

$$D_e \frac{\partial^2 c_A}{\partial x^2} = \varepsilon \frac{\partial c_A}{\partial t} \qquad (4.5)$$

Equation (4.5) has been formulated in terms of concentration c_A of the tracer species rather than as x_A. As the pressure is constant in this case, hence for simplicity (P_T x_A) of equation (4.1) has been expressed as c_A. This was solved again with the same initial conditions but with a set of four slightly different boundary conditions (see Appendix 3) as described below:

(1) The concentration of tracer at the left hand side and right hand side chamber outlets is equal to the concentration of tracer at the gas-solid interface, i.e. $c_L = c_A\big|_{x=0}$ and $c_R = c_A\big|_{x=L}$.

$$(2)\ q_L C_{in} - q_L C_L + AD_e \left(\frac{\partial C_L}{\partial x} \right)\Bigg|_{x=0} = V_L \frac{dC_L}{dt} \qquad (4.6)$$

$$(3)\ -q_R C_R - AD_e \left(\frac{\partial C_R}{\partial x} \right)\Bigg|_{x=L} = V_R \frac{dC_R}{dt} \qquad (4.7)$$

(4) The concentration of tracer i.e. c_A within the pellet from x=0 to x=L is 0, for time t=0.

4.3.1 Moments method

If a dirac delta function of tracer were introduced in the inlet stream to the left hand chamber,

then closed pulses of tracer would be observed in the outlets from each chamber.The zeroth and first moments of the transient tracer concentration from the left hand chamber are given by the following two equations (see Appendix 2 for the full derivation):

$$\alpha_0 = \frac{1 + K_1 + K_2}{1 + K_2} \qquad (4.8)$$

$$\frac{\alpha_1}{\alpha_0} = \frac{3K_1K_2K_3(1 + K_2) + 3T_1(1 + K_2)^2 + K_1(3T_2K_2 + K_3)}{3(1 + K_1 + K_2)(1 + K_2)} \qquad (4.9)$$

Likewise the right hand side zeroth and first moments are given by the following two expressions:

$$\alpha_0 = \frac{1 + K_1 + K_2}{K_2} \qquad (4.10)$$

$$\frac{\alpha_1}{\alpha_0} = \frac{6K_1K_2K_3 + 6T_1(1 + K_2) + 6T_2(1 + K_1) + \left\{3(K_1 + K_2) + 1\right\}K_3}{6(1 + K_1 + K_2)} \qquad (4.11)$$

where

$$T_1 = \frac{V_1}{q_1} \; ; \; T_2 = \frac{V_2}{q_2} \; ; \; K_1 = \frac{AD_e}{Lq_1}$$

$$K_2 = \frac{AD_e}{Lq_2} \; ; \; K_3 = \frac{L^2\varepsilon}{D_e}$$

4.3.2 Numerical solution of the isobaric model

Equation (4.5) was also solved numerically in conjunction with equations (4.6) and (4.7). Using the Crank-Nicolson numerical technique these three equations were written in finite difference form. Each of these equations are described below.

At x = 0, the equation is:

$$2u_1^* - \left(2 + \frac{1 + A_2}{A_3} + \frac{1}{A_4}\right)u_0^* = \left(2 - \frac{1 - A_2}{A_3} - \frac{1}{A_4}\right)u_0 - 2u_1 - \frac{A_1}{A_3} \qquad (4.12)$$

At 0<x<L, the equation is:

$$u_i^* - u_i = A_4(u_{i-1} + u_{i-1}^*) + A_4(u_{i+1}^* + u_{i+1} - 2u_i^* - 2u_i) \qquad (4.13)$$

At x = L, the equation is:

$$2u_{n-1}^* - \left(\frac{A_5}{A_6} + 2 + \frac{1}{A_4} + \frac{1}{A_6}\right)u_n^* = \left(2 - \frac{1}{A_4} - \frac{1}{A_6} + \frac{A_5}{A_6}\right)u_n - 2u_{n-1} \qquad (4.14)$$

Equation (4.12) at x=0 was achieved by eliminating u_{-1} and u^*_{-1} terms from the numerically formulated equations of (4.5) and (4.6); while equation (4.14) at x=L was derived from the numerical formulation of equations (4.5) and (4.7) and then eliminating terms like u_{n+1} and u^*_{n+1}. The pellet was divided into 9 equal segments and equation (4.13) was then written for each segment. Thus a total of 10 simultaneous linear equations was obtained. These were written in matrix form and solved by a Fortran program using the Nag F04ATF Fortran library routine. Full numerical analysis is available in Appendix 3.

4.4 Numerical solution of the non-isobaric model

Solution of the non-isobaric model was fairly complicated. This was for a number of obvious reasons: (1) there were two unknowns in the model, viz. x_A and P_T;

(2) D_{Ae} and D_{Be} were expressed in terms of x_A and thus equations (4.1) and (4.2) were non-linear and (3) the viscosity term as it appeared in the D'arcy equation was initially expressed in terms of the mole fraction of tracer gas A (see Appendix 1).

However this dependency of viscosity on mole fraction was not taken into account. This was further justified by the fact that the binary pair used for experimental purposes was N_2 and He with respective viscosities of 1.80×10^{-5} and 1.99×10^{-5} Ns/m^2 thus displaying a variation of only about 10%. Hence an average value of 1.895×10^{-5} Ns/m^2 was used when solving the model equations.

Thus equations (4.1), (4.2), (4.3) and (4.4) became independent of the viscosity and were written in Crank-Nicolson finite difference numerical form. The corresponding numerical equations were represented by equations (4.15), (4.16), (4.17) and (4.18) respectively as provided below which were still in the non-linear form.

$$
\begin{aligned}
& c_1\left(D^*_{Ai+1} + D^*_{Ai}\right)\left(u^*_{i+1} - u^*_i\right) - c_1\left(D^*_{Ai} + D^*_{Ai-1}\right)\left(u^*_i - u^*_{i-1}\right) \\
& + c_1\left(D_{Ai+1} + D_{Ai}\right)\left(u_{i+1} - u_i\right) - c_1\left(D_{Ai} + D_{Ai-1}\right)\left(u_i - u_{i-1}\right) \\
& + c_2\left(u^*_{i+1} + u^*_i\right)\left(u^*_{i+1} - u^*_i + v^*_{i+1} - v^*_i\right) - c_2\left(u^*_i + u^*_{i-1}\right)\left(u^*_i - u^*_{i-1} + v^*_i - v^*_{i-1}\right) \\
& + c_2\left(u_{i+1} + u_i\right)\left(u_{i+1} - u_i + v_{i+1} - v_i\right) - c_2\left(u_i + u_{i-1}\right)\left(u_i - u_{i-1} + v_i - v_{i-1}\right) \\
& - u^*_i + u_i = 0 \qquad (4.15)
\end{aligned}
$$

$$c_1\left(D^*_{Bi+1} + D^*_{Bi}\right)\left(v^*_{i+1} - v^*_i\right) - c_1\left(D^*_{Bi} + D^*_{Bi-1}\right)\left(v^*_i - v^*_{i-1}\right)$$

$$+ c_1\left(D_{Bi+1} + D_{Bi}\right)\left(v_{i+1} - v_i\right) - c_1\left(D_{Bi} + D_{Bi-1}\right)\left(v_i - v_{i-1}\right)$$

$$+ c_2\left(v^*_{i+1} + v^*_i\right)\left(u^*_{i+1} - u^*_i + v^*_{i+1} - v^*_i\right) - c_2\left(v^*_i + v^*_{i-1}\right)\left(u^*_i - u^*_{i-1} + v^*_i - v^*_{i-1}\right)$$

$$+ c_2\left(v_{i+1} + v_i\right)\left(u_{i+1} - u_i + v_{i+1} - v_i\right) - c_2\left(v_i + v_{i-1}\right)\left(u_i - u_{i-1} + v_i - v_{i-1}\right)$$

$$- v^*_i + v_i = 0 \qquad (4.16)$$

$$A_9 - A_{10}\left(u_0 + u^*_0\right) + A_{11}D_{A0}\left(u_1 - \underline{u}_1\right) + A_{11}D^*_{A0}\left(u^*_1 - \underline{u}^*_1\right) + A_{12}u_0\left(u_1 - \underline{u}_1 + v_1 - \underline{v}_1\right)$$

$$+ A_{12}u^*_0\left(u^*_1 - \underline{u}^*_1 + v^*_1 - \underline{v}^*_1\right) - u^*_0 + u_0 = 0 \qquad (4.17)$$

$$-B_{12}\left(u_n + u^*_n\right) - B_{13}D_{An}\left(u_{n+1} - u_{n-1}\right) - B_{13}D^*_{An}\left(u^*_{n+1} - u^*_{n-1}\right)$$

$$-B_{14}u_n\left(u_{n+1} - u_{n-1} + v_{n+1} - v_{n-1}\right) - B_{14}u^*_n\left(u^*_{n+1} - u^*_{n-1} + v^*_{n+1} - v^*_{n-1}\right)$$

$$- u^*_n + u_n = 0 \qquad (4.18)$$

Each of these equations was then linearised using the Newton method (Finlayson, 1980). All these linearised equations were then written in a real band matrix form. A Fortran program was developed which called F01LBF Nag Fortran library to decompose the band matrix. Then another routine F04LDF was incorporated into the main program to obtain the required solution. Detailed numerical derivation is provided in Appendix 4.

CHAPTER - 5

EXPERIMENTATION

5.1 Introduction to the experimental system

In this research, experiments were conducted to evaluate the permeability, effective diffusivity, tensile strength, surface area, porosity and pore size distribution of pelleted catalysts in cylindrical form. The first three measurements were based on single pellet techniques while the remaining measurements were based on a batch of catalysts consisting of 5 to 15 pellets. Some of the latter three measurements were conducted at the Catalysis Centre, Billingham, ICI, for which standard measurement techniques and equipment are at present available. These techniques and measurements were discussed briefly in Chapter 2 of this thesis. In the same chapter tensile strength measurement was also discussed in rather greater detail. The measurement of permeability and effective diffusivity are the main focus of this chapter and have been conducted at the University College London. No standard apparatus or technique for carrying out such measurements is commercially available as yet.

The apparatus with which all the diffusion and permeation experiments have been performed was designed and developed in the Department of Chemical and Biochemical Engineering at University College London. A schematic line diagram of the rig is shown in figure 5.1 and figure 5.2 is a photograph of the apparatus.

The rig was so designed as to be able to operate at ambient temperature and a pressure just few mm of water guage above atmospheric. The supply of process gases to the rig is maintained from gas cylinders at a regulator pressure of 55 psig. The rig consists principally of two devices which can be used to produce step changes in gas concentration at a constant flowrate

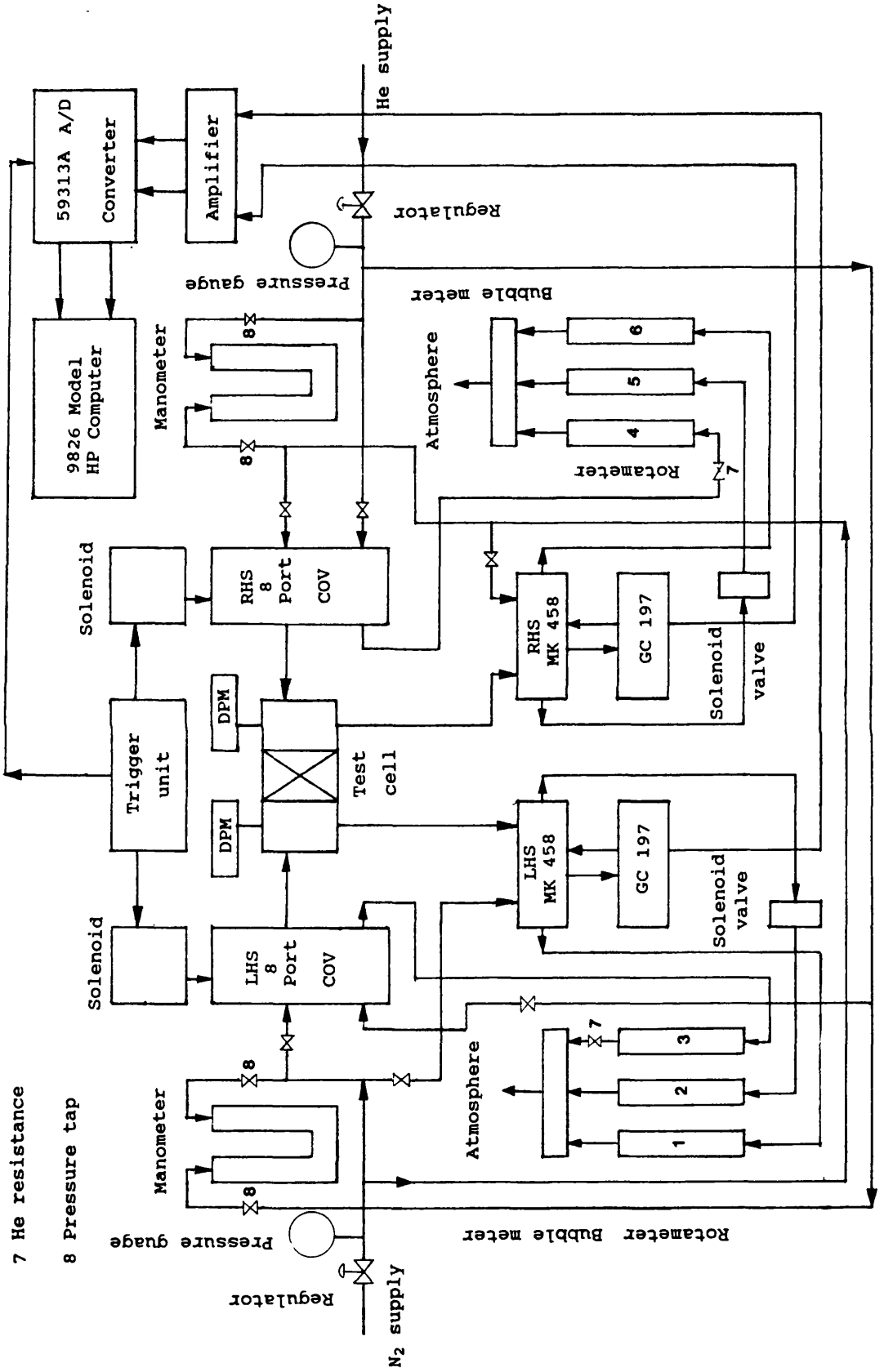

Figure 5.1. Line diagram of diffusion and permeation test apparatus.

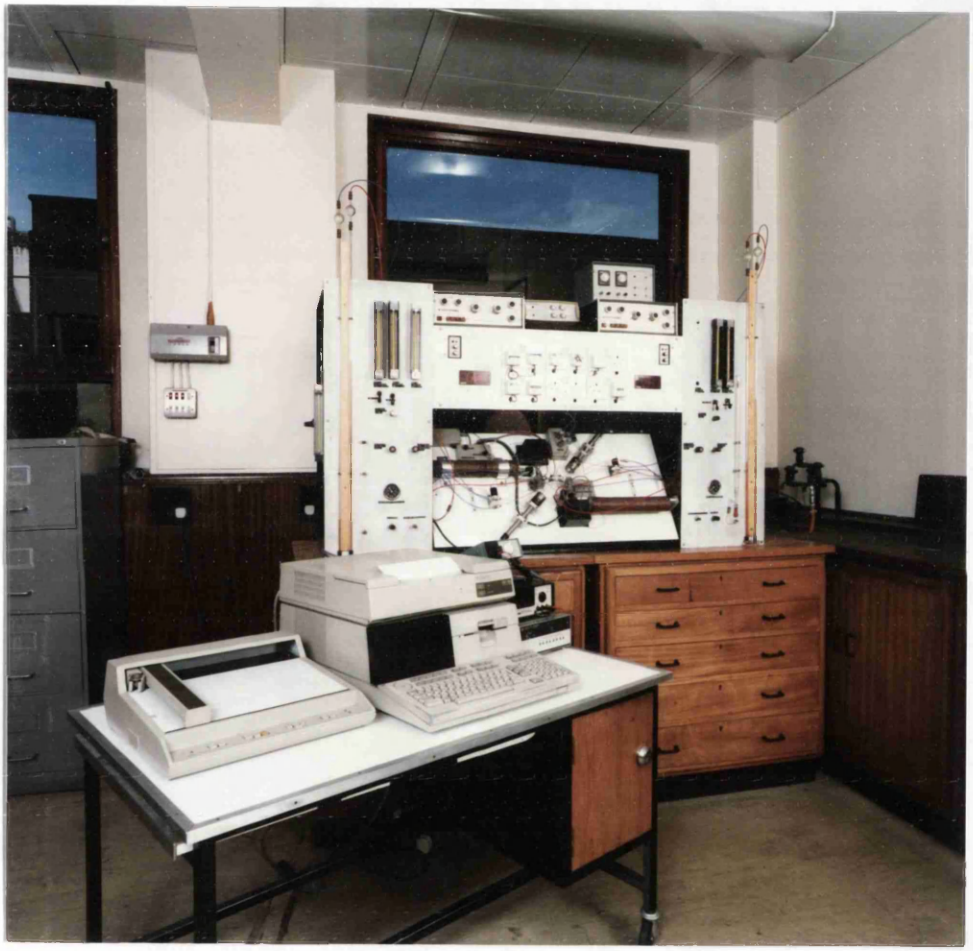

Figure 5.2. Photograph of the diffusion and permeation test apparatus.

either to the left or alternately to the right side of a diffusion cell. During experimentation, the diffusion/permeation test cell is attached to two gas distributors as mentioned in Chapter 2. Each gas distributor houses a miniature pressure transducer which reads the pressure in each end chamber (see figure 5.3). These pressures can be seen directly (in terms of millivolts) on two Digital Panel Meters (DPM).

A gas thermal conductivity detector (MK 458) with its respective control unit (GC 197) (see figure 5.1) manufactured by Taylor-Servomex is connected to each side of the single pellet diffusion and permeation test cell. The MK 458 is essentially a Wheatstone bridge with fine platinum wire filaments as the bridge elements. The reference gas, i.e. nitrogen, flows through one pair of filaments while the sample to be analysed flows over the other pair. The difference in thermal conductivities between these two gases causes a difference in temperature, and hence electrical resistance, of the filaments and hence an imbalance in the bridge. This is amplified to give an output voltage which for a binary gas pair is proportional to gas concentration. One of the detectors thus detects the gas concentration in q_{1out} and the other detects the gas concentration in q_{2out}. Both are measured in terms of millivolts and depend on the magnitude of voltages which are applied to the bridge from the GC 197 control units. These output signals are amplified,taken to a variable gain amplifier and are then sent to a 59313A model analog to digital converter (A/D) which gives binary output in two 8-bit bytes. A 9826 model Hewlett Packard (HP) computer is attached to the apparatus via this A/D converter for data acquisition. Of the four channels of the A/D converter only two are used. Channel 1 is connected to the left hand side MK 458 and channel 2 to right hand side MK 458. Each channel is capable of taking a maximum of 50 data points per second.

Two electrically operated solenoid on/off control

(A) BP pellet

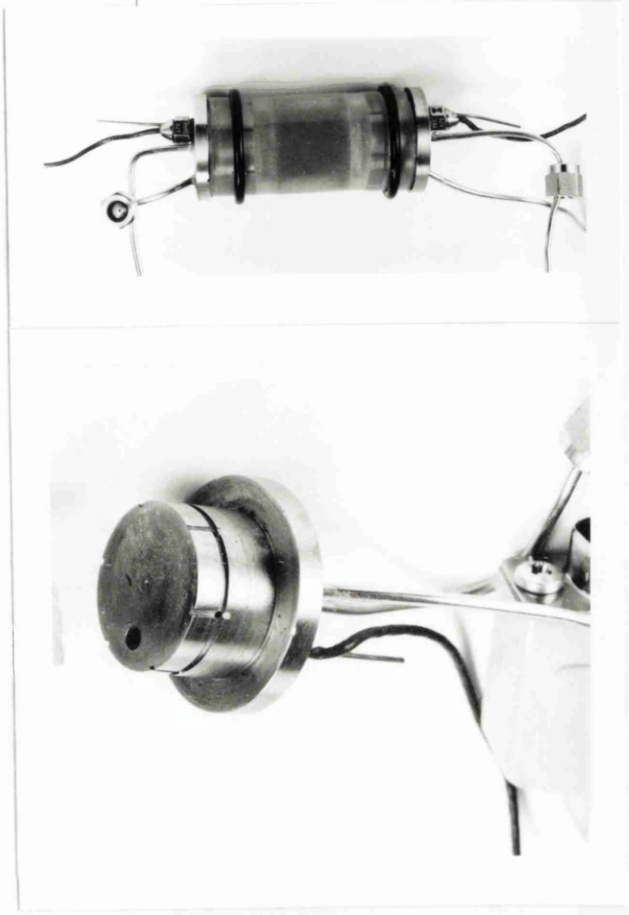

(B) ICI pellet

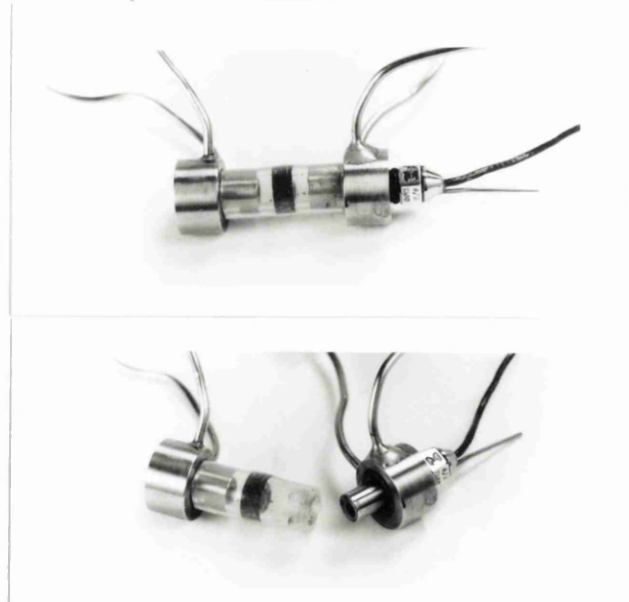

Figure 5.3. Photograph of gas distributor with pressure transducer.

valves can be opened or closed from a valve control unit and are placed at the outlet of each of the MK 458 microkatharometers. When closed, they enable the apparatus to be sealed for leak testing (see figure 5.1). Other accessory items within the rig include: two manometers for balancing the pressure of nitrogen and helium on each side of the apparatus; six rotameters (3 on each side) for observing the flow rates of nitrogen and helium and two soap bubble meters for calibrating the rotameters and for accurate measurement of flow rates.

5.2 The mechanism of step production

5.2.1 COV method

The eight port gas change over valve (COV) is a unique, reliable and fast method for producing a step change in gas concentration. All diffusion experiments were conducted using this method of step production. This is not a new method. It's development and use has already been discussed in Waldram, 1976 and Gibilaro, 1985. In this method, two identical copper coils of approximately 40 cm^3 (one containing the nitrogen carrier and the other containing either pure helium or a helium/nitrogen blend etc., depending upon the conditions of the experiment) are connected to the COV as shown in the figure 5.4.

A triggering mechanism is used to initiate the experiment. It consists of a solenoid valve and two micro switches. As soon as the solenoid is energised, the solenoid shaft hits the COV shaft and changes its position. One of the micro switches is used to cut off the power to the solenoid and the second conveys a contact closure signal to the A/D converter which triggers the start of signal sampling. On firing the solenoid, the flow paths of nitrogen and helium change completely as shown in figure 5.4. The coil is long enough so that the step response can be completed before the back end of the gas slug reaches the end chamber of the diffusion test cell. Steps produced in this manner are complete in less than 20 ms and are accompanied by

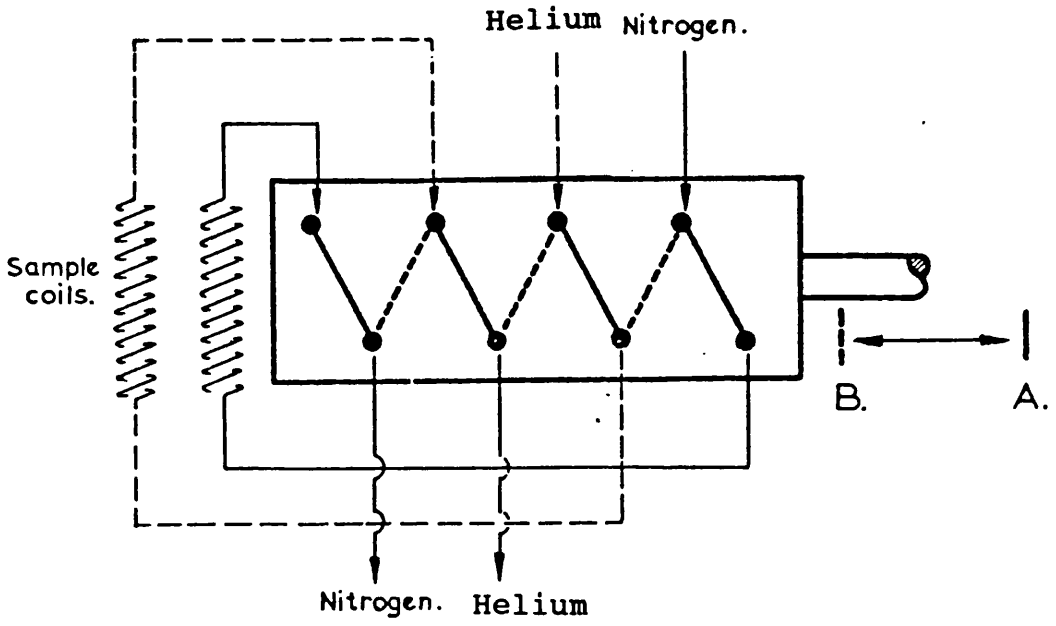

Figure 5.4. COV method of step production (quoted from Waldram, 1976).

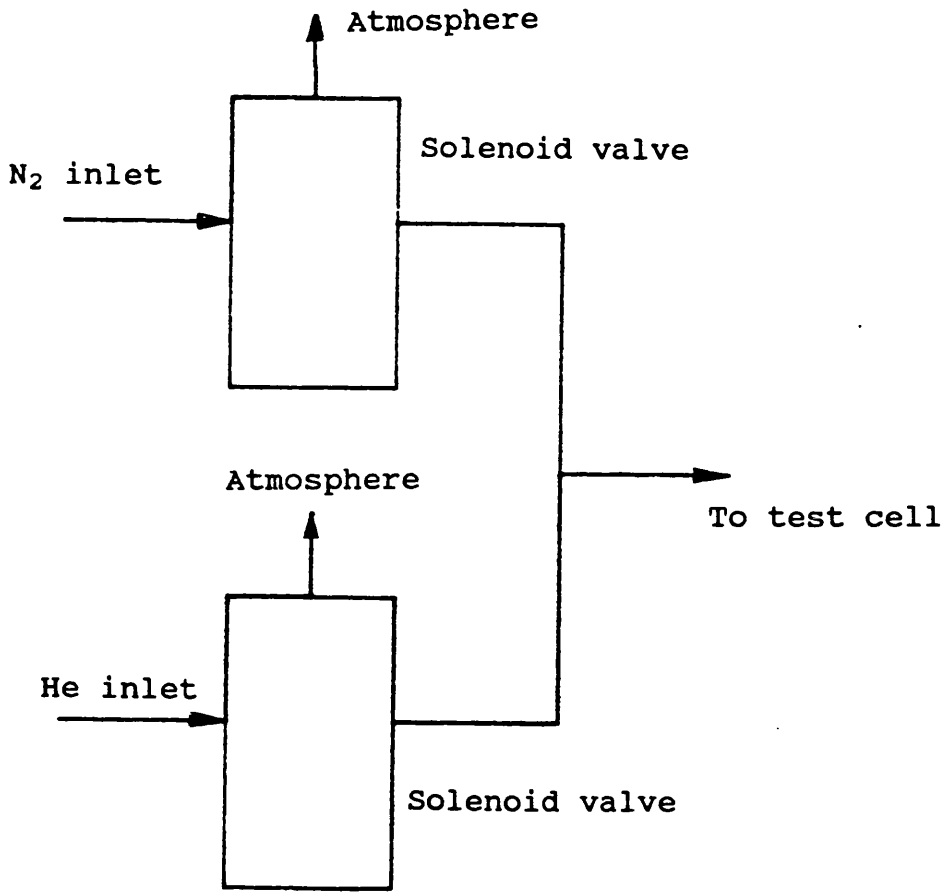

Figure 5.5. Solenoid valve method of step production.

little flow disturbance or pressure pulse.

In fact before developing this method of step production, three other alternative methods of producing steps and impulses were evaluated (Waldram, 1976). The alternatives were abandoned mainly because each was accompanied with greater pressure and flow pulsations. The present method is somewhat tedious, and not without its problems, however these are minor compared to those of the rejected systems. In this research, one other method of producing a step was tested and this is described in section 5.2.2 below.

5.2.2 Solenoid valve method

Steps can also be produced by the use of two 3 way miniature solenoid valves. This is rather a simple technique. Two such microvalves are necessary for the step to be made one for the nitrogen line and the other for the helium line. The arrangement is shown in figure 5.5. Normally nitrogen flows to the test cell and helium flows to the atmosphere. When the 3-way valves are operated simultaneously from a on/off switch, nitrogen escapes to the atmosphere and helium flows to the test cell.

Adopting this method, experimentation was carried out using two chemically inert solenoid valves with no dead volume manufactured by "The Lee Company". The internal volume of each valve was 15 microliters. The operating pressure and temperature of these valves were between 0 to 60 psig and between 4 to 40 °C respectively. The response time was 25 ms. However, this method did not work because of the same pulsation problem as experienced from the other methods tested by Waldram. Further improvement measures were not investigated because of other large volumes of work which had to be completed. However, if these pulsations can be removed or reduced greatly then this method might produce a reliable and fast step change in gas concentration. If it does, then

this would perhaps be better and simpler than the COV method. The micro switches and the COV itself would then be replaced by two microvalves and an on/off switch.

5.3 Determination of permeability

The theory of determining permeability by the differential and the integral means has been discussed in Chapter 2 of this thesis. Permeability experiments are straightforward and for ICI $Cu/Zn/Al_2O_3$ catalysts the determinations were based on the integral method. This was because only one set of readings per experiment was taken.

The sensitivity of each pressure transducer was slightly different. In order to match their sensitivity, a flow of nitrogen was taken in to the left hand side of the diffusion cell. The cell was then sealed using the solenoid valves (figure 5.1) in such a way that it gave a left hand side DPM reading of around 1800 mV (the maximum is 2000 mV). If this DPM reading was observed to be different to the right hand side one, they were equalised by adjusting the gain of the right hand side DPM. The system was then depressurised and the zeroes checked. Repressurisation was then allowed so as to see if there was any drift in DPM readings. The process was repeated for four/five times in order to get an equal pressure reading from both left hand side and right hand side DPM when the whole system was sealed at no flow conditions. Thus the sensitivity of both transducers was matched. This sensitivity was then obtained from a plot of the DPM reading versus the manometer reading as shown in figure 5.6: this was equivalent to 15.58 mV/cm of water or 1096.72 mV/psi.

It was mentioned earlier that the same diffusion apparatus and test cell can be used for conducting a permeation experiment. Again, from section 5.1, it was clear that the apparatus was designed to operate at, or near, ambient conditions only. As a consequence the gas

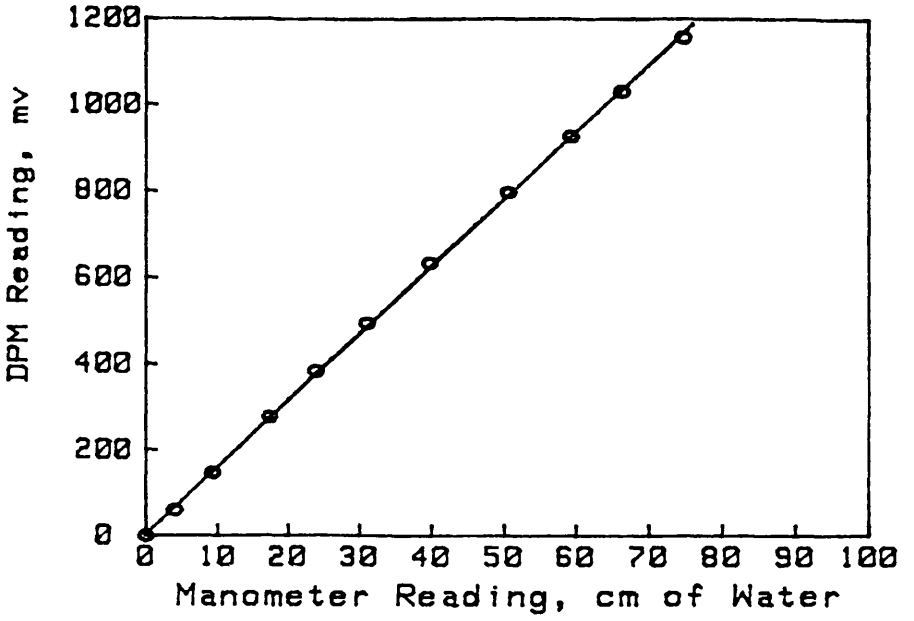

Figure 5.6. Plot of DPM reading versus manometer reading.

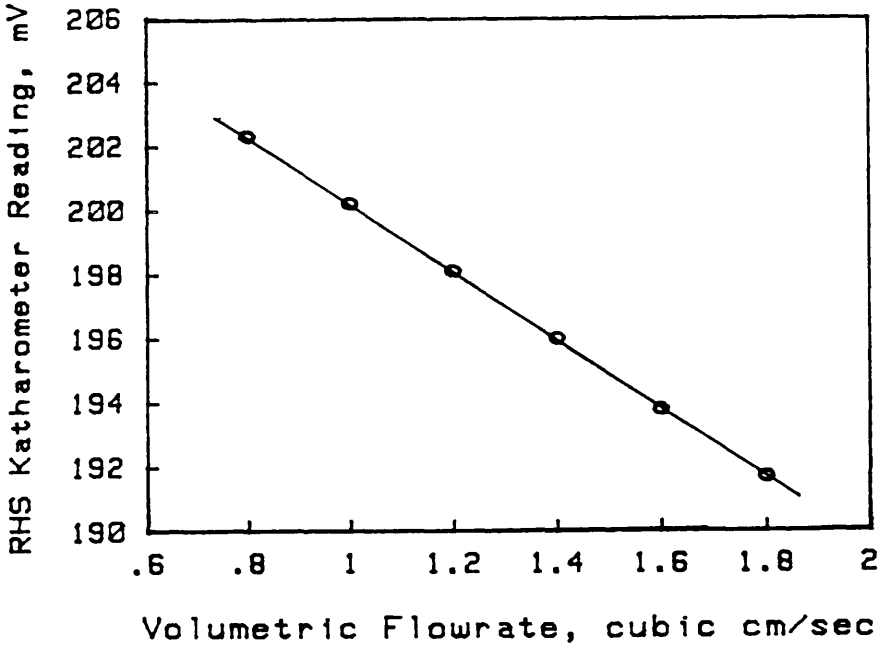

Figure 5.7. Calibration plot of right hand side MK 458 gas thermal conductivity detector.

permeation flux was in some cases very low and even using a bubble meter it was difficult to measure for an LT shift catalyst pellet of 5.4 mm diameter and 3.5 mm length. Therefore, the length of the pellet was cut to approximately one half of its original length before it was forced inside the silicone rubber tubing thereby doubling the permeation rate.

Each permeation experiment was then performed in the following manner. The permeation/diffusion test cell was placed in between the two gas distributors. A flow of nitrogen about 2.1 cm^3/s was allowed to pass through the permeation test cell from left hand side of the experimental system. Then the system was allowed to reach a steady state condition. When the steady state condition was reached, the pressures from both the left hand side and right hand side DPMs were recorded. The permeation flow rate from the left to the right hand side of the system was measured using a soap bubble meter. These data were used in equation (2.8) of Chapter 2 to evaluate the permeability. Since only one set of readings per experiment was taken, the integral method of finding permeability was applicable. A sample calculation is given in Appendix 8.

5.4 Determination of effective diffusion coefficients

Prior to the start of a diffusion experiment, the six rotameters were calibrated with nitrogen. Rotameter 3 (figure 5.1) is used when the step is made on the left hand side. The two MK 458 microkatharometers were also calibrated at appropriate ranges of flow rates of N_2 and pure He or N_2 and a blend gas at a working bridge voltage of 4 volts as shown in figure 5.7. The blend gas was a mixture of 95 volume% N_2 and 5 volume% He. This was derived from a large high pressure cylinder of purpose blended gases.

All electrical equipment was switched on for at

least two hours before any experiment was started so that electrical stability was achieved and steady signals were available from all the equipment.

The first step was to check that the apparatus was leak tight. This was done by pressurizing the system with nitrogen and then sealing all system outlets using solenoid operated valves (see figure 5.1). If there was any drop in pressure as evidenced from the DPM readings, there was leakage: constant DPM readings were obtained when the system was leak tight. This often required considerable effort to identify small leaks from couplings, joints etc. After depressurizing the system, the zeroes of the two DPMs were checked and if necessary adjusted by using the appropriate zero potentiometer setting within the DPM.

The next step was to check that the left hand side and the right hand side DPMs were showing identical readings for the same applied pressure. This was actually the matching of sensitivity of the two pressure tranducers as mentioned before during matching for the permeation experiment. It was achieved by again taking a flow of nitrogen (usually the flow at which the experiments were conducted), sealing the apparatus as described before and turning the flow off. The remainder of the procedure was exactly the same as that followed during a permeation experiment.

The final step was to adjust the helium resistance valve so that the resistances and hence the gas pressure profiles in the nitrogen and helium flow line to the COV are equal. This was done by three two way valves provided at the side panel on the apparatus with a flow controller (see figure 5.8). Valves A and B were such that they could be turned either to the system mode or to the test mode as required. In order to equalise the resistance of the nitrogen and helium lines, a flow of nitrogen (the experimental flow) was taken

through the flow controller. Valves A and B were turned to the test position; valve C was then switched to the He position. This allowed the nitrogen flow to be diverted through the helium line i.e. through rotameter 3. This rotameter was calibrated before with nitrogen. The flow rate of nitrogen through rotameter 3 was then adjusted using the helium resistance valve (see figure 5.1) so that this flow exactly matched the experimental flow of nitrogen when passing through its own normal line. The flow controller was then adjusted to set the flow to zero; valves A and B were re-positioned to the system mode and valve C was finally turned back to the nitrogen position.

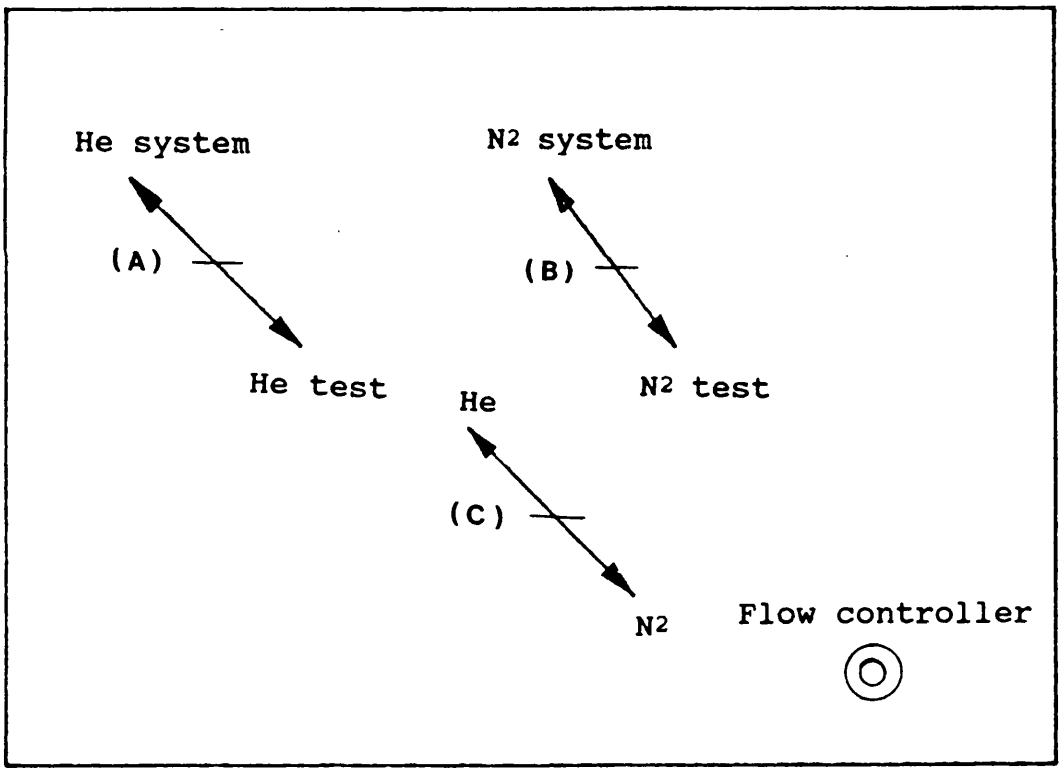

Figure 5.8. Coil resistance setting diagram.

5.4.1 Steady state measurements

The single pellet diffusion test cell, (see figure 5.1), was placed horizontally between the two purpose designed gas distributors. The two solenoid

valves (as in figure 5.1) were opened using the valve control unit and a flow of nitrogen was taken to the system from the left hand side distributor. An analogous flow of nitrogen was taken to the right hand side distributor and adjusted until the DPM readings were identical. Under these conditions, there was no convective flux through the pellet. The manometer pressure taps (see figure 5.1) were then opened and the pressures in the nitrogen and helium coils were balanced by adjusting the helium flow control valve. The bridge voltages for the two MK 458 katharometers were then applied from the katharometer control units (GC 197).

A program named "ICIDWF2" written in the BASIC computer language on the HP computer (see Appendix 10) was used to acquire both steady and transient diffusion data as well as to calculate steady state effective diffusion coefficients from the left hand side and right hand side chamber volume mass balances of the Wicke-Kallenbach cell. The software consisted of a main program and five subprograms. The first subprogram "SUB-Digitise2" samples at 10 Hz the starting signals, i.e. the base line values of channels 1 and 2 of the A/D converter, which are connected respectively to the left hand side and right hand side MK 458 katharometers. Then upon external triggering, the A/D sampling of each channel at 50 Hz was started with storage to memory of every 5th point value. These data were then subsequently plotted as a function of time (channel 1 first) and information on flow rates, amplification factors, applied voltages etc. are entered.

Subprogrammes "SUB Steady" and "SUB Steady2" calculate and store the final steady state values from the data obtained from SUB-Digitise2 for both the left hand side and right hand side response curves using the moving point average concept. In this method, the average of 10 consecutive data points is calculated. The first data point is then discarded and an 11th one is added and

the average of these next 10 points is again calculated. The process is continued until the average of five successive moving averages differs from a previous value by only 10^{-3} volts. The last point is then stored as the steady state value for the front end of the final steady state of the curve (see figure 5.9). Similarly a steady state value can be obtained for the tail end of the transient (see figure 5.9). The arithmetic mean over all points in between these two steady state values is then the required steady state voltage value.

Subprogram "SUB Mass-bal" is based on the following mass balance equation (if the step is made on the LHS):

$$Mb = \frac{c_{1o}}{c_{1i}} + \frac{q_2}{q_1} \left(\frac{c_{2o}}{c_{2i}}\right) \qquad (5.1)$$

Equation (5.1) can be derived from a mass balance around the diffusion test cell when the step is made to the left hand side of the apparatus. Under ideal conditions, i.e. if the mass balance is perfect, the right hand side of equation (5.1), in otherwords, Mb, should be equal to 1. If this is not so, then a percentage error in the mass balance can be calculated from equation (5.2).

$$\% \text{ error} = (1-Mb) \times 100 \qquad (5.2)$$

Hence this subprogram calculates and prints this mass balance error. The mass balance error plays a key role in the program. From a print out of this error one can immediately decide whether the experimental run is satisfactory or not. An error above 1% means that the experiment was regarded unsatisfactory, so a further run was necessary.

The final subprogram "SS-dif" calculates and

prints the steady state effective diffusivities based on each end chamber mass balance. If the step is made to the left hand side of the apparatus, the two following expressions for the steady state diffusion coefficients from each end chamber can be obtained (see Appendix 5):

$$D = D_L = \frac{q_2\left(\frac{C_{11}}{C_{1o}} - 1\right)}{\left(1 + \frac{q_2}{q_1} - \frac{C_{11}}{C_{1o}}\right)} \times \frac{L}{\pi R^2} \qquad (5.3)$$

$$D = D_R = \frac{q_2}{\left(\frac{C_{21}}{C_{2o}} - \frac{q_2}{q_1} - 1\right)} \times \frac{L}{\pi R^2} \qquad (5.4)$$

Incorporating these two expressions into the subprogram, two steady state effective diffusivities, one from the left hand side chamber and the other from the right hand side chamber of the diffusion test cell, can be obtained. These would be identical if the steady state experimental results represented a perfect mass balance. The tortuosity factor of the pellet can also be obtained from this subprogram, provided other relevant data values are available: these are free binary gas diffusion coefficient and the porosity of the catalyst pellet.

The main program calls all these subprograms in appropriate order. The program is written in such a way that transient diffusivity data can be printed out and a data file can be saved and protected.

After loading this program into the memory of the HP computer and on pressing the RUN key, the operator was asked to enter the file name. After entering the file name and pressing the ENTER key, the computer started digitising the base line: after about 10 seconds, an audible sound indicated that all was ready for the start of a diffusion run by external triggering. On making the step, sampling was started and the response data from the left hand side and right hand side end chambers of the test cell were sampledvia channels 1 and 2 of A/D converter until the completion of the step responses.

At this stage further information was requested from the operator, in particular entry of the volumetric flow rates, amplification factors, applied voltages etc. Upon entering these data, the steady state diffusion coefficients from the left hand side and the right hand side were printed out as was the mass balance error as discussed earlier. In practice, it was difficult to obtain a mass balance error below 1% and several runs had to be conducted in order to obtain a good and reliable average diffusion value. Precise adjustments of flow rates, resistance valve settings and pressures was the key to generating good results. The experimental curves for both left hand side and right hand side chamber outlet concentrations along with a computer print out of the steady state diffusivity results for ICI sample S-46/2 is provided below. This is typical of all experimental runs.

5.4.2. Unsteady state measurements

From section 5.4.1, the steady state effective diffusion coefficient was obtained following a step change in gas concentration from pure nitrogen to pure helium. In principle, this steady state effective diffusivity can be obtained without making such a step change in gas concentration. Now the question naturally arises as to why this step change should be made? The answer to this is to generate transient system response

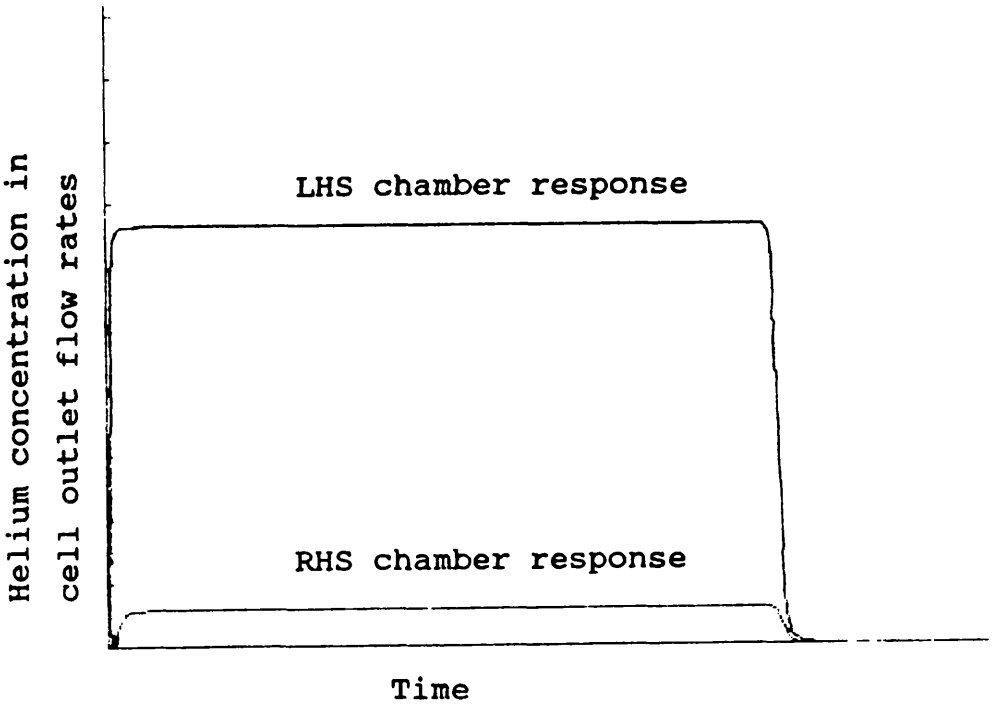

ICI462
Q(LHS) = 1.0 cm^3
Q(RHS) = 1.22 cm^3
AVERAGE BASE VALUE ON LHS = 1
STEADY STATE = 664.7
STEADY STATE = 665.0
FINAL SS VALUE ON LHS = 6649.92
AVERAGE BASE VALUE ON RHS = -1.2
STEADY STATE = 58.2
STEADY STATE = 59.2
FINAL SS VALUE ON RHS = 58.71

CO VALUE (LHS) = 6708.78 mV
CO VALUE (RHS) = 6746.04 mV
MASS BALANCE CLOSE TO WITHIN 0.19%
RADIUS OF PELLET = 0.277 CM
BINARY DIFFUSIVITY OF N_2/He = 0.7079 cm^2s^{-1}
EFFECTIVE DIFFUSIVITY CALCULATED FROM LHS = 0.00678 cm^2s^{-1}
EFFECTIVE DIFFUSIVITY CALCULATED FROM RHS = 0.00824 cm^2s^{-1}

Figure 5.9. Print out of diffusivity data with a typical step response curve for sample S-46/2.

data. From these data, the system moments can be calculated. Matching these experimental moments with the theoretical moments equations as mentioned in Chapter 4 and derived in Appendix 2, the unsteady state diffusivities from the left hand side and right hand side transients from the diffusion cell can be calculated. These unsteady state diffusivities provide more information about pellet characteristics, particularly whether any dead ended pore structure is present within the catalyst pellet or not. If there are any dead ended pores, the unsteady state diffusivities will be higher than their steady state counterparts.

Therefore no additional experiments were required for unsteady state diffusivity measurements. The transient data for each experiment was readily available together with the steady states of each diffusion experiment. Adopting the procedure described above, the unsteady state diffusivity was calculated.

CHAPTER - 6

EXPERIMENTAL RESULTS AND DISCUSSION: LT SHIFT CATALYSTS

6.1 Experimental strategy

The experiments have been designed to fall into two categories: those which explore the main effects alone and those which involve interaction effects. Main effects are those effects which correspond to the variation of one particular production parameter at one level only, keeping the remaining variables at their normal production levels. For example, the variation of calcination temperature at its low level only leads to a main effect.

When a sample is prepared with a combination of two or more production parameters at values other than their normal ones, e.g., a low value of one processing condition and a high value of the other, then the result of this is called an interaction effect. For example, when a sample is prepared from the particular combination of low pellet density and high cut size, this kind of interaction is called a first order interaction effect. Similarly if more than two processing parameters are considered simultaneously at anything other than their normal levels, this is called a higher order interaction effect.

Table 6.1 gives all the experimental results which have been generated by this research. Tables 3.2 and 3.3 specify the values of production variables (L, N, H and EH) for each of the samples listed in table 6.1. As mentioned in Chapter 5 surface area, porosity and pore size distribution measurements were based on a batch of sample consisting of 5 to 15 pellets. Measurements of the permeability and effective diffusivity of a particular catalyst batch were based on measurements from 5 individual catalyst pellets whereas tensile strength and

Table 6.1. Experimental results of ICI 52-8 LT shift catalysts.

Sample No:	Surface area (m^2/g)	Porosity	Tensile strength (MN/m^2)	Permeability $B_o \times 10^{16}$ (m^2)	Effective diffusivity $D_e \times 10^6$ (m^2/s)	Tortuosity factor
S-1	115.6	0.549	4.07 ± 1.67	1.56 ± 0.35	1.42 ± 0.55	2.95
S-2	117.3	0.554	2.91 ± 1.01	1.37 ± 0.20	1.24 ± 0.25	3.26
S-3	109.5	0.527	3.11 ± 1.87	1.87 ± 0.35	1.43 ± 0.73	2.69
S-4	96.5	0.529	3.22 ± 0.89	1.56 ± 0.39	1.52 ± 0.41	3.01
S-5	-	-	-	-	-	-
S-6	102.2	0.551	2.22 ± 0.85	1.54 ± 0.45	1.91 ± 0.65	2.46
S-7	96.5	0.495	4.33 ± 1.62	1.21 ± 0.10	0.71 ± 0.16	5.04
S-8	101.0	0.491	3.83 ± 1.29	1.39 ± 0.41	1.14 ± 0.63	3.45
S-9	112.4	0.502	3.58 ± 1.30	1.50 ± 0.29	1.13 ± 0.55	3.08
S-10	105.0	0.531	3.09 ± 1.14	1.32 ± 0.20	1.22 ± 0.25	3.02
S-11	106.2	0.513	3.67 ± 1.52	1.66 ± 0.57	1.06 ± 0.25	3.34
S-12	105.6	0.52	3.53 ± 1.23	1.12 ± 0.20	0.91 ± 0.37	3.68
S-13	115.6	0.504	4.33 ± 1.61	1.17 ± 0.20	1.03 ± 0.22	3.15
S-14	112.4	0.523	4.87 ± 2.09	1.34 ± 0.35	0.91 ± 0.41	3.53
S-15	112.6	0.528	4.54 ± 1.81	1.26 ± 0.39	1.14 ± 0.27	3.09
S-16	112.7	0.563	3.85 ± 1.59	1.50 ± 0.45	1.53 ± 0.63	2.82
S-17	115.0	0.564	2.90 ± 0.85	1.51 ± 0.51	1.40 ± 0.57	2.88
S-18	111.6	0.553	3.16 ± 1.55	1.37 ± 0.49	1.32 ± 0.37	2.96
S-19	64.2	0.460	4.27 ± 1.68	1.54 ± 0.31	2.00 ± 0.27	2.29

Table 6.1 continued

Sample No:	Surface area (m^2/g)	Porosity	Tensile strength (MN/m^2)	Permeability $B_o \times 10^{16}$ (m^2)	Effective diffusivity $D_e \times 10^6$ (m^2/s)	Tortuosity factor
S-20	110.4	0.634	1.39 ± 0.85	5.12 ± 1.21	5.60 ± 1.18	1.29
S-21	108.2	0.505	4.32 ± 1.76	0.90 ± 0.47	1.19 ± 0.27	2.56
S-22	111.5	0.616	1.13 ± 0.54	3.14 ± 0.50	4.10 ± 0.76	1.44
S-23	84.7	0.426	3.67 ± 0.89	1.14 ± 0.22	1.07 ± 0.51	2.57
S-24	55.4	0.545	0.82 ± 0.16	3.05 ± 1.25	4.10 ± 1.63	1.48
S-25	80.3	0.492	2.99 ± 0.88	1.04 ± 0.49	1.38 ± 0.29	3.00
S-26	98.0	0.449	3.70 ± 1.47	0.82 ± 0.43	1.11 ± 0.24	2.26
S-27	99.8	0.503	2.41 ± 0.95	1.14 ± 0.27	1.73 ± 0.49	2.23
S-28	85.7	0.424	4.05 ± 1.69	0.92 ± 0.31	0.69 ± 0.25	3.97
S-29	88.7	0.517	2.14 ± 0.52	2.02 ± 0.63	3.10 ± 0.57	1.24
S-30	120.1	0.561	1.88 ± 0.61	1.72 ± 0.10	1.65 ± 0.10	2.34
S-31	122.4	0.555	1.08 ± 0.24	2.01 ± 0.74	2.73 ± 0.31	1.43
S-32	89.9	0.500	2.14 ± 0.85	1.51 ± 0.06	2.60 ± 0.84	1.48
S-33	97.3	0.522	2.89 ± 0.98	2.44 ± 0.04	2.52 ± 0.41	1.54
S-34	110.5	0.581	1.09 ± 0.51	3.18 ± 1.29	2.61 ± 0.88	1.48
S-35	106.8	0.580	1.35 ± 0.47	3.94 ± 0.20	4.43 ± 1.72	0.88
S-36	119.9	0.578	1.25 ± 0.64	17.80± 3.80	3.30 ± 0.82	1.17
S-37	120.7	0.678	0.45 ± 0.33	6.33 ± 2.53	4.88 ± 0.39	0.79
S-38	118.4	0.546	2.76 ± 1.33	1.57 ± 0.20	2.70 ± 0.43	1.43
S-39	113.6	0.545	2.29 ± 0.91	1.70 ± 0.61	2.40 ± 0.82	1.61
S-40	114.4	0.578	1.30 ± 0.72	2.17 ± 1.02	3.60 ± 0.43	1.07

Table 6.1 continued

Sample No:	Surface area (m^2/g)	Porosity	Tensile strength (MN/m^2)	Permeability $B_o \times 10^{16}$ (m^2)	Effective diffusivity $D_e \times 10^6$ (m^2/s)	Tortuosity factor
S-41	111.6	0.533	2.64 ± 0.69	1.99 ± 0.67	2.60 ± 0.78	1.48
S-42	93.4	0.582	1.17 ± 0.84	3.64 ± 1.67	4.27 ± 1.88	0.54
S-43	97.9	0.657	1.68 ± 1.17	2.09 ± 0.53	3.11 ± 0.75	0.83
S-44	94.2	0.629	1.32 ± 0.63	2.60 ± 0.81	4.22 ± 1.93	0.74
S-45	100.4	0.607	2.63 ± 1.10	3.80 ± 2.87	4.83 ± 0.39	1.09
S-46	91.0	0.435	5.29 ± 2.63	0.40 ± 0.17	0.66 ± 0.38	3.01
S-47	85.3	0.462	5.63 ± 3.28	1.03 ± 0.70	0.91 ± 0.21	3.19
S-48	90.9	0.633	2.89 ± 1.71	2.41 ± 0.74	3.40 ± 1.55	2.59
S-49	86.7	0.433	5.83 ± 2.21	0.64 ± 0.41	0.81 ± 0.75	2.72
S-50	88.0	0.442	7.52 ± 2.80	0.88 ± 0.58	1.31 ± 1.06	2.77
S-51	57.3	0.422	4.54 ± 1.44	0.48 ± 0.22	0.72 ± 0.29	2.11
S-52	117.7	0.610	1.27 ± 0.53	5.10 ± 4.25	4.42 ± 0.75	0.85
S-53	103.1	0.447	5.83 ± 3.23	0.47 ± 0.11	0.79 ± 0.48	1.97
S-54	112.4	0.566	2.57 ± 1.66	1.33 ± 0.98	1.53 ± 0.86	1.72
S-55	100.2	0.447	4.14 ± 1.14	1.91 ± 0.71	1.33 ± 0.99	2.34
S-56	94.8	0.477	5.14 ± 1.84	1.15 ± 0.23	1.44 ± 0.32	1.90
S-57	96.9	0.481	6.29 ± 1.89	0.67 ± 0.43	1.19 ± 0.45	1.84
S-58	103.9	0.579	2.62 ± 2.45	5.10 ± 1.31	3.85 ± 0.07	1.38
S-59	101.5	0.522	3.96 ± 1.14	1.24 ± 0.81	1.69 ± 0.69	1.36
S-60	96.0	0.507	4.38 ± 2.60	0.96 ± 0.18	1.57 ± 0.62	1.47

Table 6.1 continued

Sample No:	Surface area (m^2/g)	Porosity	Tensile strength (MN/m^2)	Permeability $B_o \times 10^{16}$ (m^2)	Effective diffusivity $D_e \times 10^6$ (m^2/s)	Tortuosity factor
S-61	110.5	0.614	1.34 ± 0.71	4.91 ± 2.02	4.25 ± 0.69	0.79
S-62	95.7	0.537	3.76 ± 2.03	1.74 ± 1.36	1.71 ± 0.27	2.16
S-63	76.4	0.505	3.63 ± 1.59	1.42 ± 1.15	1.82 ± 0.50	2.37
S-64	106.7	0.656	0.90 ± 0.23	9.05 ± 8.00	7.13 ± 3.00	0.54
S-65	122.1	0.648	1.45 ± 0.43	3.39 ± 1.70	4.67 ± 1.19	0.83
S-66	114.5	0.65	1.22 ± 0.49	10.7 ± 4.30	5.24 ± 0.89	0.74
S-67	128.1	0.69	1.88 ± 0.94	6.97 ± 4.12	-	-
S-68	117.6	0.52	2.51 ± 1.23	60.10 ± 36.30	1.28 ± 0.49	3.01
S-69	111.6	0.503	3.27 ± 1.77	30.23 ± 26.80	1.21 ± 0.61	3.19
S-70	102.5	0.653	0.92 ± 0.51	82.63	-	-
S-71	124.2	0.495	1.99 ± 0.94	213.26 ± 53.92	1.42 ± 0.11	2.72
S-72	106.5	0.476	1.37 ± 0.73	213.29 ± 71.18	1.39 ± 0.36	2.77
S-73	-	0.555	1.23 ± 0.82	239.23 ± 218.71	1.83 ± 0.53	2.11
S-74	110.3	0.608	0.68 ± 0.36	17.12 ± 14.90	4.54 ± 1.26	0.85
S-75	109.0	0.481	2.13 ± 0.77	155.87 ± 104.17	1.96 ± 0.33	1.97
S-76	130.1	0.616	1.11 ± 0.56	233.61	2.24 ± 0.48	1.72
S-77	96.0	0.522	2.14 ± 1.40	177.18 ± 90.68	1.65 ± 0.21	2.34
S-78	101.3	0.519	1.41 ± 0.58	177.20 ± 37.50	2.03 ± 0.24	1.90
S-79	106.9	0.518	2.77 ± 1.21	5.45 ± 4.50	2.10 ± 0.51	1.84
S-80	116.0	0.636	1.61 ± 0.76	26.79 ± 21.00	-	-
S-81	96.7	0.563	1.73 ± 0.77	102.29	2.84 ± 0.89	1.36
S-82	91.5	0.549	2.10 ± 1.25	44.02 ± 28.41	2.62 ± 0.55	1.47
S-83	-	0.620	1.00 ± 0.65	14.19 ± 7.00	4.88 ± 1.95	0.79
S-84	70.3	0.548	2.84 ± 1.89	2.99 ± 2.16	1.78 ± 0.88	2.17
S-85	69.6	0.489	2.97 ± 1.14	2.22 ± 0.68	-	-

Weibull modulus determinations were based on sample sizes of between 15 to 56 pellets. As a consequence, the results of permeability, diffusivity and tensile strength are quoted as average values with standard deviations at the 95% confidence limit. The tortuosity factor appearing in table 6.1 has been calculated from the average experimental value of the steady state effective diffusivity using the Bosanquet extrapolation formula (see Appendix 9 for a sample calculation).

6.2 Discussion of experimental results

Based on the type of effects, discussion of experimental results can be divided into two groups: (1) discussion based on all main effect results and (2) discussion based on all interaction effect results.

6.2.1 Discussion based on all main effect results

Experimental results based on the main effects are presented in circular diagrams as shown in figures 6.1 to 6.5. In those figures, L represents low, N represents normal, H represents high and EH represents extra high values of a particular production parameter.

6.2.1.1 Surface area

Figure 6.1 represents the surface area of the green catalysts which varied from 55.3 to 117.3 m^2/g with a base sample area of 115.6 m^2/g. That is, this property can be varied by a factor of 117.3/55.3 = 2.12 and can be decreased by (115.6 - 55.3) x 100/115.6 = 52.16% below the base sample value. However, it can only be increased above the base sample case by (117.3 - 115.6) x 100/115.6 = 1.47%. From a production point of view, we always require high surface area to enhance the probability of more surface reaction. The figure shows that surface area can be slightly increased above the base case area by choosing a low lubricant concentration only (S-2). Apart from this, all surface areas fell below the base case.

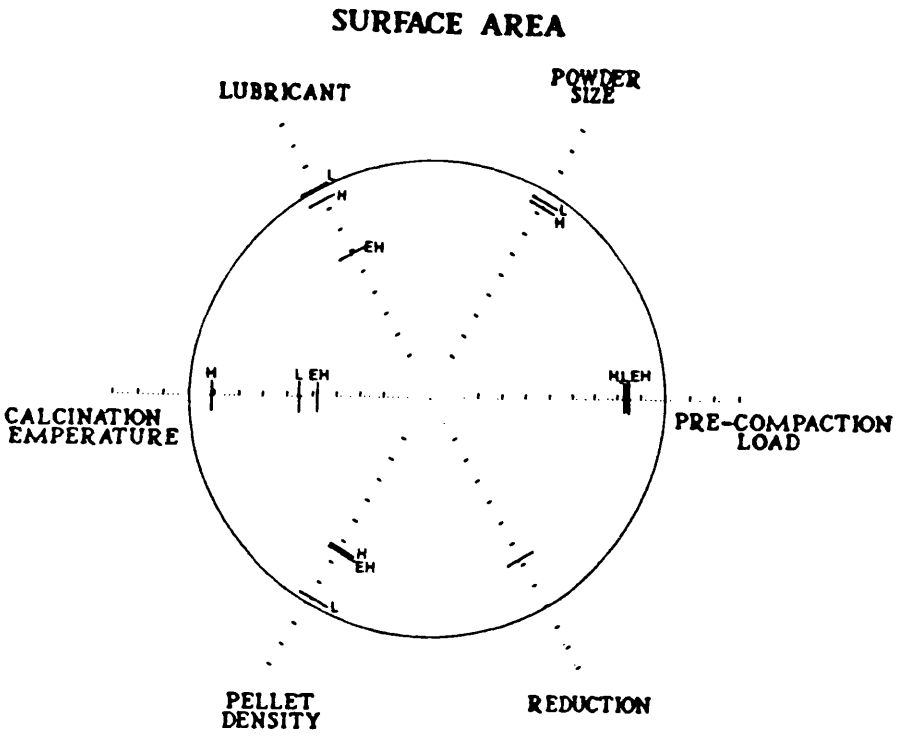

Figure 6.1. Variation of surface area with the five catalyst production parameters at their low, normal, high and extra high levels.

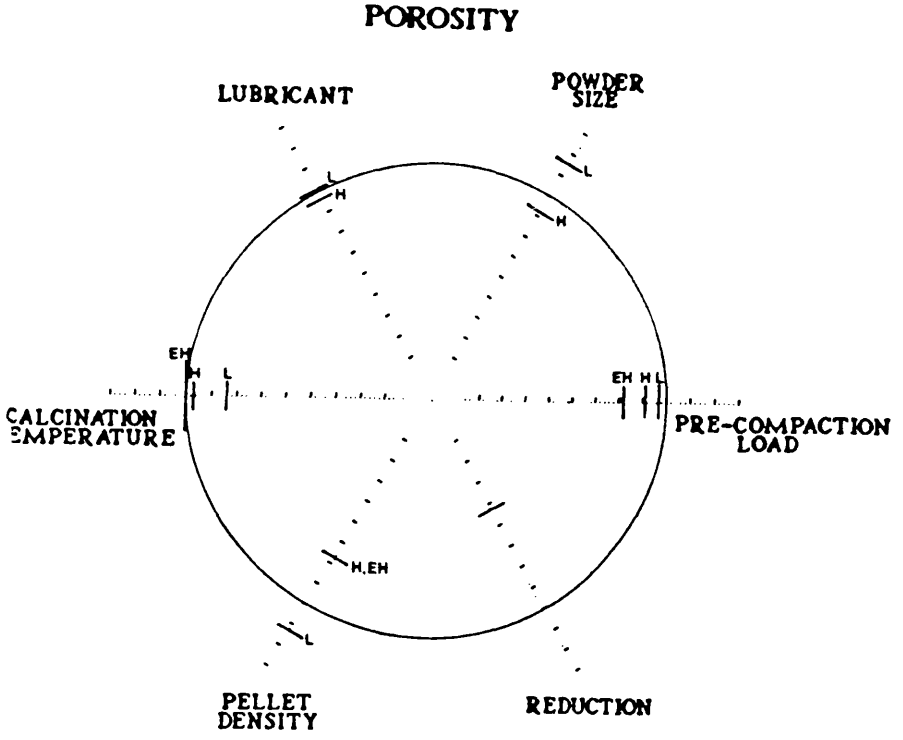

Figure 6.2. Variation of porosity with the five catalyst production parameters at their low, normal, high and extra high levels.

From this figure, it is also seen that surface area changed by only 17% ((115.6-96.5) x 100/115.6 = 16.5%, S-4 and S-7) and 14% (S-27) in response to changes in either preliminary compaction load or particle cut size. A regular decreasing tendency was observed as the amount of lubricant was raised to high and extra high levels (S-3 and S-25). Although the surface area was observed to fall with high pellet density by 27%, which could be expected, there was no further change observed at the extra high level. Minimum surface areas i.e. 64.2 m^2/g and 55.4 m^2/g were found in samples prepared with low and extra high calcination temperatures (S-19 and S-24). At low calcination temperature, due to the presence of trace amounts of water, carbonates, nitrates etc. the materials are more compressive during the pre-compaction stage. Thus surface area due to micropores is lost. On the other hand, at extra high calcination temperature, sintering occurs and thus surface area decreases. However, a value of 110 m^2/g (S-10) was observed at a high calcination temperature level. This means that at this temperature, the material property is little different than at the normal calcination temperature.

6.2.1.2 Porosity

Figure 6.2 represents the changes in porosities with the same five production steps varied when the green catalyst samples were prepared. The overall variation of porosity was in the range of 0.426 to 0.634, i.e. a factor of 0.634/0.426 = 1.49 only, with the reference base case porosity of 0.549.

The amount of lubricant added and the pre-compaction load showed an overall variation of 18% (S-26) on the porosity and decreased in a regular fashion with increasing levels. On the other hand, the effect of calcination temperature was the reverse, that is, porosity was increased from 0.460 to 0.545 with increasing calcination temperature (S-19, S-10 and S-24).

Sharp reduction of porosities was observed i.e. from 0.634 to 0.505 (S-20 and S-21) for primary particle cut size and from 0.616 to 0.426 (S-22 and S-23) for pelleting density when these variables were altered from their low to high levels. However, these variations did not continue significantly with further increases to extra high level. This means porosity can be increased by (0.634-0.549) x 100/0.549 = 15.48% above the base sample by choosing a low particle cut size. If the particle sizes are small, it is more difficult to compress them and hence more pore spaces within the pellet result and will increase the porosity value. A similar increase of porosity by about 12% for a low pellet density is due to the lack of sufficient compression load. Alternatively, porosity can be decreased below the base sample by (0.549 -0.424) x 100/0.549 = 22.77% (case S-28) by increasing the pellet density.

6.2.1.3 Permeability

Figure 6.3 represents the results of all green pellet permeabilities which varied from o.82 x 10^{-16} m^2 to 5.12 x 10^{-16} m^2, with the base case value of 1.56 x 10^{-16} m^2. This property shows a 5.12/0.82 = 6.24 factor of overall variation. It can be increased by (5.12 - 1.56) x 100/1.56 = 228.21% above the base sample which of course may be very attractive from a reaction engineering point of view. A decrease of (1.56 - 0.82) x 100/1.56 = 47.44% below the base case sample is also observed and this will in general be unattractive.

Pre-compaction load does not have a very marked effect at low and high levels but decreased permeability by approximately 45% at the extra high level (S-26) which can be expected. Addition of lubricant at its high level increased the permeability by 20% (S-3), a surprising result but the value decreased at both the extra high level and the low level respectively by 33% and 12%. Extra high calcination temperature increased

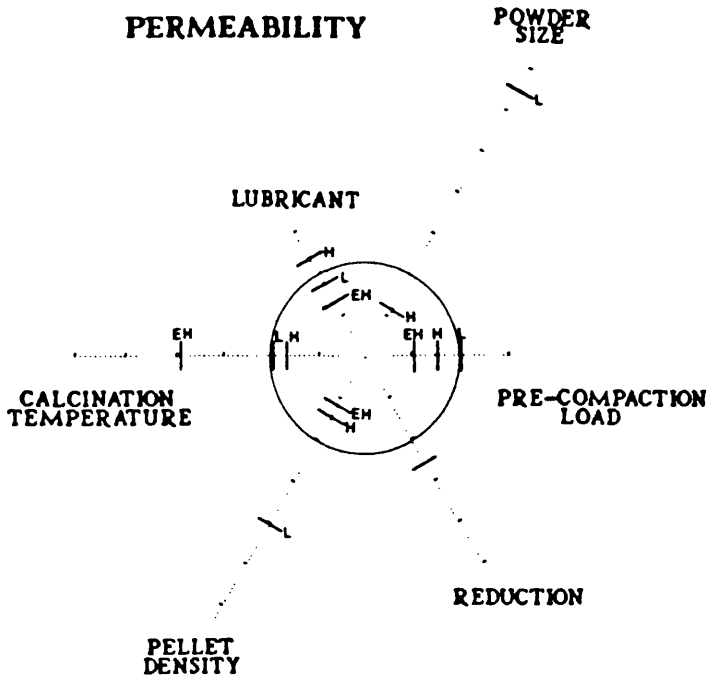

Figure 6.3. Variation of permeability with the five catalyst production parameters at their low, normal, high and extra high levels.

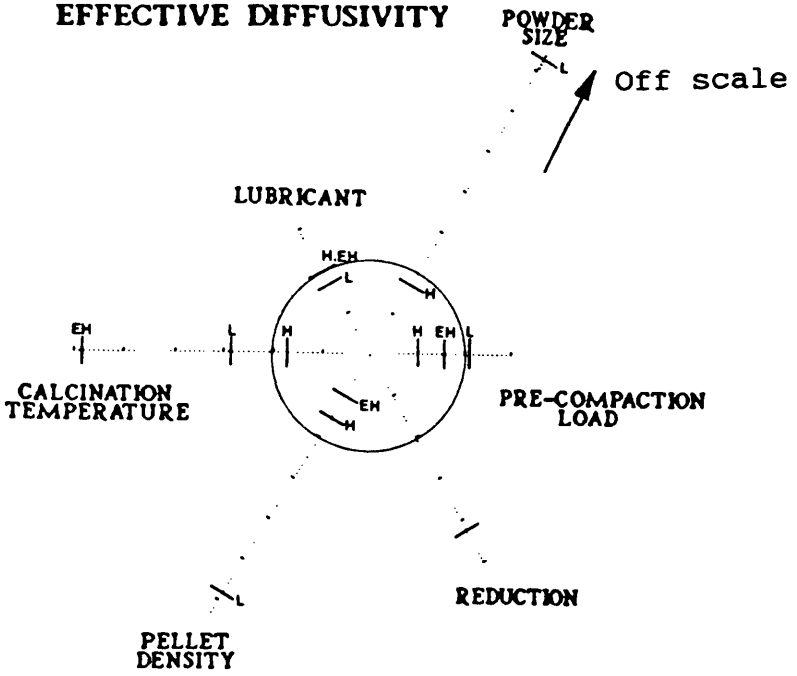

Figure 6.4. Variation of effective diffusivity with the five catalyst production parameters at their low, normal, high and extra high levels.

permeability by a factor of almost 2 (S-24). Due to sintering at extra high calcination temperature, smaller particles join each other to become large. Hence much of the porosity will appear as macroporosity. From pore size distribution data (see section 6.2.4) it can be seen that the average pore diameter has increased from 15.6 nm (S-1) to 18.2 nm (S-24). Since at low Reynolds number the permeation flux is proportional to the 4th power of the pore radius, we would expect to observe increased permeability.

Cut size and pellet density produced similar results to those observed for porosity. That is, a 20% increase in the porosity resulting from a low cut size has an associated permeability increase of more than 200% (S-20). A 100% increase of permeability can be achieved by using a low pellet density (S-22).

6.2.1.4 Effective diffusivity

Figure 6.4 represents the results for effective diffusivities of all green catalyst samples. This property has varied from 0.70×10^{-6} m^2/s to 5.60×10^{-6} m^2/s and has a base value of 1.40×10^{-6} m^2/s. An overall variation by a factor of 5.6/0.70 = 8.00 has been achieved. It can be increased above the base case sample by (5.60 - 1.40) x 100/1.40 = 300%. This trend is obviously desirable for free movement of gas molecules so that they can reach the active sites of the catalyst particles easily, and quickly, for potential reaction. Diffusivity can be decreased by (1.40 - 0.70) x 100/1.40 = 50% below the base case sample value.

In an analogous manner to the discussion in 6.2.1.1 to 6.2.1.3, the variation of diffusivities due to the five production parameters followed similar trends. Very little change i.e 14% (S-2) was observed due to the addition of lubricant. A decreasing trend i.e. from 1.50×10^{-6} m^2/s (S-4) to 0.70×10^{-6} m^2/s (S-7) in the values of diffusivity was observed with higher pre-compaction

load. This was a decrease of exactly 50% over the base sample. However, these variations were nowhere near as pronounced as the variations resulting from calcination temperature, cut size and pelleting density. A 43% increase in diffusivity was obtained at low calcination temperature whereas at extra high calcination temperature the increase was approximately 200% (S-24). Diffusivity was increased by a factor of about 3 following low pellet density (S-22) and variations with particle cut size are even greater (S-20).

The tortuosity factor of the green catalyst samples can be calculated from the diffusivity results and varied from 1.29 (S-20) to 5.04 (S-7) but most of them were found to be in the range of 2 to 3.5. As mentioned earlier, each tortuosity factor was calculated from the Bosanquet extrapolation formula assuming that the porosity was equivalent for both bulk and Knudsen diffusion coefficient terms. The tortuosity factor is inversely proportional to the diffusivity value. Thus a low tortuosity factor is an indication of high diffusivity and vice versa.

6.2.1.5 Tensile strength and Weibull modulus

The tensile strength of the green catalyst samples varied from 0.82 MN/m^2 to 4.33 MN/m^2 with the corresponding reference case value of 4.07 MN/m^2. This property can be varied by as much as a factor of 4.33/0.82 = 5.28. It can be increased above the base sample by (4.33 - 4.07) x 100/4.07 = 6.39% or can be decreased below the base sample by (4.07 - 0.82) x 100/4.07 = 79.85%. Any catalysts with low tensile strengths will be more prone to breakage and attrition which in an industrial context is a great disadvantage. This will lead to high reactor pressure drops and, in severe cases, premature plant shut down.

Figure 6.5 represents these variations with all processing variables considered during the sample

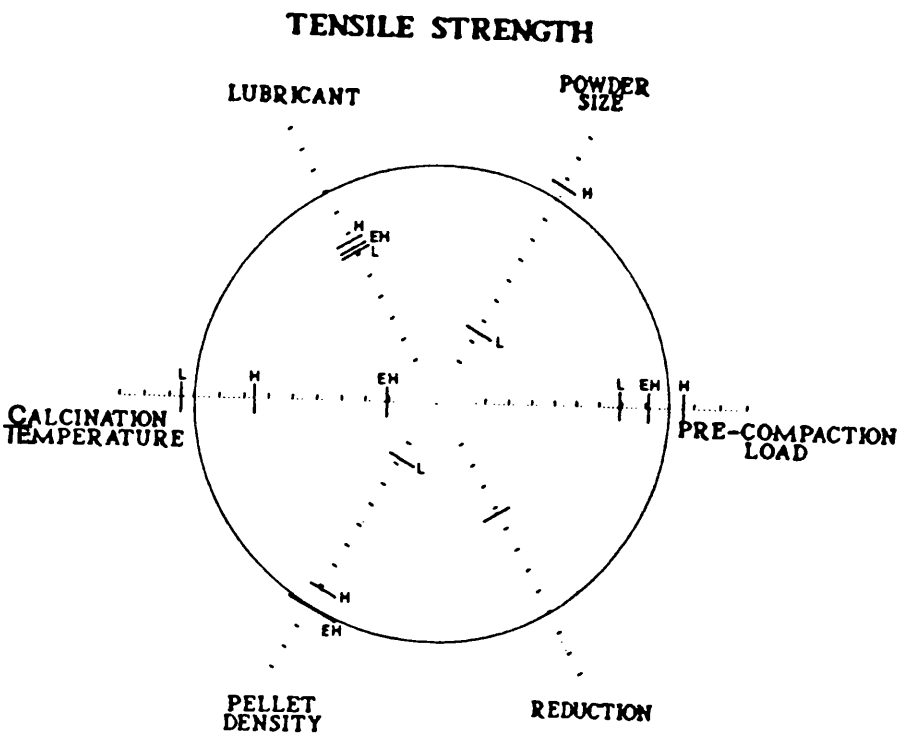

Figure 6.5. Variation of tensile strength with the five catalyst production parameters at their low, normal, high and extra high levels.

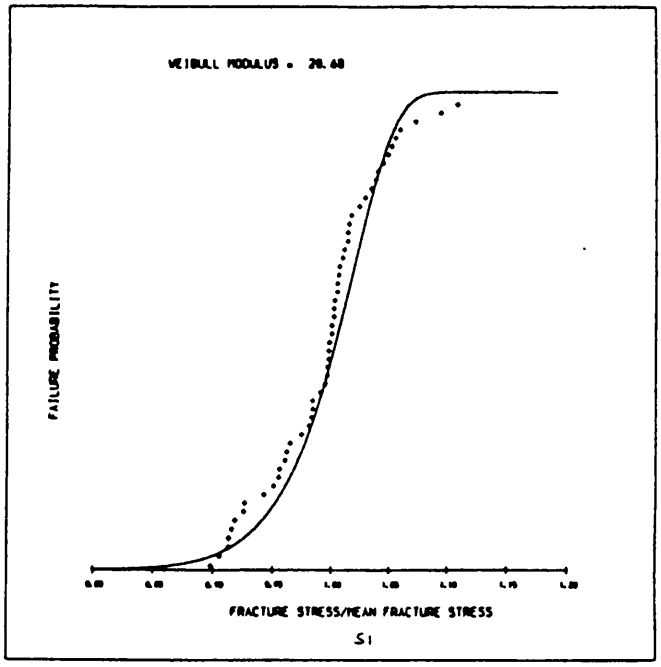

Figure 6.6. Failure probability versus fracture stress plot for sample S-1.

preparation at their low, high and extra high levels. Again, from the figure, the amount of lubricant added did not have a significant effect on the tensile strength. A comparison with the base sample showed that tensile strength was decreased by approximately 24% and 27% due to addition of lubricant at higher levels (S-3 and S-25). Neither were strong variations observed with changes in pre-compaction load: this was in contrast to variations associated with calcination temperature or pellet density. The pellet tensile strength was reduced by a factor in excess of 3 with increased calcination temperature (S-24) as well as with low cut size (S-20) and low pellet density (S-22). This reduction can be partly explained from the corresponding porosity values. During each of these production conditions, the porosity has increased. This causes the pellet strength to be reduced.

The Weibull moduli for a set of catalyst particles were determined for samples S-1, S-24 and S-28 respectively using a computer program supplied by Professor J.M. Newton of the School of Pharmacy. The program asks its user to enter the following data values: number of groups of data, the true solid density, the punch diameter, number of pellets in groups followed by group number, tablet weight, formation pressure, tablet thickness, tablet diameter and tensile failure load. From the program then, for each sample, a plot of failure probability versus fracture stress was obtained along with the Weibull modulus for the test sample. These plots are shown in figures 6.6, 6.7 and 6.8 with corresponding Weibull moduli of 27.91, 28.68 and 30.08 respectively. These indicate that $Cu/Zn/Al_2O_3$ catalysts are not particularly brittle materials. Brittle materials are those materials which are hard but can be broken easily. Usually the Weibull modulus lies between 5 to 40. A value less than 10 would indicate high brittleness. For materials of equal brittleness, (as seen for the ICI LT shift catalysts), the Weibull modulus would remain

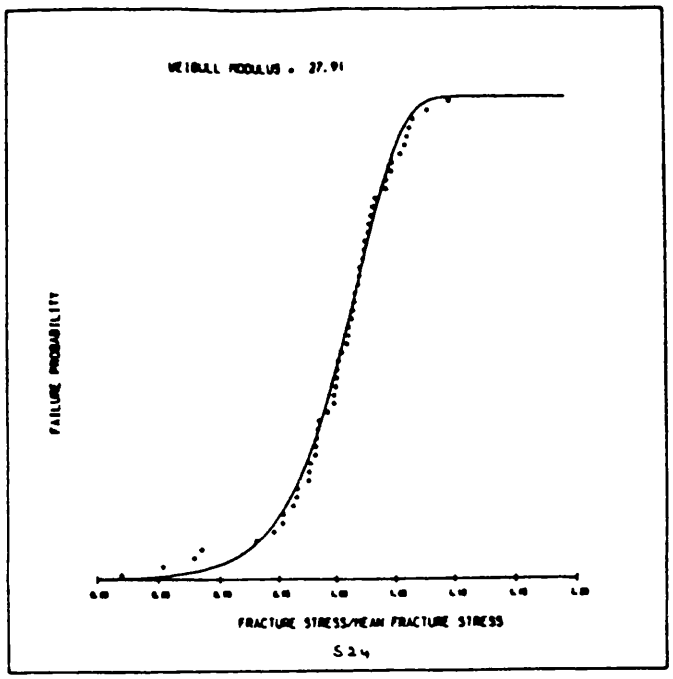

Figure 6.7. Failure probability versus fracture stress plot for sample S-24.

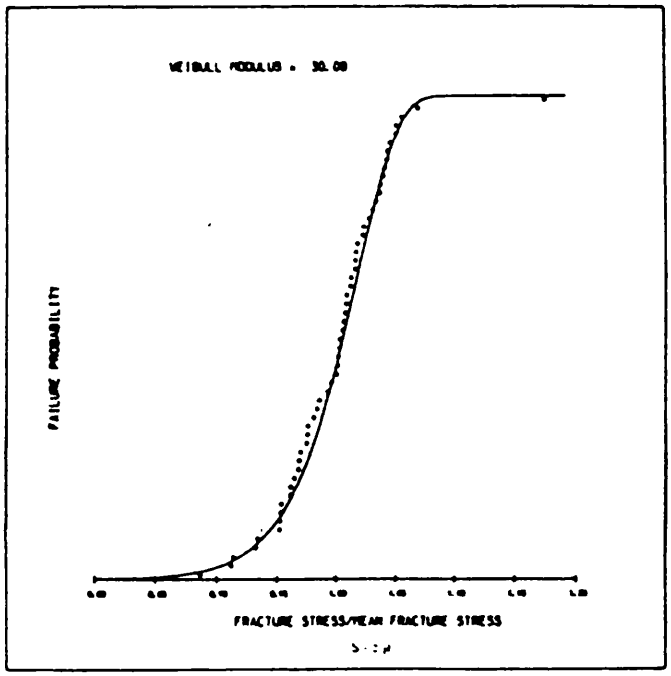

Figure 6.8. Failure probability versus fracture stress plot for sample S-28.

essentially unchanged even if the mean fracture stress changes.

Reviewing the discussions on the main effects of all production parameters on the physical properties of the green catalysts, it can be seen that neither the amount of lubricant added nor the value of the pre-compaction load play a significant role in determining pellet properties. The calcination temperature, cut size or pellet density influence strongly the final pellet properties. Again, from figures 6.1 to 6.5 it is clear that surface area and porosity change by factors of only 2.12 and 1.49 respectively whereas permeability, effective diffusivity and tensile strength change by factors of 6.24, 8.00 and 5.28 respectively. For marketing purposes, a good quality catalyst is always desirable. That is, a catalyst must be produced in such a way that the finished product can fulfill its customer demand. High permeability or high diffusivity catalysts will usually be attractive from a reaction engineering point of view, particularly for co-precipitated catalysts, and hence these can be prepared by choosing a low particle cut size, a low pellet density or an extra high calcination temperature. But these factors also reduce the tensile strength significantly which no potential catalyst producer or customer wants. On the other hand, stronger catalysts can be prepared by increasing the pellet density. But this factor reduces the permeability as well as effective diffusivity significantly. It is seen that tensile strengths are inversely related to diffusivity or permeability when the variables of low cut size, extra high calcination temperature or low pellet density are altered. Therefore, in order to prepare a good quality catalyst there has to be a compromise among each of these production variables at some prescribed intermediate level.

However such a compromise among production

parameters based on their main effects only may provide an optimum condition for regular catalyst manufacture only if the factors considered are independent of each other i.e. noninteracting. If they interact, as will be true in actual practice, this must be taken into account. In this case, a factorial design of experiments is necessary to reduce the overall total number of experiments to manageable proportions.

6.2.2 Discussion based on interaction effects

It is difficult to represent the results of interactions in circular diagrams. Hence all interaction effect results are presented in rectangular x-y plots. These are shown in figures 6.9 to 6.14.

In these figures, values of production variables, or combination of such variables, are as follows: L represents low, H represents high, EH represents extra high, LL represents low-low, LH represents low-high, LEH represents low-extra high, HL represents high-low, HH represents high-high and HEH represents high-extra high. For example, in figure 6.9, LH represents the interaction between low calcination temperature and high cut size and HEH represents the interaction of high calcination temperature and extra high cut size and so on. Only first order interactions have been considered when discussing the results presented in table 6.1.

6.2.2.1 Interaction between calcination temperature and cut size

Figures 6.9 and 6.10 represent the variation of the five physical properties due to the first order interaction between calcination temperature and cut size. In each plot, the main individual effect was also included so that a clear picture could be drawn between each individual effect and their interactions. It is observed from figure 6.9 that the effect of primary particle cut size at all levels was dominant in conjunction with the low calcination temperature. This

can easily be verified from the two main effects of L calcination temperature and L cut size. The LL point is closer to the L cut size point than the L calcination temperature. But it is unclear which parameter is dominant at a high level of calcination temperature. Another clearly obvious point from figure 6.9 is that the low surface areas due to the individual effects of both low and extra high calcination temperature can be increased by interaction with the primary particle cut sizes.

In figure 6.10 for permeability, L calcination temperature was observed dominant for LL and LH points. The LEH point was seen to be dominated by EH cut size. Point HL was dominated by L cut size but for points HH and HEH it was difficult to specify a dominant effect. For diffusivity, LL was dominated by L calcination temperature and LH and LEH were dominated by H and EH cut size respectively. Point HL was dominated by L cut size but the dominant effect in points HH and HEH was unclear. Finally for tensile strength, points LL and LH were dominated by L and H cut size respectively while point LEH was dominated by L calcination temperature. However for points HL, HH and HEH, it was difficult to specify a dominant effect.

6.2.2.2 Interaction between calcination temperature and pelleting density

Figures 6.11 and 6.12 represent the above interaction. In figure 6.11 for surface area and porosity at LL and HL, the effect of L pellet density was dominating but points LH and HH fell in between their two individual effects. Similar effects for LL and HL were observed for permeability, diffusivity and tensile strength in figure 6.12. For LH and HH, the effect of H pellet density was dominant.

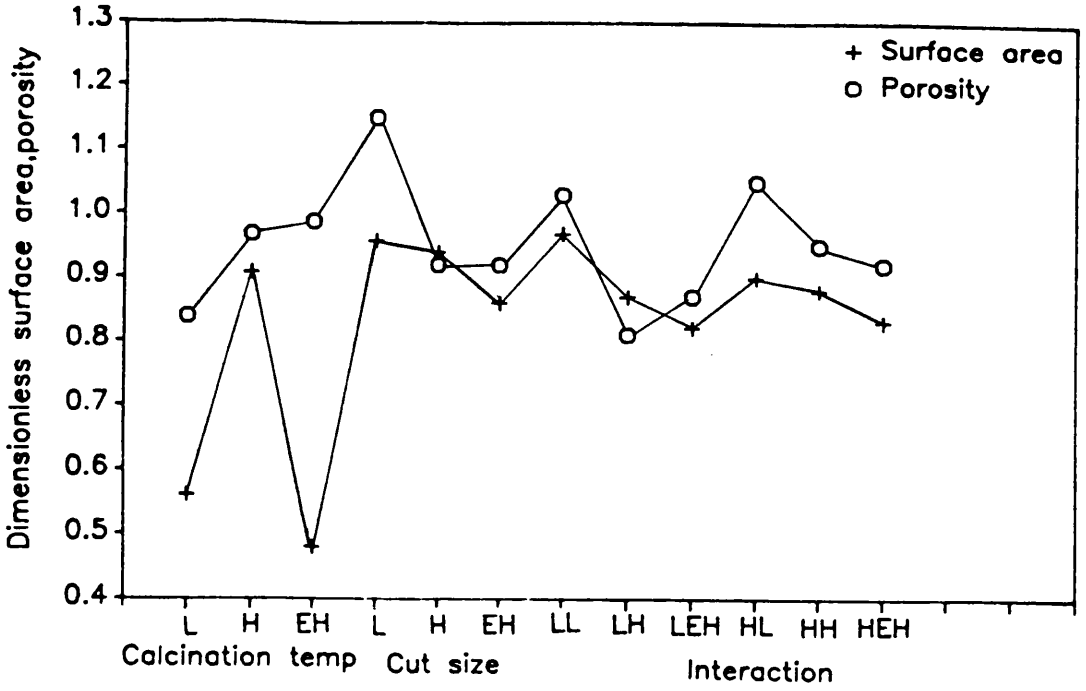

Figure 6.9. Interaction between calcination temperature and cut size.

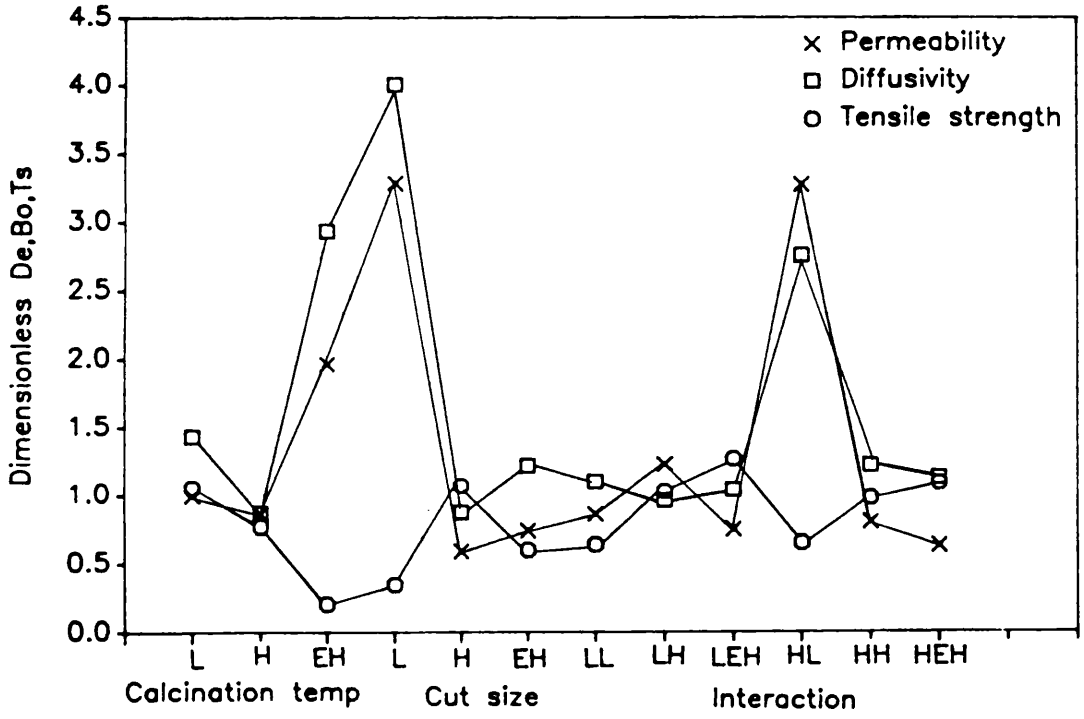

Figure 6.10. Interaction between calcination temperature and cut size.

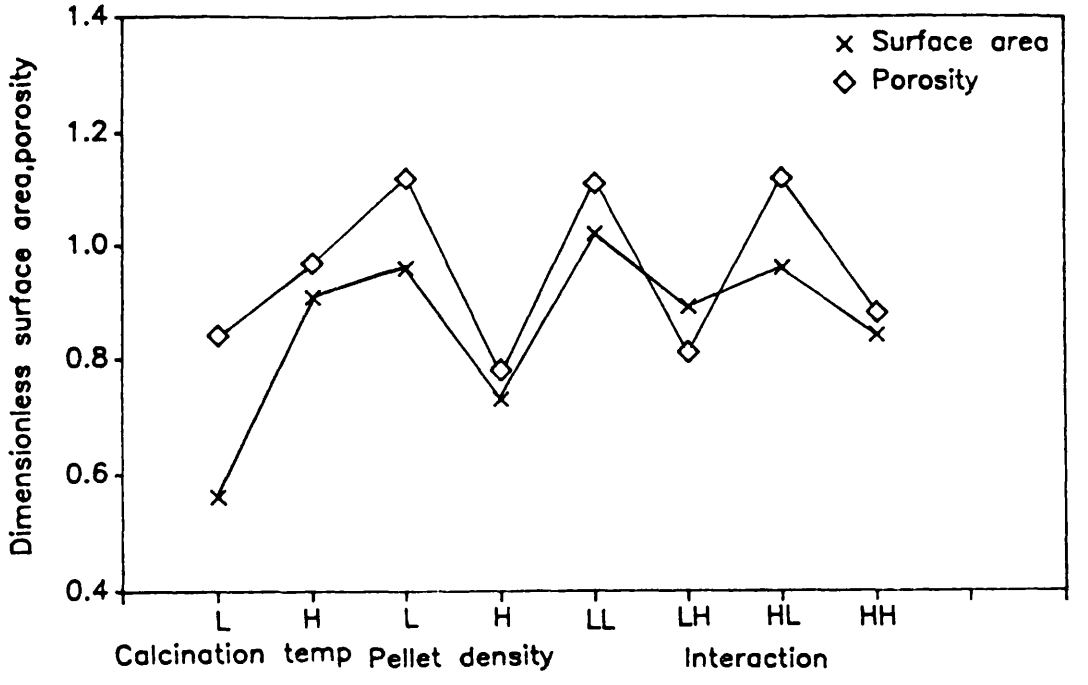

Figure 6.11 Interaction between calcination temperature and pellet density

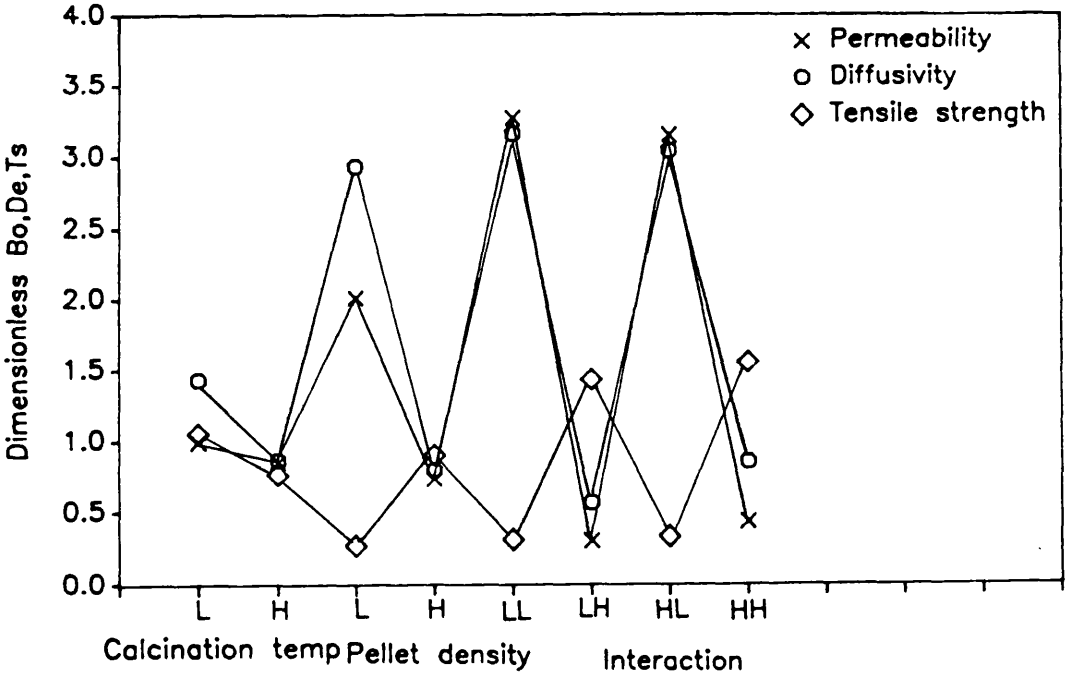

Figure 6.12 Interaction between calcination temperature and pellet density

6.2.2.3 Interaction between cut size and pelleting density

From figure 6.13, it is seen that surface area is weakly dependent on interactions between cut size and pellet density. In the case of porosity, the effect of L cut size has dominated over H or EH pellet density but it is unclear whether the L cut size or the L pellet density is dominant. However at HL and EHL, the effect of low pellet density has prevailed.

In figure 6.14, as with porosity, so also for permeability, diffusivity and tensile strength, the effect of L cut size is dominant. The dominant effect in points HL, HH and HEH is unclear but at EHL it is the low pellet density which is dominant.

Reviewing the discussion of the first order interactions between the calcination temperature, cut size and pelleting density, it is still not possible to specify completely optimum pellet production conditions because second and higher order interactions have not yet been investigated.

6.2.3 Effect of reduction on the five physical properties

As mentioned in Chapter 3, LT shift catalysts are used in reactors after activation by chemical reduction. Therefore, it is desirable to investigate the impact of this reduction on the catalyst's physical properties. Reduction is a chemical transformation process and thus changes in the innermost structure of each individual catalyst particle can be expected.

Upon reduction of the green catalyst samples, porosity was typically increased by 10-15% and permeability and diffusivity by a factor more than 3. Tensile strength decreased by a factor in excess of 3. Of all surface area measurements, about 70% were increased following the reduction step. The results of reduction as

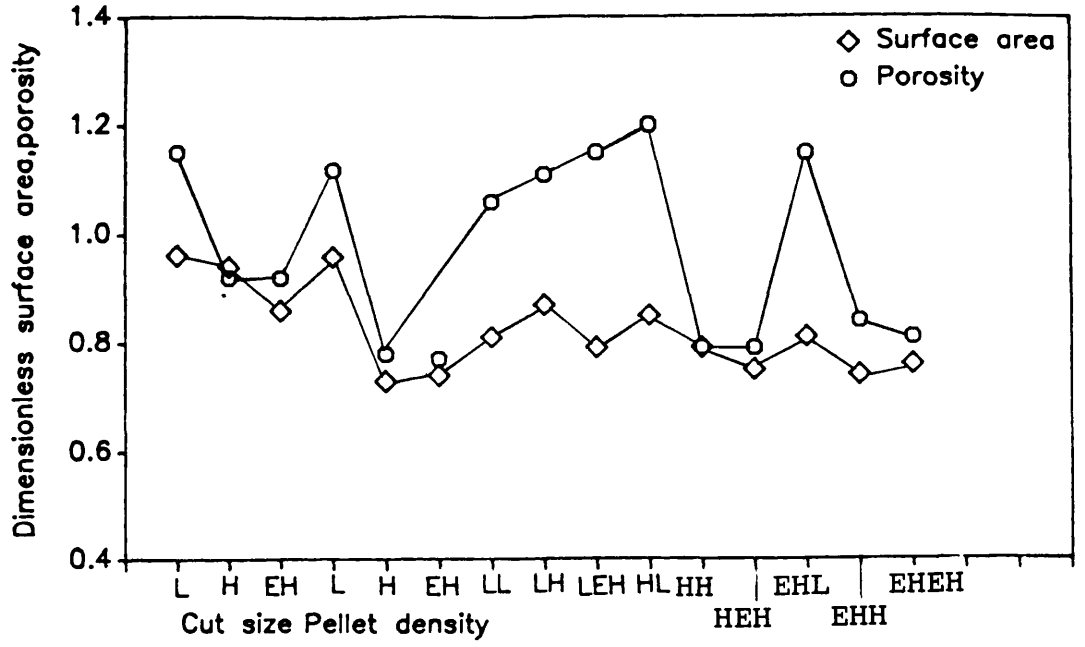

Figure 6.13 Interaction between cut size and pellet density

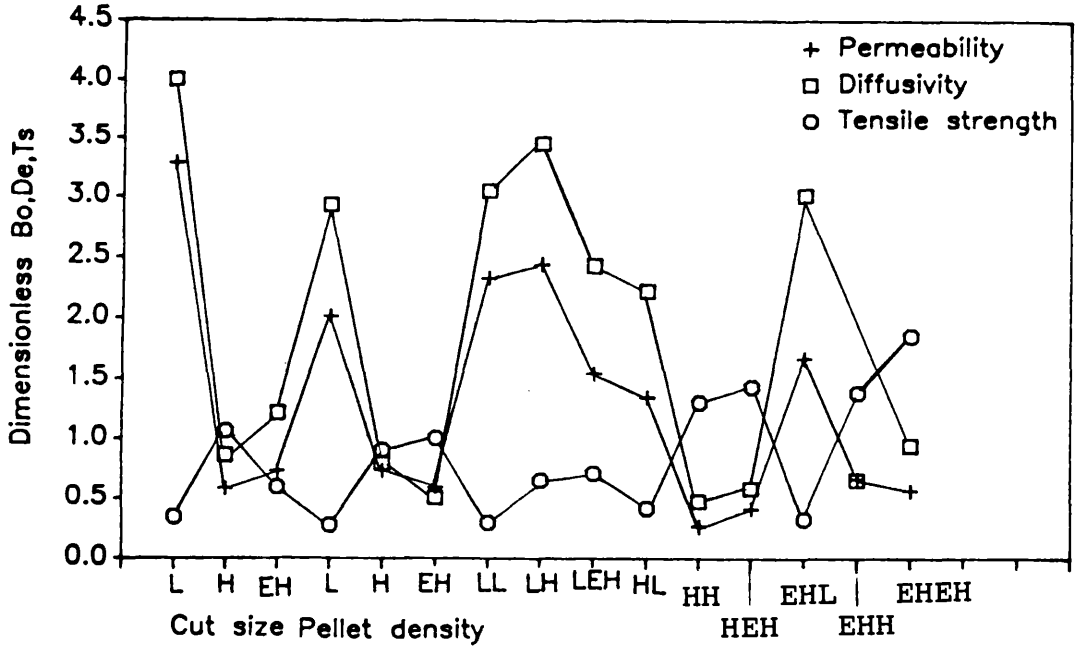

Figure 6.14 Interaction between cut size and pellet density

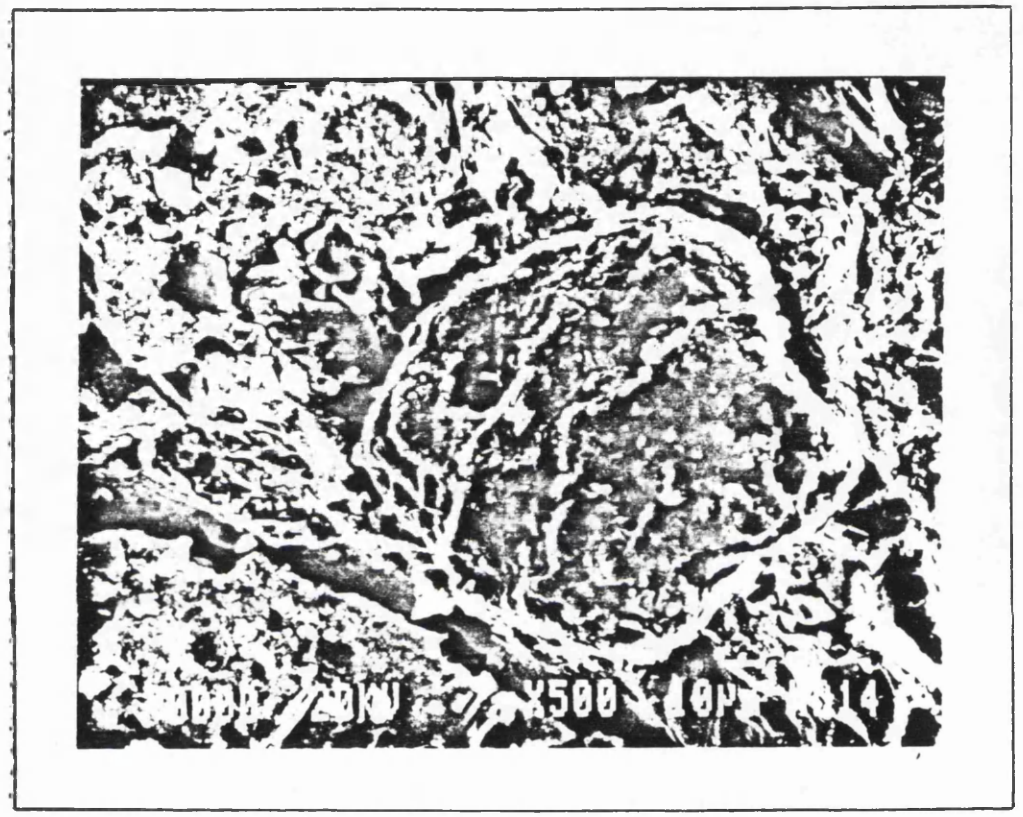

Figure 6.15. SEM photograph for sample S-76 showing the formation of microscopic cracks within the catalyst pellet after reduction.

shown in circular diagrams (figures 6.1 to 6.5) were for the base case sample only: surface area, porosity and tensile strength decreased while permeability and effective diffusivity increased upon reduction.

The most interesting results were found for the permeabilities of some of the reduced catalyst samples. An increase in excess of 400 fold was observed though the effective diffusivity for those same samples had increased by a factor of only 2. The only explanation for this seemed to be the possible development of microscopic cracks formed during the chemical reduction process. The presence of these was subsequently confirmed by visual inspection using the Scanning Electron Microscope (JEOL, JSM-820) as shown in the figure 6.15. Part of all properties other than tensile strength, tend to increase on reduction.

One important point is clear here that the effective diffusion coefficient is strongly dependent on the porous geometry of the individual catalyst particle.

6.2.4 Pore size distribution

It is not possible to discuss and include all the results and plots of pore size distribution in this thesis. Hence some selected ones will be discussed only. It can be recalled from Chapter 2 of this thesis that pore size distribution measurements are required to predict the effective diffusion coefficient within a porous catalyst particle.

The pore size distribution of the base case sample (S-1), using mercury intrusion porosimetry, is presented in table 6.2 and in figure 6.16 respectively. From table 6.2, it is evident that at a maximum pressure of 412.85 MN/m^2 (equivalent to 59878.4 psia) mercury would penetrate pores of up to 3.6 nm (18 A radius) diameter only. The cumulative pore volume of 0.2856 dm^3/g is an apparent value because there will be more pore

MICROMERITICS REPORT: MERCURY INTRUSION POROSIMETRY

ICI MICROMERITICS LABORATORY

Sample description: S-1

Analysis summary		Total volume intruded	0.2856 ml/g
Contact angle = 141.3		Total area calculated	72.777 m^2/g
Surface tension	= 480	Median pore size (vol)	86 A° rad
(dynes/cm)		Median pore size (area)	68 A° rad
		Average pore size (4V/A)	78 A° rad

Pressure (psia)	Pore Size (A° rad)	Cum.volume (ml/g)
1.3919	780662	0.0000
2.5	440136	0.0007
5	217806	0.0014
7.5	145417	0.0019
9.9	109304	0.0021
12.5	86893	0.0026
14.6	74386	0.0028
20	54411	0.0030
29.6	36740	0.0031
38.8	27999	0.0031
58.9	18455	0.0031
81	13414	0.0031
102.2	10627	0.0033
160	6792	0.0034
291.7	3725	0.0039
407.9	2664	0.0040
658	1651	0.0046
1018.4	1067	0.0052
1535.1	708	0.0061
2495.3	435	0.0077
3968.4	274	0.0119
6456.8	168	0.0351
10032.9	108	0.0817
15009.2	72	0.1822
20194.5	54	0.2485
25022.6	43	0.2660
30014.8	36	0.2728
35126.1	31	0.2770
40461	27	0.2796
45438.3	24	0.2817
50490.1	22	0.2833
55482.3	20	0.2845
59878.4	18	0.2856

Table 6.2. Pore size distribution using mercury porosimetry for sample S-1.

volume associated with pores of less than 3.6 nm diameter. The largest part of the pore volume was found in pores between 33.6 to 10.8 nm radius. These constitute about 75% of the total pore volume. The average pore diameter based on a volume divided by area basis was 15.6 nm. At standard conditions of temperature and pressure, the mean free path of He is 274.5 nm (Weast, 1978). A 33.6 nm diameter pore is approximately 10 times less, and a pore diameter of 3691 nm is approximately 10 times greater than the mean free path of He. Hence the meso pore region (transition diffusion region) chosen for He was from pore diameters between 33.6 to 3691 nm. Below 33.6 nm, it was assumed that there was pure Knudsen diffusion and above 3691 nm, there was pure bulk diffusion.

Figure 6.16 simply represents the differential as well as the cumulative distribution of pores according to their radius. For the differential distribution only one peak was seen because mercury porosimetry can not be used to investigate pore radii below 1.8 nm. In this particular case, there was essentially no penetration below 2.7 nm.

A pore size distribution measurement on the base sample S-1, was also carried out after chemical reduction. The average pore radius did not change significantly but the cumulative pore volume was decreased by about 11%.

For a sample prepared with an extra high calcination temperature, the average pore diameter was measured as 18.2 nm with a cumulative pore volume of 0.2496 dm^3/g. About 66% of the total pore volume was found in pores of diameter between 14.3 to 54.4 nm. In this case, two peaks, that is, a bimodal pore size distribution was observed (see figure 6.17).

The pore size distribution of a sample prepared

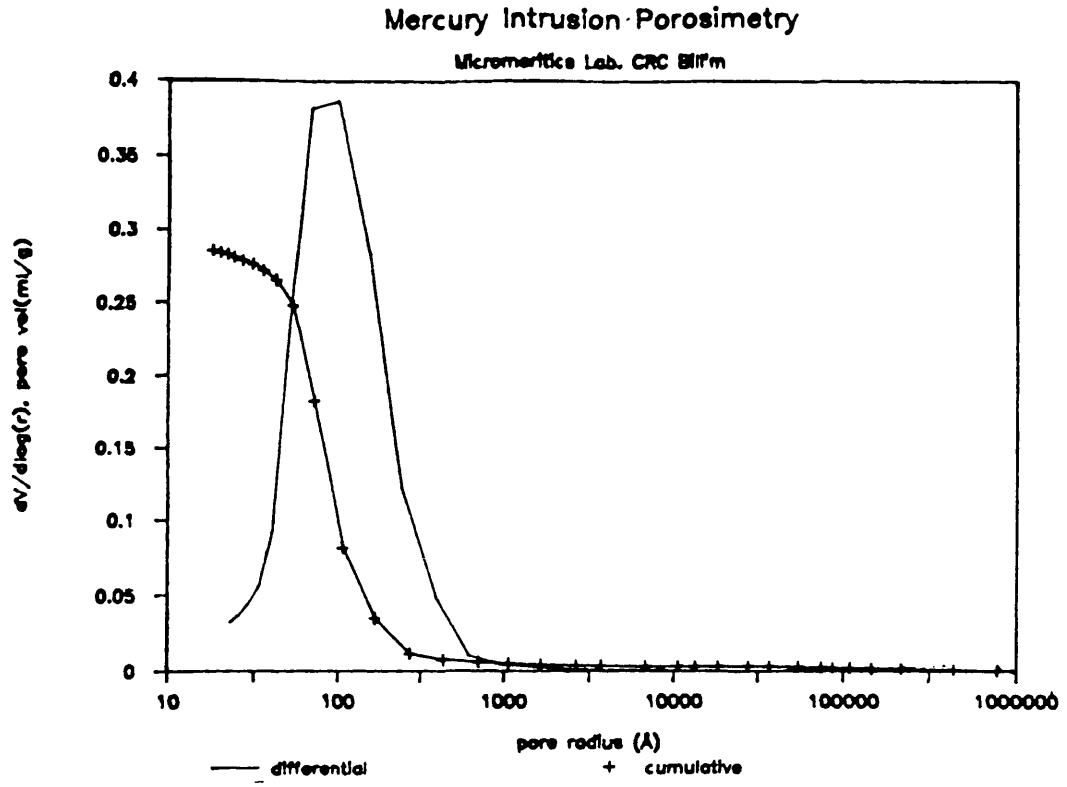

Figure 6.16. Differential and cumulative pore volume distribution for sample S-1.

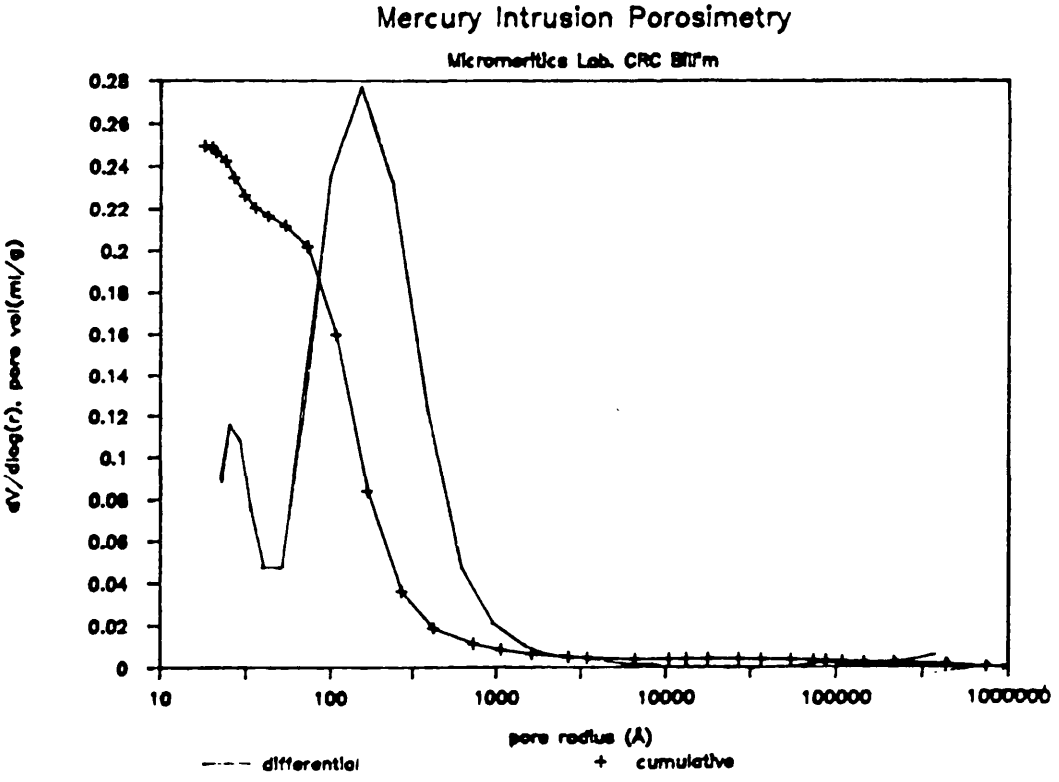

Figure 6.17. Differential and cumulative pore volume distribution for sample S-24.

with a extra high pelleting density showed an average pore diameter of 11.4 nm and a cumulative pore volume of 0.1846 dm^3/g. These figures correspond to a decrease in both pore diameter and pore volume by about 27% and 35% respectively with respect to the base sample S-1.

The sample which exhibited a relative permeability value in excess of 400 following reduction was seen to have an average pore radius of 8.6 nm with a cumulative pore volume of 0.3497 dm^3/g. Thus an increase of about 22% in the pore volume and about 10% in the pore radius were observed for this sample in comparison to the base case sample.

6.3 Other investigations

As the calcination temperature plays a part during catalyst manufacture, investigations at calcination temperatures of 200 ^oC (S-51), 500 ^oC (S-62) and 600 ^oC (S-63) other than low, normal, high and extra high levels were also carried out (see table 3.3, Chapter 3). At 200 ^oC, apart from the tensile strength which has increased slightly, the remaining four properties have decreased. However, increase of tensile strength by 1.15%, decrease of surface area and porosity by 50.43% and 23.13% relative to sample S-1, were comparable to the low calcination temperature of 250 ^oC (S-19). But in the case of effective diffusivity and permeability, such a trend did not exist. That is a decrease of 69.23% in permeability and a decrease of 49.30% in diffusivity were noticed.

At 500 ^oC which was slightly higher than the high level of calcination temperature (S-10), a 17.21% decrease in surface area and a 7.62% decrease in tensile strength, with porosity unchanged, were observed. At this temperature effective diffusivity and permeability increased only slightly.

At 600 ^oC, surface area was decreased by 33.91%.

Porosity, tensile strength and permeability decreased only slightly while effective diffusivity increased by 28.17%. Thus with the increase of the calcination temperature, a tendency of achieving reduced surface area, reduced porosity and reduced tensile strength were obvious. Hence one should expect to observe high effective diffusivity and high permeability.

During the first phase of the work some second order interactions between the amount of the lubricant added, pre-compaction load and calcination temperature were also studied. Samples S-14, S-15, S-17 and S-18 represent these interaction effects (see Chapter 3, table 3.2). As the investigation proceeded, it was observed that the amount of lubricant added and the pre-compaction load do not noticeably alter the final physical characteristics of the catalysts. Hence the results of these interactions were of little commercial or academic interest.

6.4 Matching of experimental results with the model solution

6.4.1 Matching of experimental results with the isobaric model solution

6.4.1.1 Moments method

The diffusion coefficient obtained from the left hand side chamber equation tends to be dominated by the mixing characteristics within the left hand chamber rather than the values of the diffusion coefficients. However, the diffusion coefficient obtained from the right hand side chamber equation depends strongly on both D_{Ae} and D_{Be} and hence gives more reliable estimates of these parameters. All unsteady state diffusivities which are reported for both ICI $Cu/Zn/Al_2O_3$ LT shift catalysts and for the BP porous carbon samples (see Chapter 7) were interpreted from the right hand side experimental tracer response curve using the right hand side moments equation. Taking the unsteady state diffusivity as the correct value, the %difference between the steady and

Sample No:	Experimental Steady State $D_e \times 10^6$ m^2/s	Unsteady State $D_e \times 10^6$ m^2/s using Moments method	% variation between D_e steady state & unsteady state value
S-60	1.60 ± 0.80	1.70 ± 0.12	5.88
S-62	1.70 ± 0.30	1.40 ± 0.30	21.43
S-68	1.30 ± 0.30	1.40 ± 0.20	7.14

Table 6.3. Comparison of experimental steady state D_e with the unsteady state value as obtained from the isobaric model solution using moments method.

Sample No:	Experimental steady state $D_e \times 10^6$ m^2/s	Unsteady state $D_e \times 10^6$ m^2/s from non-isobaric model	% variation between D_e steady state & unsteady state value
S-1/7	1.20	1.40	14.29
S-24/2	4.04	2.61	54.79
S-37/2	4.73	5.82	18.23
S-46/2	0.75	0.82	8.24

Table 6.4. Comparison of experimental steady state D_e with the unsteady state value as obtained from the non-isobaric model solution using numerical method.

unsteady state diffusivities was (for example for sample S-60) (1.70 - 1.60) x 100 / 1.70 = 5.88%. Thus an agreement within +/- 21% between steady and unsteady state diffusivities was observed for all the samples tested (see table 6.3).

6.4.1.2 Numerical method

Equation (4.5) was also solved numerically for ICI sample S-1/7 using the following known or estimated data: $q_{1in}=1*10^{-6}$ m^3/s; $q_{1out}=0.994*10^{-6}$ m^3/s; $q_{2in}=1.77*10^{-6}$ m^3/s; $q_{2out}=1.776*10^{-6}$ m^3/s; V_1 $=6.75*10^{-8}$ m3; V_2=7.20*10-8 m3; ε=0.549 and D_e=1.2*10-6 m2/s. The D_e value used to solve the model was the experimentally obtain steady state value. The numerically based predictions were compared with the observed experimental transients as shown in figure 6.18. Clearly poor agreement exists between theory and experiment, illustrating the need for the more complex non-isobaric model.

On the other hand, the BP porous carbon experiments (see Chapter 7) were conducted making a step change in gas mole fraction from N_2 to 95 mole% N_2 and 5 mole% He (almost an isobaric condition). Numerical solution for sample C2 using the following sample data: $q_{1in}=q_{1out}=$ 1 cm^3/s; $q_{2in}=q_{2out}=1.77$ cm^3/s; V_1 = V_2= 0.25 cm3; ε=0.61 and D_e=0.14 cm2/s (experimental steady state value) showed very good agreement with experiment as shown in figure 6.19. This demonstrates that for some classes of porous materials an isobaric model can be adequate for describing diffusion and flow within a porous catalyst particle. The model can then be used to describe given experiments and diffusion coefficients evaluated by an appropriate parameter estimation and extraction routine.

6.4.2 Matching the experimental results with the non-isobaric model solution

Using the same data values from section 6.4.1.2 for q_{1in}, q_{1out}, q_{2in}, q_{2out}, V_1, V_2 and ε and assuming

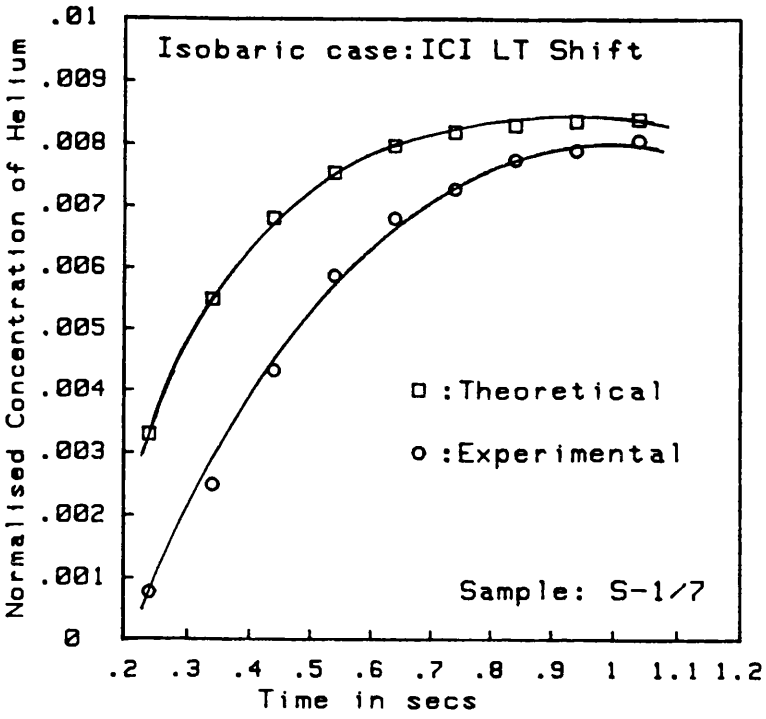

Figure 6.18. Matching of experimental results with the isobaric model for ICI LT shift catalyst.

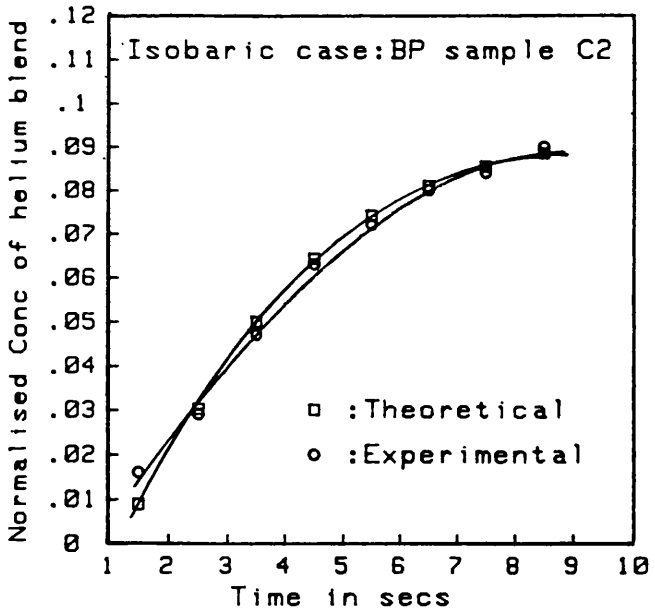

Figure 6.19. Matching of experimental results with the isobaric model for BP porous carbon system.

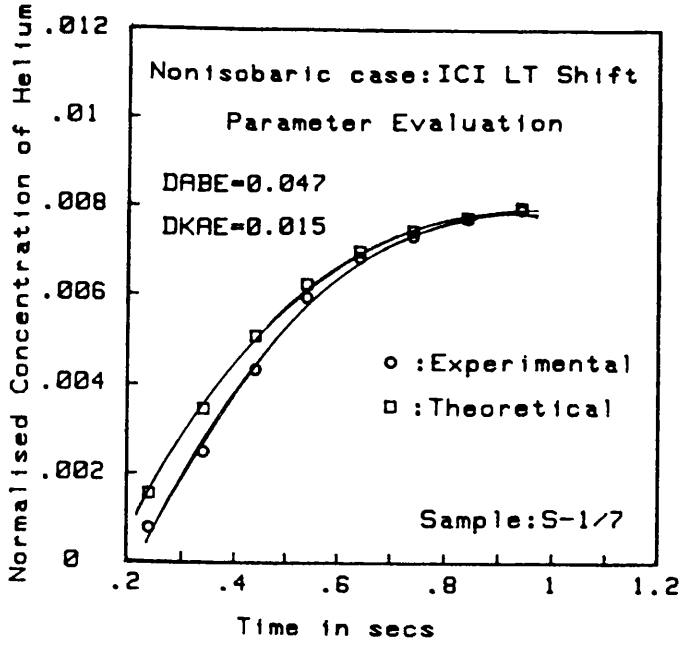

Figure 6.20. Solution of the non-isobaric model using the initial guesses for D_{ABe}=0.047 cm^2s^{-1} and D_{KAe}=0.015 cm^2s^{-1} (Sample S-1/7).

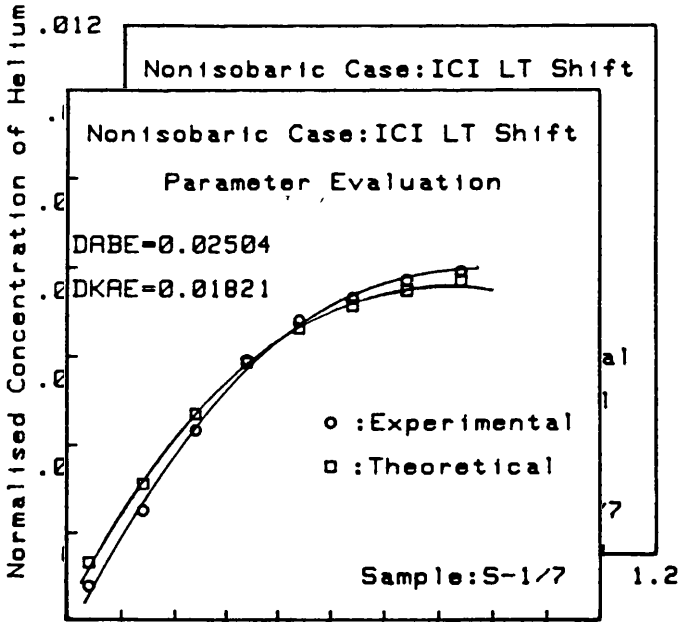

Figure 6.21. Solution of the non-isobaric model showing best match with the experiment for D_{ABe} = 0.025 and D_{KAe} = 0.018 cm^2s^{-1} (Sample S-1/7).

$D_{ABe}=4.7*10^{-6}$ m^2/s and $D_{KAe}=1.5*10^{-6}$ m^2/s as the starting iteration points, equations (4.1) and (4.2) were solved for sample S-1/7 and the predicted transient in the mole fraction of helium in flow rate q_{2out} was compared with the experimentally observed value. A comparison of these is shown in figure 6.20.

An optimal parameter search routine for D_{ABe} and D_{KAe} was then incorporated into the main Fortran computer program. The routine takes the starting two values of D_{ABe} and D_{KAe} and calculates the transient mole fraction values. A sum of the square of the differences between the experimental and transient mole fraction values is then calculated by the routine. If this sum is less than a specified value, then the search procedure is terminated and the final values are reported. Otherwise the program recalculates this sum for a new set of D_{ABe} and D_{KAe} values and continues until the above condition is satisfied. This method showed that values of $D_{ABe}=2.5*10^{-6}$ m^2/s and $D_{KAe}=1.8*10^{-6}$ m^2/s provided the best match with the experimental transient curve as shown in figure 6.21. The unsteady state diffusivity was then calculated using the composition dependency of diffusion coefficient formula as shown below.

Sample calculation for diffusivity prediction using composition dependency of diffusion coefficient

Sample no S-1/7

An optimum parameter search routine provided a D_{ABe} value of 0.025 cm^2/s and a D_{KAe} value of 0.018 cm^2/s.

Now $$D_{Ae} = \frac{D_{ABe}\, D_{KAe}}{(1 - \alpha_{AB} x_A) D_{KAe} + D_{ABe}}$$

$$\alpha_{AB} = 1 - (M_A / M_B)^{0.5} = 0.622 \text{ (see nomenclature)}$$

$$x_A = 1 \text{ (for pure helium)}$$

$$\text{Hence} \quad D_{Ae} = \frac{0.025 \times 0.018}{(1 - 0.622 \times 1)0.018 + 0.025}$$

$$= \underline{0.0141}\ \underline{cm^2/s}$$

Using Bosanquet extrapolation formula, D_{Ae} is calculated to be

$$D_{Ae} = \frac{D_{ABe}\, D_{KAe}}{D_{ABe} + D_{KAe}} = \frac{0.025 \times 0.018}{0.025 + 0.018}$$

$$= \underline{0.0105}\ \underline{cm^2/s}$$

For this sample, a value of $1.4*10^{-6}$ m^2/s resulted which compared with the steady state diffusivity of $1.2*10^{-6}$ m^2/s. Again taking the unsteady state diffusivity as the base case value, the %difference in the steady state diffusivity value was (1.4 - 1.2) x 100 / 1.4 = 14.3%. That is, both agreed to within 20% (see table 6.4).

Some investigators claim that it is not necessary to use an expression for diffusion which takes into account this composition dependency of both bulk and Knudsen diffusion coefficients. Rather a Bosanquet extrapolation formula is sufficient. This discrepancy was observed here. For example, for sample S-1/7, using composition dependency of the diffusion coefficient a value for D_{Ae} was found to be 1.40×10^{-6} m^2/s whilst the Bosanquet formula would yield a value for D_{Ae} of 1.05×10^{-6} m^2/s and so be 25% lower. This indicates that use of the Bosanquet approximation for ICI LT shift catalysts can lead to an underestimated D_{Ae} by as much as one quarter.

Using the pore size distribution data for sample S-1 from section 6.2.4 table 6.2, and using equation (1.4) for D_{KAe} from Chapter 1, under the assumption that

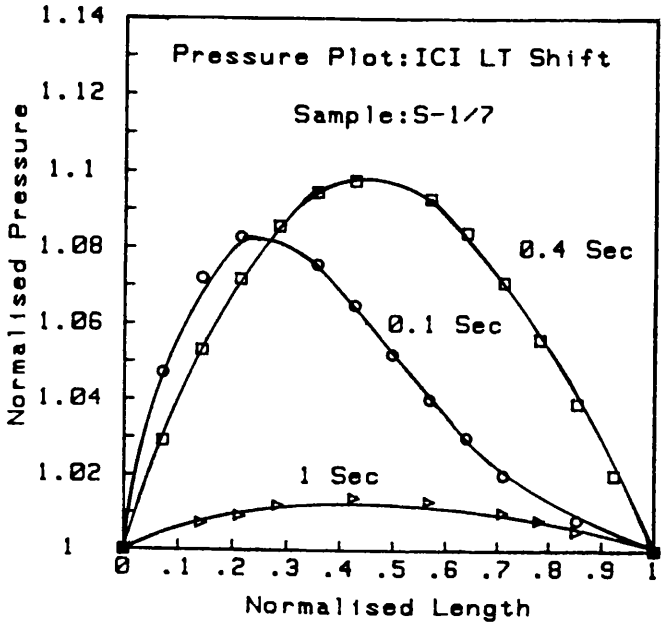

Figure 6.22. Development of pressure within the pellet as obtained from the non-isobaric model solution for sample S-1/7.

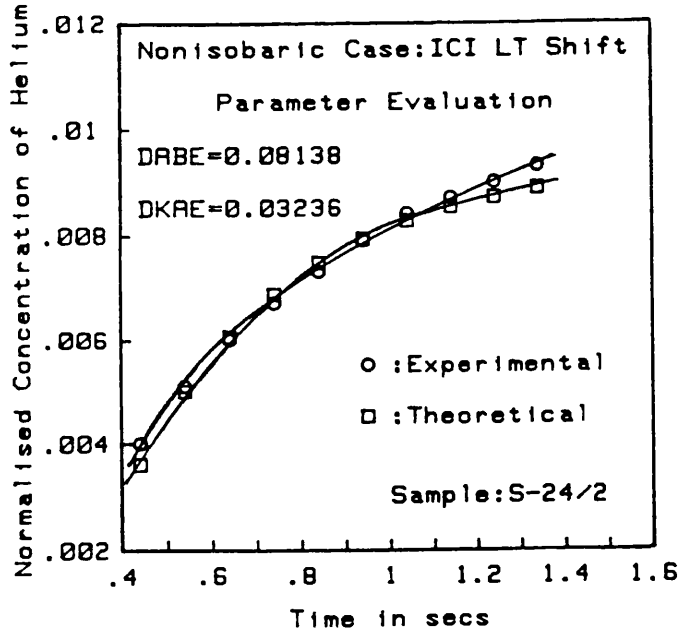

Figure 6.23. Solution of the non-isobaric model showing best match with the experiment for D_{ABe} = 0.081 and D_{KAe} = 0.032 cm^2s^{-1}(Sample S-24/2).

the diffusion process is solely by a Knudsen mechanism, the tortuosity factor for sample S-1/7 was found to be 1.41 . Using the model provided by Waldram et al for the tortuosity factor, which is equation (1.1) of Chapter 1, a tortuosity factor for the Knudsen diffusivity was predicted to be 2.35 (see Appendix 6 for this calculation). Thus for this sample and for Knudsen diffusion, equation (1.1) holds only very approximately. For bulk diffusion agreement is worse (see Appendix 6).

The theoretical prediction for the increase of pressure within the porous pellet is shown in figure 6.22 for sample S-1/7. Since He diffuses faster into the porous pellet than N_2 counter diffuses, some He accumulates inside the porous pellet due to net flow. This leads to the development of pressure build-up within the pellet. At time 0.1s, the increase of pressure was rapid and steep. When the time was 0.4s, the pressure rise was maximum at about the centre line of the pellet. As time proceeded further, the pressure started to fall and finally approached unity when the steady state condition was attained. This indicates clearly that LT shift catalysts need a non-isobaric model for adequate description of transient diffusion and flow phenomena within them.

The non-isobaric model was also tested for samples S-24/2 (figure 6.23), S-37/2 (figure 6.24) and S-46/2 (figure 6.25) and the results are tabulated in table 6.4. It was observed that apart from sample S-24/2, the steady and unsteady state diffusivities of the other samples tested agreed to within 20%. Sample S-24/2 showed a worse deviation of more than 50%. Samples S-24/3 as well as S-24/4 showed a similar trend. The only explanation for these large deviations is either that the experiment was conducted with substantial error or that a more refined model of the porous matrix is required to describe this particular sample.

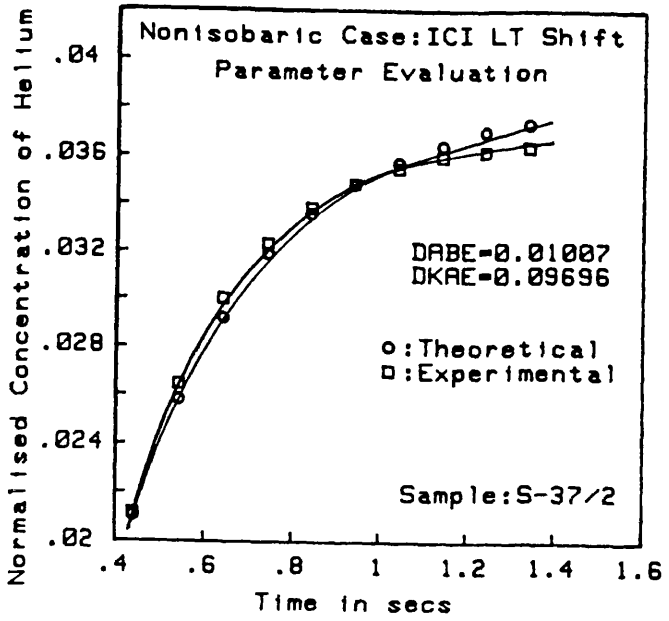

Figure 6.24. Solution of the non-isobaric model showing best match with the experiment for D_{ABe} = 0.0101 and D_{KAe}=0.097 cm^2s^{-1}(Sample S-37/2).

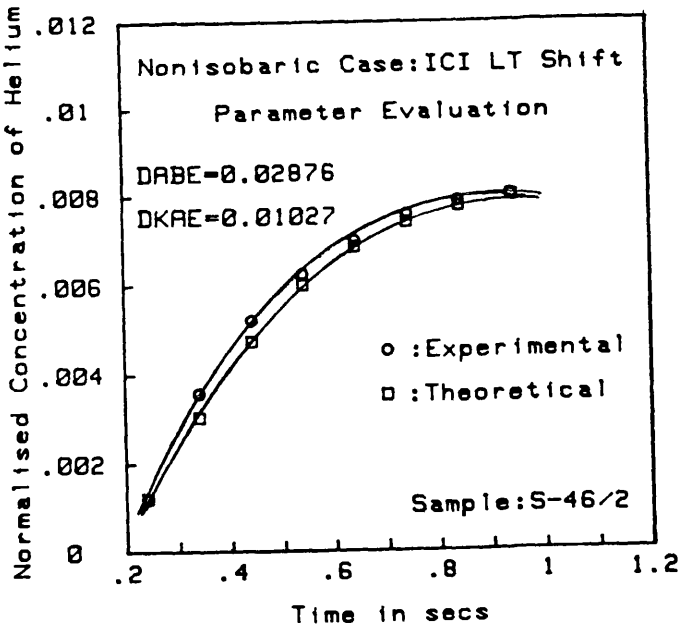

Figure 6.25. Solution of the non-isobaric model showing best match with the experiment for D_{ABe} = 0.029 and D_{KAe} = 0.0103 cm^2s^{-1}(SampleS-46/2).

CHAPTER - 7

EXPERIMENTAL RESULTS AND DISCUSSION: POROUS CARBON SUPPORT MATERIALS

7.1 Introduction

For a brief period porous carbon support materials were studied in addition to LT shift catalysts. This resulted from a research contract between UCL and BP Research Centre, Sunbury and made use of the same permeability and diffusivity apparatus as was used for the LT shift catalyst studies. The results are reported here because they present an interesting contrast with the results for LT shift catalysts. In addition the carbon materials are of great potential interest as their method of preparation allows the properties of the porous carbon matrix to be tailor made for specific duties. Porosity, pore size distribution and the relative balance between macro and micro porosity can be adjusted by varying the detailed production conditions for the carbons. These materials appear to be in use already as supports for a new ruthenium based ammonia synthesis catalyst (Twigg, 1989).

Four cylindrical carbon specimens of approximately 105 mm length and 18 mm diameter were supplied by BP. They were prepared from a range of primary particle size carbon resins as detailed below:

Sample no	Primary particle size (μm)
A	<50
B	50-100
C	150-200
D	200-250

The objective was to determine the steady and the unsteady state binary gas effective diffusion coefficients for He/N_2 and also the permeation coefficients.

7.2 Theory

Theories and derivations for determining the above have been presented in Chapters 2 and 4 of this thesis as well as in Bhowmik, 1989; Bhowmik 1990; Waldram 1985a and Burghardt and Smith, 1979.

7.3 Sample preparation

All porous carbon samples were prepared in the Material Sciences Branch of BP Research Centre, Sunbury, following the steps shown in figure 7.1 (Bhowmik, 1990).

The commercial Novolak resin was partially cured and then ground and sieved to obtain the four previously mentioned particle size ranges. Hexamethylene tetramine was added as a cross linking agent to these powdered materials and they were then heated to 150 ^{o}C for further cross linking and chemical bonding.

The porous phenolic resin was then carbonised at 900 ^{o}C in a nitrogen atmosphere for a period of 18 hours during which the resin lost approximately 50% of its weight and shrank both axially and radially by 30% roughly.

7.3 Experiments and results

A total of 8 carbon rods i.e. two from each sample were supplied by BP. From these eight 18 mm length specimens were cut to give pellets with length to diameter ratio exactly equal to 1. Permeabilities were determined by both the integral and differential methods. A plot of permeation volumetric flow rate versus pressure differential is given in figure 7.2.

From the slope of this plot at $\Delta P = 0$ and using equation (2.7) from Chapter 2, the permeability is determined. This method is called the differential method of finding the permeability. However the integral method provides one permeability value (equation 2.8 of Chapter 2) from each measured permeation volumetric flow rate and

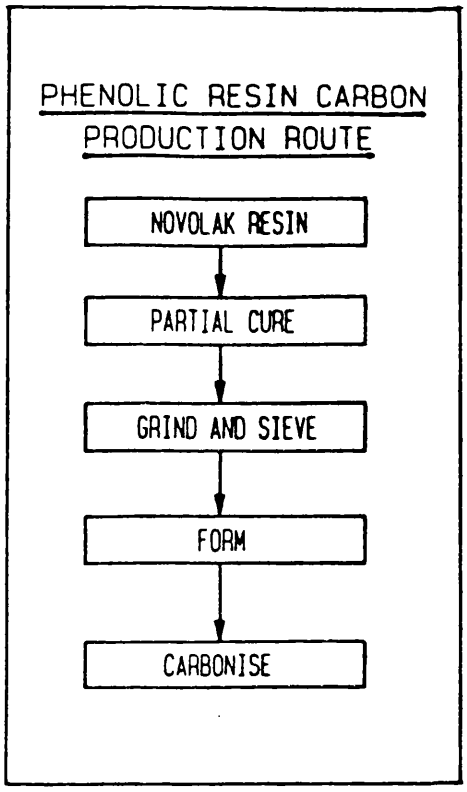

Figure 7.1. Production route for porous carbon material.

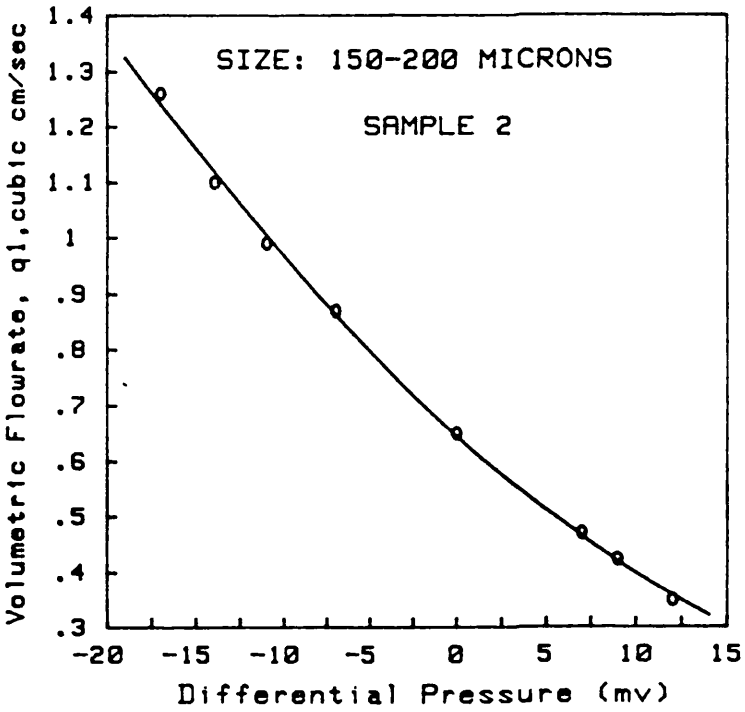

Figure 7.2. Plot of permeation volumetric flow rate versus pressure differential for sample C2.

pressure differential. Hence a mean value of permeability with standard deviation is quoted, whenever the integral method is used. See Appendix 8 for a sample calculation. Steady state binary gas diffusion coefficients were determined by making a step change from pure N_2 to a blend of 95 mole% N_2 and 5 mole% He. Unsteady state diffusivities were computed by equating the expression for the first moment of the system response obtained from the model equations (equations 4.10 and 4.11 of Chapter 4) with the reading obtained experimentally from the right hand side of the test cell.

The unsteady state effective diffusion coefficient is dependent on the pellet porosity. At the time of the diffusion measurements ε was not known. So plots of D_e versus ε were given for each material and the relationships were expressed analytically by regression analyses. This enabled BP to evaluate D_e once they measured ε. Samples A1, A2 and D1 showed a second order fit between D_e and ε while a linear relation was observed for the remaining five samples. Coefficients of the regression analysis are provided in Appendix 7. Results of diffusivity depend on the porosity and are shown in table 7.1. Table 7.2 represents all the results for the porous carbon materials. Note here that the bulk and skeletal densities as well as the porosity as appearing in table 7.2 were determined at BP Research Centre, Sunbury. Detailed experimental procedures are available in sections 2.5 and 2.6 of Chapter 2 and in sections 5.3 and 5.4 of Chapter 5 of this thesis and also in Bhowmik, 1989 and Bhowmik, 1990.

7.4 Discussion and conclusions

Permeabilities determined from both methods agreed to within 4% apart from for sample D and increased by a factor more than 5 with the same factor increment in the primary carbon particle size. A trend of decreasing diffusivity was obvious from the tabulated data with increasing particle size and a 36% decrease was observed

Table 7.1. Results of diffusivity as a function of porosity.

Sample		Effective diffusivity, D_e, $\times 10^4$, (m^2/s)				
		Steady state	Unsteady state			
			ε = 0.31	ε = 0.41	ε = 0.51	ε = 0.61
A < 50 μm	1	0.25	0.17	0.21	0.23	0.26
	2	0.25	0.15	0.18	0.22	0.23
B 50–100 μm	1	0.21	0.13	0.15	0.17	0.19
	2	0.19	0.12	0.14	0.16	0.18
C 150–200 μm	1	0.14	0.10	0.12	0.14	0.16
	2	0.14	0.11	0.13	0.15	0.17
D 200–250 μm	1	0.15	0.12	0.13	0.16	0.18
	2	0.17	0.11	0.13	0.15	0.17

Table 7.2. Experimental results for BP porous carbon.

Sample		Density ρ /g cm^{-3}		Porosity ϵ		Effective Diffusivity De x $10^4/(m^2s^{-1})$		Permeability Bo x $10^{12}/m^2$	
		1 Skeletal	2 Bulk	3	4	Steady State	Unsteady State	Integral Method	Differential Method
A < 50 μm	1	1.890	0.715	.62	-	.25	.26	3.1 St. Dev = 0.23	3.2
	2		0.523	.72	.64	.25	.24	3.8 St. Dev = 0.56	3.8
B 50-100 μm	1	1.859	-	-	-	.21	-	3.5 St. Dev = 0.30	3.5
	2		0.719	.61	.52	.19	.18	2.3 St. Dev = 0.16	2.4
C 150-200 μm	1	1.904	0.758	.60	.52	.14	.16	5.6 St. Dev = 0.40	5.7
	2		0.736	.61	.47	.14	.17	7.3 St. Dev = 0.87	7.2
D 200-250 μm	1	1.889	0.699	.63	.50	.15	.19	13.0 St. Dev = 2.7	11.1
	2		0.679	.64	.69	.17	.18	16.2 St. Dev = 2.8	14.9

1 Determined from Helium Pycnometry

2 Determined from mercury immersion

3 Determined from skeletal and bulk densities

4 Determined from mercury porosimetry

for sample D relative to sample A. Both steady and unsteady state diffusivities were close to each other and such closeness led to the conclusion that most of the pores within the porous carbon were open and interconnected.

CHAPTER - 8

OVERALL DISCUSSION, CONCLUSIONS AND RECOMMENDATIONS FOR FUTURE WORK

8.1 Overall discussion

In this thesis, the physical and transport properties of ICI's well established 52-8 $Cu/Zn/Al_2O_3$ LT (low temperature) shift catalysts were measured and analysed. This catalyst is used largely in ammonia synthesis plants for converting CO gas into CO_2 gas at a relatively low temperature in the range between 200 to 250 ^oC. This is necessary because CO gas deactivates the multipromoted iron catalyst which initiates the reaction between N_2 and H_2 gases to produce NH_3. In addition, the physical properties of some novel forms of carbon materials supplied by BP Research International were also investigated. Attention was particularly focussed on the measurements of surface area, porosity, pore size distribution, permeability, effective diffusivity and tensile strength of a single or a small batch (where appropriate) of catalyst particles.

Each of these properties can change significantly with alterations in key physical processing steps during catalyst preparation. To produce and market good quality catalysts with appropriate and tightly controlled final pellet properties, the effects on these properties of all the preparation steps during catalyst manufacture must be considered. Investigations of this type have not appeared in the open literature previously.

When fine powders are compressed and given a regular pellet structure, a pore system and hence both external and internal surfaces are developed within each individual catalyst particle. Often the internal surface area of such a pelleted catalyst is higher by several orders of magnitude than the external surface area. It is this internal surface where the potential for most

reaction resides. Without the knowledge of this surface area, the activity of a particular catalyst can not be specified quantitatively and, the effective diffusion coefficient (especially the Knudsen diffusion coefficient) can not be predicted. A standard BET technique is available to measure this surface area and this has been discussed briefly in Chapter 2 of this thesis.

Because of the development of a pore system, a catalyst pellet consists of both a solid volume and the pore volume. Porosity is a measure of this pore volume which is usually comprised of large pores, medium pores and small pores. Based on these pore sizes, there is a macro pore volume, a meso pore volume and the micro pore volume. The total porosity of the pellet can be obtained by the addition of macroporosity, mesoporosity and the microporosity. This property, like surface area, is equally important as without this, a dynamic isobaric or non-isobaric model of diffusion can not be fully specified and solved: hence unsteady state diffusivities can not be evaluated. A helium pycnometer can be used to measure the total porosity of a small batch of say 5 to 15 catalyst pellets and this has been discussed, together with other methods, in Chapter 2.

The macro pore region, meso pore region and the micro pore region of a single pellet, or a small batch of catalyst, can only be identified through a pore size distribution measurement. Hence from this measurement it can be decided whether a particular diffusing species will exhibit bulk diffusion, Knudsen diffusion or transition diffusion. Such pore size distributions can be measured by the mercury porosimeter or nitrogen desorption methods. These were also discussed in Chapter 2. Thus surface area, porosity and pore size distribution measurements are fundamental to the characterisation of any porous catalysts and if these are not known, then the prediction of effective diffusivities clearly becomes

impossible.

Catalyst particles are sensitive to breakage and attrition during transportation and loading into reactors. In addition thermal shock during operation can lead to further break up of catalyst particles. Thus finer particles tend to accumulate at the bottom of the reactor and these then cause excessive pressure drop within the reactor vessel, thereby reducing the effective life of the catalyst. In order to minimise catalyst breakage and hence maximise the duration of effective life, catalysts should be produced in such a way that their strength should lie above a certain minimum level. Catalysts can break more easily along their diameter in a tensile mode than along their axis in a compressive mode. Therefore the study and determination of catalyst tensile strength is essential in order to be able to guarantee the effective life of a particular catalyst as well as for producing good quality catalysts. The study of Weibull modulus, which is partly related to catalyst tensile strength, reflects the brittleness of a particular catalyst sample: this brittleness is governed by the flaw distribution within the porous material. Brittle materials are hard but break relatively easily. These also have been discussed in Chapter 2.

Finally the permeation and effective diffusion coefficients are two interrelated and extremely important properties of catalysts. Bulk diffusion is a mass transfer process and irrespective of media (porous or free gas) is caused by a gradient in mole fraction of the diffusing species. The term effective diffusivity is often used when discussing diffusion through porous media. Within a catalyst pellet both diffusion and chemical reaction usually occur simultaneously; it is the slowest step which tends to control the overall rate. In a situation when the isothermal effectiveness factor, a ratio of overall observed rate to the true intrinsic chemical rate, is unity, the overall rate is controlled

by the intrinsic reaction kinetics alone. However the effectiveness factor in real catalytic systems is often less than unity and effective diffusion coefficients must be known in order to predict conversion. Thus without the value of an effective diffusion coefficient, reactor model equations can not be solved and reactor performance can not be specified. Again if the catalyst particle exhibits a substantial internal pressure gradient, then together with the effective diffusion coefficient the permeation coefficient is also needed to solve the model equations. Permeation is a viscous flow phenomena and is caused by a gradient in total pressure within the catalyst particle. Hence all these properties in some way or the other do contribute to specifying the performance of a reactor and therefore assume great importance. Methods of measuring these two properties are also discussed in Chapter 2. Unlike surface area or the pore size distribution measurements, there is still a complete lack of standard equipment to measure these two properties.

For the measurements and investigation of these properties, both "green" and "reduced" catalyst samples were prepared under carefully controlled conditions at ICI's Billingham Catalysis Research Centre. The starting material was copper oxide/zinc oxide/alumina co-precipitated dried powder taken from a batch of industrial catalyst produced at the ICI catalyst plant located at Clitheroe. Then varying five standard catalyst production parameters at their "low", "normal", "high" and "extra high" levels, the powders were finally compressed and pelleted to a regular cylindrical form. These five production parameters were:

(1) Amount of lubricant added
(2) Pre-compaction load
(3) Calcination temperature
(4) Primary particle cut size
(5) Final pelleting density.

The "green" cylindrical catalysts were 3.6 mm

long with a standard diameter of 5.4 mm and were the subject of these investigations. As catalysts used in situ in reactors are operating under "reduced" condition, the green samples were reduced and stabilised and the effect of this reduction was investigated.

A dynamic, non-isobaric isothermal model describing combined diffusion and permeation within a single cylindrical catalyst pellet has been developed for a binary gas system. The model is written for a Wicke-Kellenbach type diffusion test cell and assumes that the porous medium is isotropic and that the adsorption of the tracer species on the porous matrix is negligible. In addition to these assumptions, the end chamber volumes of the Wicke-Kallenbach diffusion cell are assumed to be perfectly mixed. The non-equimolal counter diffusion flux of the model has been expressed with a Fickian type equation taking into account the contribution of composition dependency of both bulk and Knudsen diffusion coefficients. The permeation, or the viscous, flux was described by a D'arcy type equation. These two fluxes were simply added to develop the complete non-isobaric model of diffusion.

The development and solution of a non-isobaric model is not new. Such a model was developed earlier by Mason and co-workers using the theoretical dusty gas model but was written in a more complex form. This was later solved numerically by McGreavy and Asaeda using simple boundary and initial conditions. The non-isobaric model as developed in this thesis has been formulated in a very simple way from the first principles. Moreover, for it's solution complex derivative type boundary conditions were used.

The model so developed is also based theoretically on the dusty gas model (see Chapter 1). A dusty gas model neither talks about the pore structure nor provides a means for predicting the effective

diffusion coefficient which at present can be obtained by experimentation alone. This is in a sense good because the pore structure of commercially marketed catalysts is extremely complicated and impossible to characterise fully. Pore models like the parallel path pore model or the random pore model, etc., can also never accurately describe such a complicated pore structure. In these situations, it is better to avoid trying to describe the geometrical structure of pores and the dusty gas model does just this. One other advantage of the dusty gas model is that the equations developed can be used to describe any kind of diffusion i.e. bulk, Knudsen or transition diffusion.

The complete model was solved using a Crank-Nicolson finite difference numerical technique. At low gas concentration the viscosity term which appeared in the D'arcy equation was expressed in terms of mole fraction of component A (see Appendix 1). To make the solution more simple, this viscosity variation was not taken into account. This was further justified from the fact that the binary pair used for experimental purposes was N_2 and He with respective viscosities of 1.8×10^{-5} Ns/m^2 and 1.99×10^{-5} Ns/m^2, a variation of only about 10% between the two. Hence an average of these two values was used. For large pores, the model predictions became essentially identical to those of an isobaric model. Such a model was solved using both a numerical method and the moments method (Chapter 4).

Parts of the experimental programme, i.e. measurements of surface area, porosity, pore size distribution and catalyst reduction were performed at the ICI Catalysis Centre, Billingham, as standard equipment for measuring these properties and carrying out chemical reduction were readily available there. For example, pellet porosity was determined at ICI using a 1320 Micromeritics Pycnometer and surface area by a Micromeritics Digisorb 2020. At University College

London, the remaining porosity and surface area measurements were carried out using a 1330 helium pycnometer manufactured again by Micromeritics Corporation and an Omnisorp 100 size analyser developed by the Omicron Technology Corporation. Pore size distribution measurements were carried out both at ICI and at UCL using mercury porosimetry. The catalyst tensile strength tests were conducted at the School of Pharmacy of the University of London using a CT40 load tester designed specifically for this purpose by Systems Engineering Nottingham.

As mentioned earlier no standard apparatus is yet available in the market for the measurement of effective diffusion coefficients or permeation coefficients. These measurements were conducted at University College London where a purpose designed apparatus was developed and built to measure these two catalyst properties based on a single pellet measurement technique.

The idea of a single pellet diffusion/permeation experimental technique was developed first by Wicke and Kallenbach in 1941 and later was modified by Weisz. Despite its main potential drawback of leakage around the external curved surfaces of the pellet, it is experimentally simple and keeps the number of unknown system parameters to only one. Therefore, the unsteady state effective diffusivity can be obtained directly from the first moment of the system response. Along with the above advantages, the adoption of this technique in this thesis was primarily based on two important factors. The first was that the experimental apparatus was already available in the department and the second was that if all the characteristic features of a single pellet are known then the behaviour of a single tube containing several hundreds of such catalyst pellets can in principle be predicted provided that the tube voidage, catalyst effective thermal conductivity, etc., are known. A full reactor model can then be built up from several

hundreds of such individual tubes (e.g., a primary reformer).

But this single pellet measurement technique can be criticised on at least two grounds. First, while tonnes of catalysts are used in a reactor, measurement on just 1 pellet or 5 pellets or even 10 pellets may not be representative of the whole batch of catalyst. However, testing a large number of catalyst pellets means that experimental time increase significantly. Second, as diffusion takes place simultaneously with chemical reaction, measurements of diffusion in the absence of chemical reaction, or without the consideration of realistic process conditions for pressure and temperature can provide misleading results.

An alternative which enables these latter two problems to be addressed is to use the pulse or chromatographic technique where the behaviour of a few hundreds of catalyst pellets can be observed from a single experiment. Moreover, measurements of diffusion under reacting conditions as well as at actual process pressure and temperature can be carried out using this pulse method. A fixed column packed with catalyst pellets constitutes the chromatographic column. Initially a tracer or reactant gas is allowed to pass through the column and then a pulse of another gas is suddenly introduced and both inlet and outlet responses of the pulse as a function of time are recorded. But this poses a serious drawback when interpreting the data, that is a second moment, i.e. the system variance, is needed to evaluate the unsteady state diffusivity. Also it may be difficult to carry out an experiment under reacting conditions. Moreover, pellet to pellet variations of properties can not be investigated by this method and this is vital for good quality control of catalysts. The model equations needed to describe these type of experiments are quite complex, involve a number of poorly known, or unknown, parameters and also involve model

assumptions which are at best questionable, e.g., a flat velocity profile across the radius of the chromatographic column.

Now the question naturally arises whether it is necessary to carry out an unsteady state test such as the pulse or chromatographic test and if so when, or whether, it is better simply to stick to a steady state Wicke-Kallenbach diffusion test. An unsteady state test, in addition to providing a diffusion coefficient can reflect the presence of any dead ended pore structure. If the steady state diffusion coefficient value is used to predict the concentration transient from a dynamic test then it will differ from the experimentally obtained transient. In order to match these two curves, a higher diffusivity value will be needed and this highlights the fact that all the pore system plays a part in a transient diffusion test whereas only the interconnected pores are involved in steady state diffusion.

If the pores within a pellet are all sufficiently big so that only bulk diffusion occurs, the chance of having a non-interconnected porous structure is less likely. The gradient of total pressure within the pellet will be small and hence a non-isobaric model will usually not be required to predict the performance of such a catalyst. In this case, a steady state diffusion test will be sufficient. This situation was found both experimentally and theoretically for the BP porous carbon samples. Mathematical predictions and experimental results were presented in Chapter 4 and Chapter 7 of this thesis: it was clear that there was no significant difference between steady and unsteady state diffusivities, although with an increase in primary particle size some variation between these two were noticed. These variations might be due to the fact that with an increase of particle size, the diffusivity is increasingly dominated by micro pores rather than as a whole by macropores within the pellet. An isobaric model

solution, as shown in Chapter 6 for sample C2, provided a good match between the theory and the experiments. This demonstrates that for some forms of porous materials an isobaric model can be quite adequate for describing diffusion within them.

But this was not the case for the high surface area ICI $Cu/Zn/Al_2O_3$ LT shift catalyst. An isobaric model was first solved to see the agreement with experimental results. In the experimental system a time lag of about 0.06 s was observed. The time lag is the time taken by the first tracer to reach the detector unit after the step is initiated. This was calculated by measuring the volume of the apparatus between the step production point up to the detector unit and then dividing by the volumetric flow rate. Hence from each time point of the experimentally obtained concentration profile, this 0.06 s was deducted so that the time scale between theory and experiment matched each other on the concentration profile plots. This was given in figure 6.18 of Chapter 6. A poor agreement between theory and experiments was found. This led us on to the development and solution of the more complex non-isobaric model.

The non-isobaric model was solved first for sample S-1/7 adjusting the value of D_{ABe} and D_{KAe} in such a way that the D_{Ae} value using the Bosanquet extrapolation formula was equal to the experimentally obtained steady state diffusivity value. This solution was compared with the experiment as shown in figure 6.20 of Chapter 6. Better agreement was observed than that for the isobaric model case. Using a parameter estimation search routine, best values for D_{ABe} and D_{KAe} were picked so that using these two values, the calculated concentration profile matched the experimental one. The unsteady state diffusivity was then calculated using the composition dependency of diffusion coefficient. Assuming the unsteady state diffusivity as the base value, the %difference in the steady state diffusivity was 14.3%.

But an overall agreement within 21% was obtained for all the samples tested except S-24/2. Poor agreement in this latter case may have been attributable to experimental error (see table 6.4, Chapter 6) or perhaps to non-uniformity of this particular sample. Using the Bosanquet extrapolation formula, for sample S-1/7, the unsteady state diffusivity was found to be 25% less than that obtained from the composition dependency of diffusion coefficient.

From all experimentally obtained steady state diffusivities, the tortuosity factor was calculated using again the Bosanquet formula. For green catalyst samples, the tortuosity factor varied from 1.29 to 5.04. However the majority of the samples showed a tortuosity factor between 2 and 3.5. After reduction of the green samples diffusivity values have increased and so the tortuosity factors are lower.

From the pore size distribution data, and assuming that the diffusion process has proceeded solely by Knudsen mode, the tortuosity factor for the base sample S-1/7 was found to be 1.41 (see Appendix 6). Using the model provided by Waldram et al for the tortuosity factor, equation (1.1) of Chapter 1, a tortuosity for the Knudsen diffusivity has been predicted to be 2.35. Thus for this sample and for Knudsen diffusion, the tortuosity factor model proposed by Waldram et al, shows relatively poor agreement with that calculated from the usual Knudsen diffusion expression.

Some unsteady state diffusion coefficients for the ICI catalysts (see table 6.3 of Chapter 6) were also determined using moments equations. An agreement within 21% was found for all the samples tested. However, because of time shortage, for the same pellet, the moments method and the non-isobaric numerical method were not compared to observe the deviation between the two.

Nearly all the unsteady state diffusivities using the moments method and the non-isobaric numerical method were above the experimental steady state diffusivities. This confirms the presence of some dead ended pores within the pellet. Again significant internal pellet pressure gradients were found when the non-isobaric model was solved. Therefore, unlike the BP porous carbon materials, ICI $Cu/Zn/Al_2O_3$ catalysts require a non-isobaric model in order to describe diffusion. Thus here it can be concluded that the adoption of a single pellet measurement technique or a pulse technique and hence the use of an isobaric model or a non-isobaric model depends largely on the type of catalysts and their inherent porous nature. However it can be emphasised that the single pellet technique is the most useful for an initial screening test when no on hand information for a particular catalyst is available.

The diffusion tests, which were the complex part of this research were all based on single pellet measurement technique using a Wicke-Kallenbach type test cell. This test cell was attached to two purpose designed gas distributors. For each test, the effective diffusivity was determined by making a step change in gas mole fraction entering the left hand gas distributor. The mole fractions of this gas leaving each gas distributor were detected by Taylor-Servomex gas thermal conductivity detectors. The data from each experiment was collected by a 9826 model HP computer via an analog to digital converter (see Chapter 5). There were two advantages of this apparatus. First, the step change in gas mole fraction could in principle be made either to the left hand side or to the right hand side of the apparatus. The same effect could be achieved by simply reversing the position of the test cell. Using these means a study of pellet anisotropy can also be performed. This however requires a slightly different set of steady state diffusion equations to be used. Such equations were derived and are provided in Appendix 7. The second

advantage is that from a single experiment a total of four i.e. two steady state diffusivity values and two unsteady state diffusivity values can be obtained. The two steady state values would show exact agreement if a perfect experimental tracer mass balance was observed. To all results presented in this thesis the tracer mass balance was within +/- 0.5%.

Permeability experiments were simple and were performed using the same diffusion apparatus and the test cell. A pressure gradient was imposed across the pellet and the convective flux through it was measured. For the BP porous carbon systems, both the differential and the integral method of evaluating permeability were used. For the ICI $Cu/Zn/Al_2O_3$ only the integral method was used. This was because the permeation flux from a pellet of only 0.24 cm^2 cross-sectional area and with an average pore diameter of approximately 16 nm was very small even for the maximum allowable pressure differential across the pellet corresponding to a digital voltmeter reading of 1800 mV. For each pellet, only one set of data was taken.

Determinations of catalyst tensile tests were also simple. These involved placing the single pellet horizontally on the platten of the CT40 load tester and then splitting it by the application of a load from the top across the diameter. The tensile strength was then calculated from a relationship between catalyst pellet length, diameter, applied load and the tensile strength itself (Chapter 2, equation (2.9)).

The results for all "green" catalyst samples with the five processing parameters are summarised below:

BET surface area varied from 55.3 m^2/g to 117.3 m^2/g with a base case sample area of 115.6 m^2/g. That is, it can be varied by a factor of 2.12. A decrease of 52% below the base sample or an increase of only 1.5% above

the base sample can be achieved.

The overall variation of porosity was between 0.426 to 0.634 with the reference porosity being 0.549. This corresponds to a variation by a factor of only 1.56 and it was the physical property which showed least sensitivity to variations in pellet production conditions. Porosity can only be increased above the base sample by 20% and can be decreased below the base sample by 23%.

Permeability of the "green" catalyst varied from 0.82×10^{-16} m^2 to 5.12×10^{-16} m^2 with the base case value of 1.56×10^{-16} m^2. An overall variation by a factor of 6.24 is observed. It can be increased by 228% above the base sample or can be decreased by 47% below the base sample.

Effective diffusivity showed a variation between 0.70×10^{-6} m^2/s and 5.60×10^{-6} m^2/s with a base value of 1.40×10^{-6} m^2/s. An ultimate change by a factor of 8.0 is noticed. It can be increased above the base sample by 300% but can be decreased by only 50% below the base sample.

The tensile strength of the green catalyst samples changed from 0.82 MN/m^2 to 4.33 MN/m^2 with the corresponding reference case value of 4.07 MN/m^2. This property can be varied as much as by a factor of 5.28 and can be increased above the base sample by 6.39% or can be decreased by 80% below the base sample.

The Weibull modulus for a set of catalyst particles for samples S-1, S-24 and S-28 were found to be 27.91, 28.68 and 30.08 respectively. These indicate that the $Cu/Zn/Al_2O_3$ catalysts are not particularly brittle. Typically the Weibull modulus lies between 5 to 40. A value less than 10 would indicate high brittleness. The Weibull modulus would remain essentially identical for

materials of equal brittleness even though the mean fracture stress changes.

From the results, it is clear that surface area and porosity change by a factors of 2.12 and 1.56 only respectively whereas changes in permeability, effective diffusivity and tensile strength are by factors of 6.24, 8.00 and 5.28 respectively. The changes in all five properties were due mainly to choice of calcination temperature, primary particle cut size and final pelleting density. The amount of lubricant added and the pre-compaction load had hardly any effect on the variation of properties. For marketing purposes a good quality catalyst is always desirable. That is, a catalyst must be produced in such a way that the finished product can fulfill its customer demand. High permeability and high diffusivity catalysts, which a user of that particular catalyst wants, can be prepared by considering a low cut size, a low pellet density or an extra high calcination temperature. But these reduce the tensile strength substantially which of course will be unacceptable. On the other hand, stronger catalysts can be prepared only by increasing the pellet density. But this factor reduces the permeability as well as effective diffusivity significantly. Therefore, in order to prepare a good quality catalyst with specific properties there must be a compromise between these production variables at some prescribed intermediate level.

However such a compromise among production parameters based on their main effects only may provide an optimum condition for regular catalyst manufacture if the factors considered are independent of each other i.e. non-interacting. In actual practice factors do interact and these effects must be taken into account. In these cases, a factorial design of experiments is necessary to reduce the overall total number of experiments.

In this thesis, the first order interactions

among calcination temperature, cut size and pelleting density were investigated. It was observed that in most cases the first order interaction resulted in a variation of properties between the two equivalent individual main effects. It was also clearly observed that by choosing an appropriate combination of interaction, a particular property can be increased.

The interaction effects have not yet been fully studied because second and higher order interactions have not been considered. In order to determine an optimum condition for a particular catalyst to be produced, it is recommended that along with first order interactions, second and higher order interactions should be investigated. Then based on these interactions, a factorial design of experiments can be carried out so as to reduce the overall number of experiments and experimental time to manageable proportions.

Upon reduction of the green catalyst samples, porosity was typically increased by 10 to 15% and permeability and diffusivity by a factor more than 3. Tensile strength decreased by a factor in excess of 3. Of all the surface area measurements about 70% were increased following a reduction step. The results of reduction as shown in figures 6.1 to 6.5 (Chapter 6) were for the base case sample S-1 only.

The most interesting results were found for permeabilities of some pre-reduced catalyst samples. An increase in permeabilities in excess of 400 fold was observed though the effective diffusivity for those same samples increased by a factor of only 2. The only logical explanation for this seemed to be the possible development of microscopic cracks formed during the chemical reduction step. Part of all properties other than the tensile strength tended to increase on reduction. What is certainly apparent is that chemical reduction can affect the physical properties of the LT

shift catalyst very significantly. It is vital that this process is carried out under very carefully controlled conditions. Otherwise the virtues of producing a high quality "green" catalyst with closely specified physical, and chemical, properties may be lost, the catalyst significantly weakened and catalyst activity and life profoundly shortened.

The pore size distribution measurements using mercury intrusion porosimetry showed a variation of pore diameter between 11.4 nm to 18.2 nm with the base sample value of 15.6 nm. The mesopore region i.e. transition diffusion region chosen for He (table 6.2 of Chapter 6) was from pore diameters of 33.6 nm to 3691 nm. This range was from pore diameters approximately 10 times smaller than the mean free path of He of 274.5 nm at one extreme and at the other was approximately 10 times higher. Exact choices of the pore diameters at either end of the transition diffusion band had to made for specific points on the pore size distribution data.

8.2 Conclusions

This project has been financially supported by ICI Chemicals and Polymers Group. The purpose was to focus attention on the measurements of all possible physical properties of their 52-8 LT shift catalysts when changes in key preparation steps were imposed. After careful analysis and investigation on a total of 85 "green" and "reduced" catalyst samples, the following conclusions can be drawn:

* The frequently quoted BET surface area and pellet porosity are not critically dependent on the physical production conditions. Hence for quality control purposes, routine measurements of these properties are of limited value. On the other hand, permeability, effective diffusivity and tensile strength of catalyst particles are strongly dependent on some of the production variables, particularly on extra high calcination

temperature, low particle cut size and low pelleting density. Therefore, to obtain better quality products, frequent measurements of these properties are essential. On the catalyst production plant good control systems are vital for calcination temperature, particle cut size and pelleting density. The latter depends on the mass of powder fed to each die on the Manesty tabletting machines.

* For the open market, LT shift catalysts are normally quoted as having a pore volume of 0.25 dm^3/g, a BET surface area of 75 m^2/g and an average pore diameter of 13.4 nm (Twigg, 1989). To these, can now be added three more physical properties, namely, permeability, diffusivity and tensile strength. This means that catalyst manufacturers might need to quote as many as six physical properties in order to characterise their products more completely. This in turn will enable the buyer of a particular catalyst to discriminate between two nominally similar rival catalyst products.

* In order to search for an optimum set of routine production conditions, the number of experiments to be conducted obviously would be enormously high. To reduce the overall total number of experiments to manageable proportions, a factorial design of experiments is recommended.

* The modelling of diffusion and flow in porous media can potentially be applied in other areas such as oil field modelling, hydrology, geology etc.

It is obvious from the above conclusions that research of this type can have a significant implication in the commercial marketplace of catalysts. Therefore, it might be anticipated that catalyst manufacturers would devote significant research effort to studies of the type reported in this thesis. In order to produce better quality catalyst products, there is a crucial need at

present for the development of purpose built instrumentation for diffusion and permeation measurements.

The existing single pellet instrument at University College London has some disadvantages. First, only pellets of regular geometries can be studied. Spherical particles can be investigated by using a Weisz correction factor (Waldram, 1985), which is unity for the case of cylindrical catalyst pellets. A similar correction factor for the measurement of permeability of spherical particles can be defined. The permeability and diffusivity for any irregular shaped catalysts (like iron catalysts or ring or cross-partition ring type steam reforming catalysts) can not be investigated using a Wicke-Kallenbach apparatus.

The only option to resolve this problem is to develop an instrument using the pulse or chromatographic method as mentioned earlier. This then can be used to monitor the quality of each batch of regular or irregular catalysts. Diffusivities can then be measured under reacting or non-reacting conditions and can then be used directly for reactor modelling and studies for scale up of chemical plant. The measurement of permeabilities in a chromatographic type apparatus has not been attempted and there are no obvious techniques by which this could be achieved.

The chemical properties of catalysts such as bonding, oxidation state, etc., are often relatively well established compared with physical properties (Twigg, 1989). This is mainly because of the lack of standard instrumentation for the latter.

All the above conclusions are new in the field of heterogeneous catalysis of solid-gas system. Therefore this thesis has considerable value in the design, manufacture and marketing of large scale porous solid

catalysts.

8.3 Recommendations for future work

Following the overall discussion and conclusions, it is evident that more experimental and research work needs to be carried out in order to partially fulfill the present demand of the catalyst industry. Suggestions for future work can be made in three different ways: (i) experimental work, (ii) theoretical work and (iii) other related work.

8.3.1 Experimental work

To develop a diffusion and permeation test apparatus based on the single pellet measurement technique, the following improvements are necessary:

(i) Finding a new and simple method of creating a fast step change in gas concentration unaccompanied by pressure pulsations.

(ii) Installation of gas concentration analysers which give a reading independent of flow rate.

(iii) Installation of on-line flowrate measuring instruments.

(iv) Development of the apparatus so that measurements of diffusivity and permeability can be carried out over a wider range of pressures and temperatures.

(v) Development of a diffusion apparatus based on the chromatographic method.

(vi) Studying pellet anisotropy.

8.3.2 Theoretical work

(i) To take into account the variation of viscosity with composition during the non-isobaric model solution.

(ii) Development of a criterion to decide whether an isobaric model or a non-isobaric model of diffusion and permeation is required.

(iii) Improvement in the modelling of diffusion experiments based on the chromatographic column method.

8.3.3 Other related work

(i) Studying the variation of upstream catalyst production parameters such as crystallization rate, aging time, pH etc., on catalyst properties.

(ii) Study of higher order interaction effects and designing the experiments factorially.

(iii) Investigating the cause of cracking during chemical reduction and hence conditions to be avoided.

(iv) Studies on porous carbons with known and carefully controlled pore structures, e.g., only macroporosity, only microporosity and both. These will enable to test the validity of the theory of diffusion (e.g., Bosanquet formula) from experimental observations.

(v) Comparison of results derived from the transient experiments by the moments equation with those from the full non-isobaric model for the same catalyst sample pellet.

APPENDICES

APPENDIX - 1

Development of the non isobaric model of diffusion for a binary gas mixture A and B

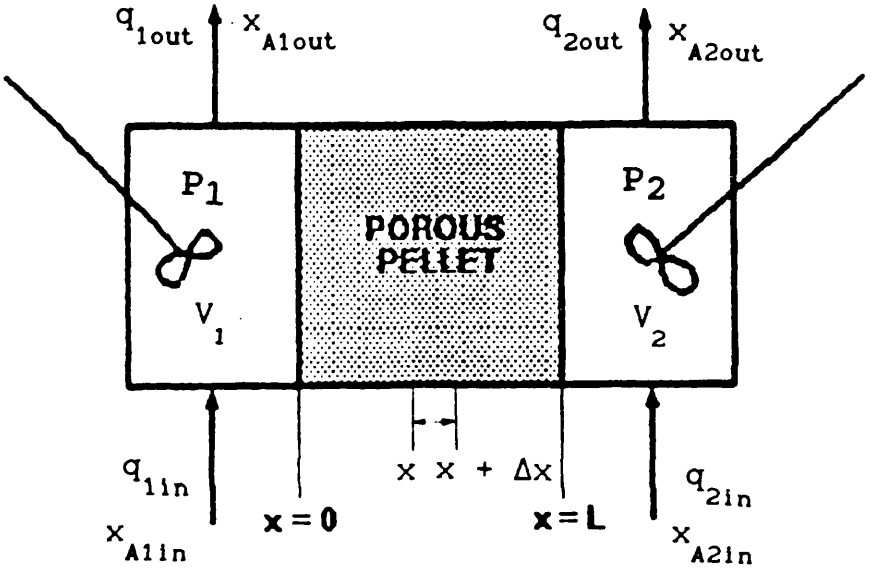

Mass balance on A on the differential volume Δx (see figure)

$$\left(-D_{Ae}A\frac{\partial C_A}{\partial x}\right)\Bigg|_x + \left(D_{Ae}A\frac{\partial C_A}{\partial x}\right)\Bigg|_{x+\Delta x} - \left(\frac{AB_0}{\mu_m}C_A\frac{\partial P_T}{\partial x}\right)\Bigg|_x + \left(\frac{AB_0}{\mu_m}C_A\frac{\partial P_T}{\partial x}\right)\Bigg|_{x+\Delta x}$$

$$= \varepsilon\ A\ \Delta x\frac{\partial}{\partial t}(C_A)$$

or, in terms of molefraction of A:-

$$-\left(D_{Ae}\frac{\partial}{\partial x}\left(\frac{P_T x_A}{RT}\right)\right)\Bigg|_x + \left(D_{Ae}\frac{\partial}{\partial x}\left(\frac{P_T x_A}{RT}\right)\right)\Bigg|_{x+\Delta x} - \left(\frac{B_0}{\mu_m}\frac{P_T x_A}{RT}\frac{\partial P_T}{\partial x}\right)\Bigg|_x$$

$$+ \left(\frac{B_0}{\mu_m}\frac{P_T x_A}{RT}\frac{\partial P_T}{\partial x}\right)\Bigg|_{x+\Delta x} = \varepsilon\ \Delta x\frac{\partial}{\partial t}\left(\frac{P_T x_A}{RT}\right)$$

or,

$$\frac{\left[D_{Ae}\frac{\partial}{\partial x}\left(P_T x_A\right)\Big|_{x+\Delta x} - D_{Ae}\frac{\partial}{\partial x}\left(P_T x_A\right)\Big|_{x}\right]}{\Delta x} +$$

$$\frac{B_0\left[\frac{P_T x_A}{\mu_m}\frac{\partial P_T}{\partial x}\Big|_{x+\Delta x} - \frac{P_T x_A}{\mu_m}\frac{\partial P_T}{\partial x}\Big|_{x}\right]}{\Delta x} = \varepsilon\frac{\partial}{\partial x}\left(P_T x_A\right)$$

or,

$$\frac{\partial}{\partial x}\left(D_{Ae}\frac{\partial}{\partial x}\left(P_T x_A\right)\right) + B_0\frac{\partial}{\partial x}\left(\frac{P_T x_A}{\mu_m}\frac{\partial P_T}{\partial x}\right) = \varepsilon\frac{\partial}{\partial x}\left(P_T x_A\right) \ldots\ldots(1)$$

Overall mass balance on the differential volume Δx

$$-\left(D_{Ae}A\frac{\partial C_A}{\partial x}\right)\Big|_{x} + \left(D_{Ae}A\frac{\partial C_A}{\partial x}\right)\Big|_{x+\Delta x} - \left(D_{Be}A\frac{\partial C_B}{\partial x}\right)\Big|_{x} + \left(D_{Be}A\frac{\partial C_B}{\partial x}\right)\Big|_{x+\Delta x}$$

$$-\left(\frac{AB_0}{\mu_m}C_T\frac{\partial P_T}{\partial x}\right)\Big|_{x} + \left(\frac{AB_0}{\mu_m}C_T\frac{\partial P_T}{\partial x}\right)\Big|_{x+\Delta x} = \varepsilon A\,\Delta x\frac{\partial C_T}{\partial t}$$

or, in terms of molefraction of A and B

$$\frac{\left(\frac{D_{Ae}}{RT}\frac{\partial}{\partial x}\left(P_T x_A\right)\right)\Big|_{x+\Delta x} - \left(\frac{D_{Ae}}{RT}\frac{\partial}{\partial x}\left(P_T x_A\right)\right)\Big|_{x}}{\Delta x} +$$

$$\frac{\left(\frac{D_{Be}}{RT}\frac{\partial}{\partial x}\left(P_T x_B\right)\right)\Big|_{x+\Delta x} - \left(\frac{D_{Be}}{RT}\frac{\partial}{\partial x}\left(P_T x_B\right)\right)\Big|_{x}}{\Delta x} +$$

$$\frac{B_0\left[\frac{P_T}{RT}\frac{1}{\mu_m}\frac{\partial P_T}{\partial x}\right]_{x+\Delta x} - B_0\left[\frac{P_T}{\mu_m RT}\frac{\partial P_T}{\partial x}\right]_{x}}{\Delta x} = \frac{\varepsilon}{RT}\frac{\partial P_T}{\partial t}$$

or,

$$\frac{\partial}{\partial x}\left(D_{Ae}\frac{\partial}{\partial x}\left(P_T x_A\right)\right) + \frac{\partial}{\partial x}\left(D_{Be}\frac{\partial}{\partial x}\left(P_T x_B\right)\right) + B_0\frac{\partial}{\partial x}\left(\frac{P_T}{\mu_m}\frac{\partial P_T}{\partial x}\right) = \varepsilon\frac{\partial P_T}{\partial t}$$

or,

$$\frac{\partial}{\partial x}\left(D_{Ae}\frac{\partial}{\partial x}\left(P_T x_A\right)\right) + \frac{\partial}{\partial x}\left(D_{Be}\frac{\partial}{\partial x}\{P_T(1 - x_A\}\right) + B_0\frac{\partial}{\partial x}\left(\frac{P_T}{\mu_m}\frac{\partial P_T}{\partial x}\right) = \varepsilon\frac{\partial P_T}{\partial t}$$

or,

$$\frac{\partial}{\partial x}\left[\left(D_{Ae} - D_{Be}\right)\frac{\partial}{\partial x}\left(P_T x_A\right)\right] + \frac{\partial}{\partial x}\left(D_{Be}\frac{\partial P_T}{\partial x}\right) + B_0\frac{\partial}{\partial x}\left(\frac{P_T}{\mu_m}\frac{\partial P_T}{\partial x}\right) = \varepsilon\frac{\partial P_T}{\partial t} \quad ..(2)$$

End chamber balance:

L.H.S. chamber -

$$q_{1in}c_{A1in} - q_{1out}c_{A1out} + AD_{Ae}\frac{\partial C_A}{\partial x}\bigg|_{x=0} + A\frac{B_0}{\mu_m}\left(C_A\frac{\partial P_T}{\partial x}\right)\bigg|_{x=0} = V_1\frac{dC_{A1out}}{dt}$$

or, in terms of molefraction of A

$$q_{1in}\frac{P_T}{RT}x_{A1in} - q_{1out}\frac{P_T}{RT}x_{A1out} + AD_{Ae}\frac{\partial}{\partial x}\left(\frac{P_T}{RT}x_A\right)\bigg|_{x=0} + \frac{AB_0}{\mu_m}\left(\frac{P_T x_A}{RT}\frac{\partial P_T}{\partial x}\right)\bigg|_{x=0} = V_1\frac{d}{dt}\left(x_{A1out}\frac{P_T}{RT}\right)$$

or,

$$q_{1in}x_{A1in}P_T - q_{1out}x_{A1out}P_T + AD_{Ae}\frac{\partial}{\partial x}\left(P_T x_A\right)\bigg|_{x=0} + A\frac{B_0}{\mu_m}\left(P_T x_A\frac{\partial P_T}{\partial x}\right)\bigg|_{x=0} = V_1\frac{d}{dt}\left(P_T x_{A1out}\right) \quad .....(3)$$

Similarly for R.H.S. chamber -

$$q_{2in}x_{A2in}P_T - q_{2out}x_{A2out}P_T - AD_{Ae}\frac{\partial}{\partial x}\left(P_T x_A\right)\bigg|_{x=L} - A\frac{B_0}{\mu_m}\left(P_T x_A\frac{\partial P_T}{\partial x}\right)\bigg|_{x=L} = V_2\frac{d}{dt}\left(P_T x_{A2out}\right) \quad .....(4)$$

where

D_{Ae} = Effective diffusivity of A, m^2/s and defined by

$$= \frac{1}{\frac{1 - \alpha_{AB}x_A}{D_{ABe}} + \frac{1}{D_{KAe}}} = \frac{D_{ABe}D_{KAe}}{\left(1 - \alpha_{AB}x_A\right)D_{KAe} + D_{ABe}}$$

D_{Be} = Effective diffusivity of B, m^2/s and defined by

$$= \frac{1}{\frac{1 - \alpha_{BA} x_B}{D_{ABe}} + \frac{1}{D_{KBe}}} = \frac{D_{ABe} D_{KBe}}{(1 - \alpha_{BA} x_B) D_{KBe} + D_{ABe}}$$

$$\alpha_{AB} = 1 - \sqrt{\frac{M_A}{M_B}} \; ; \; \alpha_{BA} = 1 - \sqrt{\frac{M_B}{M_A}}$$

The viscosity of the gas mixture is represented by

$$\mu_m = (1.78 + 0.46 \, x_A) \times 10^{-5} \; Ns/m^2$$

APPENDIX - 2

Solution of isobaric diffusion equation using moments method

$$D_e \frac{\partial^2 c_A}{\partial x^2} = \varepsilon \frac{\partial c_A}{\partial t}$$

Subject to at $x = 0,\ c_A = c_{A1}$

$x = L,\ c_A = c_{A2}$

Let $z = x/L \therefore x = zL$

Putting this value and applying Laplace transformation

$$\frac{D_e}{L^2} \frac{d^2\bar{c}_A}{dz^2} = \varepsilon s \bar{c}_A$$

or,

$$\frac{d^2\bar{c}_A}{dz^2} = \frac{L^2 \varepsilon s \bar{c}_A}{D_e}$$

Let $\alpha^2 = \frac{L^2 \varepsilon s}{D_e} \therefore \frac{d^2\bar{c}_A}{dz^2} - \alpha^2 \bar{c}_A = 0,$

$z = 0,\ \bar{c}_A = \bar{c}_{A1}$.....(1)

$z = 1,\ \bar{c}_A = \bar{c}_{A2}$.....(2)

or,

$$D^2\bar{c}_A - \alpha^2\bar{c}_A = 0$$

or,

$$(D + \alpha)(D - \alpha)\bar{c}_A = 0$$

or,

$$\bar{c}_A = Ae^{\alpha z} + Be^{-\alpha z} \quad \text{.....} \quad (3)$$

Applying (1) to (3),

$$\bar{c}_{A1} = A + B \quad \text{.....} \quad (4)$$

Applying (2) to (3),

$$\bar{c}_{A2} = Ae^{\alpha} + Be^{-\alpha} \quad \text{.....} \quad (5)$$

From (4) and (5),

$$\bar{c}_{A2} = Ae^{\alpha} + \left(\bar{c}_{A1} - A\right)e^{-\alpha}$$

or,

$$A = \frac{\bar{c}_{A2} - \bar{c}_{A1}e^{-\alpha}}{e^{\alpha} - e^{-\alpha}}$$

and

$$B = \frac{\bar{c}_{A1}e^{\alpha} - \bar{c}_{A2}}{e^{\alpha} - e^{-\alpha}}$$

Substituting the value of A and B in equation (3) the solution becomes

$$\bar{c}_A = \frac{\bar{c}_{A2} - \bar{c}_{A1}e^{-\alpha}}{e^{\alpha} - e^{-\alpha}}e^{\alpha z} + \frac{\bar{c}_{A1}e^{\alpha} - \bar{c}_{A2}}{e^{\alpha} - e^{-\alpha}}e^{-\alpha z} \quad \ldots\ldots\ldots \quad (6)$$

Differentiating (6) with respect to z,

$$\frac{d\bar{c}_A}{dz} = \frac{\left(\bar{c}_{A2} - \bar{c}_{A1}e^{-\alpha}\right)\alpha e^{\alpha z}}{e^{\alpha} - e^{-\alpha}} - \frac{\left(\bar{c}_{A1}e^{\alpha} - \bar{c}_{A2}\right)\alpha e^{-\alpha z}}{e^{\alpha} - e^{-\alpha}}$$

or,

$$\left(\frac{d\bar{c}_A}{dz}\right)\Bigg|_{z=0} = \frac{\left(\bar{c}_{A2} - \bar{c}_{A1}e^{-\alpha}\right)\alpha}{e^{\alpha} - e^{-\alpha}} - \frac{\left(\bar{c}_{A1}e^{\alpha} - \bar{c}_{A2}\right)\alpha}{e^{\alpha} - e^{-\alpha}}$$

$$= \frac{2\alpha\bar{c}_{A2} - \alpha\bar{c}_{A1}\left(e^{\alpha} + e^{-\alpha}\right)}{e^{\alpha} - e^{-\alpha}} \quad \ldots\ldots\ldots \quad (7)$$

$$\left(\frac{d\bar{c}_A}{dz}\right)\Bigg|_{z=1} = \frac{\left(\bar{c}_{A2} - \bar{c}_{A1}e^{-\alpha}\right)\alpha e^{\alpha}}{e^{\alpha} - e^{-\alpha}} - \frac{\left(\bar{c}_{A1}e^{\alpha} - \bar{c}_{A2}\right)\alpha e^{-\alpha}}{e^{\alpha} - e^{-\alpha}}$$

$$= \frac{\alpha\bar{c}_{A2}\left(e^{\alpha} + e^{-\alpha}\right) - 2\alpha\bar{c}_{A1}}{e^{\alpha} - e^{-\alpha}} \quad \ldots\ldots\ldots \quad (8)$$

L.H.S. chamber equation

$$q_1 c_{Ain} - q_1 c_{A1} + AD_e\left(\frac{\partial c_A}{\partial x}\right)\Bigg|_{x=0} = V_1\frac{dc_{A1}}{dt}$$

or,

$$c_{Ain} - c_{A1} + \frac{AD_e}{q_1 L}\left(\frac{\partial c_A}{\partial z}\right)\Bigg|_{z=0} = \frac{V_1}{q_1}\frac{dc_{A1}}{dt}$$

Let $\frac{AD_e}{q_1 L} = K_1$ and $\frac{V_1}{q_1} = T_1$

$$\therefore c_{Ain} - c_{A1} + K_1\left(\frac{\partial c_A}{\partial z}\right)\Bigg|_{z=0} = T_1 \frac{dc_{A1}}{dt}$$

On Laplace transformation

$$\bar{c}_{Ain} - \bar{c}_{A1} + K_1\left(\frac{d\bar{c}_A}{dz}\right)\Bigg|_{z=0} = T_1 s\bar{c}_{A1}$$

or,

$$\left(\frac{d\bar{c}_A}{dz}\right)\Bigg|_{z=0} = \left(\frac{T_1 s + 1}{K_1}\right)\bar{c}_{A1} - \frac{\bar{c}_{Ain}}{K_1} \quad \ldots\ldots\ldots\ldots \quad (9)$$

R.H.S. chamber equation

$$-q_2 c_{A2} - AD_e\left(\frac{\partial c_A}{\partial x}\right)\Bigg|_{x=L} = V_2 \frac{dc_{A2}}{dt}$$

or,

$$c_{A2} + \frac{AD_e}{q_2 L}\left(\frac{\partial c_A}{\partial z}\right)\Bigg|_{z=1} = -\frac{V_2}{q_2}\frac{dc_{A2}}{dt}$$

Let $\frac{AD_e}{q_2 L} = K_2$ and $\frac{V_2}{q_2} = T_2$

$$\therefore c_{A2} + K_2\left(\frac{\partial c_A}{\partial z}\right)\Bigg|_{z=1} = -T_2 \frac{dc_{A2}}{dt}$$

On Laplace transformation

$$\bar{c}_{A2} + K_2\left(\frac{d\bar{c}_A}{dz}\right)\Bigg|_{z=1} = -T_2 s\bar{c}_{A2}$$

or,

$$\left(\frac{d\bar{c}_A}{dz}\right)\Bigg|_{z=1} = -\left(\frac{T_2 s + 1}{K_2}\right)\bar{c}_{A2} \quad \ldots\ldots\ldots\ldots\ldots \quad (10)$$

Equating (8) and (10) we have

$$\frac{\alpha\bar{c}_{A2}\left(e^{\alpha} + e^{-\alpha}\right) - 2\alpha\bar{c}_{A1}}{e^{\alpha} - e^{-\alpha}} = -\left(\frac{T_2 s + 1}{K_2}\right)\bar{c}_{A2}$$

or,

$$\frac{\alpha\bar{c}_{A2}\left(2\cosh\alpha\right) - 2\alpha\bar{c}_{A1}}{2\sinh\alpha} = -\left(\frac{T_2 s + 1}{K_2}\right)\bar{c}_{A2}$$

or,

$$\bar{c}_{A2} = \frac{\alpha K_2 \bar{c}_{A1}}{\alpha K_2 \cosh\alpha + (T_2 s + 1)\sinh\alpha} \quad \ldots\ldots\ldots\ldots \qquad (11)$$

Comparing Equations (7) and (9)

$$\frac{2\alpha\bar{c}_{A2} - \alpha\bar{c}_{A1}\left(e^{\alpha} + e^{-\alpha}\right)}{e^{\alpha} - e^{-\alpha}} = \left(\frac{T_1 s + 1}{K_1}\right)\bar{c}_{A1} - \frac{\bar{c}_{Ain}}{K_1}$$

or,

$$\frac{2\alpha\bar{c}_{A2} - \alpha\bar{c}_{A1}\left(2\cosh\alpha\right)}{2\sinh\alpha} = \left(\frac{T_1 s + 1}{K_1}\right)\bar{c}_{A1} - \frac{\bar{c}_{Ain}}{K_1}$$

or,

$$\left(\alpha\bar{c}_{A2} - \alpha\cosh\alpha\bar{c}_{A1}\right)K_1 = \left(T_1 s + 1\right)\sinh\alpha\bar{c}_{A1} - \bar{c}_{Ain}\sinh\alpha$$

or,

$$K_1\alpha\bar{c}_{A2} = K_1\alpha\cosh\alpha\bar{c}_{A1} + \left(T_1 s + 1\right)\sinh\alpha\bar{c}_{A1} - \bar{c}_{Ain}\sinh\alpha$$

Now substituting for $\bar{c}_{A2}$ from equation (11),

$$K_1\alpha\left[\frac{\alpha K_2 \bar{c}_{A1}}{\alpha K_2\cosh\alpha + \left(T_2 s + 1\right)\sinh\alpha}\right] = \left[K_1\alpha\cosh\alpha + \left(T_1 s + 1\right)\sinh\alpha\right]\bar{c}_{A1}$$

$$- \bar{c}_{Ain}\sinh\alpha$$

or,

$$\alpha^2 K_1 K_2 \bar{c}_{A1} = \left[K_1 \cosh\alpha + (T_2 s + 1)\sinh\alpha\right]\left[\alpha K_2 \cosh\alpha + (T_2 s + 1)\sinh\alpha\right]\bar{c}_{A1}$$

$$- \bar{c}_{Aln} \sinh\alpha \left[\alpha K_2 \cosh\alpha + (T_2 s + 1)\sinh\alpha\right]$$

or,

$$\bar{c}_{A1} = \frac{\left\{\alpha K_2 \cosh\alpha + (T_2 s + 1)\sinh\alpha\right\}\sinh\alpha \bar{c}_{Aln}}{\left[\left\{K_1 \cosh\alpha + (T_1 s + 1)\sinh\alpha\right\}\left\{\alpha K_2 \cosh\alpha + (T_2 s + 1)\sinh\alpha\right\} - \alpha^2 K_1 K_2\right]}$$

$$= \frac{\left\{\alpha K_2 \cosh\alpha + (T_2 s + 1)\sinh\alpha\right\}\sinh\alpha \bar{c}_{Aln}}{\left[\alpha^2 K_1 K_2 \cosh^2\alpha + \left\{\alpha K_2 (T_1 s + 1) + \alpha K_1 (T_2 s + 1)\right\}\sinh\alpha\cosh\alpha\right.}$$

$$\left. + (T_1 s + 1)(T_2 s + 1)\sin^2\alpha - \alpha K_1 K_2\right]$$

$$\bar{c}_{A1} = \frac{\left\{\alpha K_2 \cosh\alpha + (T_2 s + 1)\sinh\alpha\right\}\sinh\alpha \bar{c}_{Ain}}{\left[\alpha^2 K_1 K_2 + \alpha^2 K_1 K_2 \sinh^2\alpha + \left\{\alpha K_2 (T_1 s + 1) + \alpha K_1 (T_2 s + 1)\right\}\sinh\alpha\cosh\alpha \right.}$$

$$\left. + (T_1 s + 1)(T_2 s + 1)\sinh^2\alpha - \alpha^2 K_1 K_2\right]$$

$$= \frac{\left\{\alpha K_2 \cosh\alpha + (T_2 s + 1)\sinh\alpha\right\}\sinh\alpha \bar{c}_{Ain}}{\sinh\alpha\left[\left\{\alpha^2 K_1 K_2 + (T_1 s + 1)\ \ (T_2 s + 1)\right\}\sinh\alpha \right.}$$

$$\left. + \left\{\alpha K_2 (T_1 s + 1) + \alpha_1 (T_2 s + 1)\right\}\cosh\alpha\right]$$

$$= \frac{\left\{\alpha K_2 \cosh\alpha + (T_2 s + 1)\sinh\alpha\right\}\bar{c}_{Ain}}{\left\{\alpha^2 K_1 K_2 + (T_1 s + 1)(T_2 s + 1)\right\}\sinh\alpha + \left\{\alpha K_2 (T_1 s + 1) + \alpha K_1 (T_2 s + 1)\right\}\cosh\alpha}$$

$$\bar{c}_{A2} = \frac{\alpha K_2 \bar{c}_{Ain}}{\left\{\alpha^2 K_1 K_2 + (T_1 s + 1)(T_2 s + 1)\right\}\sinh\alpha + \left\{\alpha K_1 (T_2 s + 1) + \alpha K_2 (T_1 s + 1)\right\}\cosh\alpha}$$

Transfer function relating $\bar{c}_{A1}$ and $\bar{c}_{Ain}$ is

$$G(s) = \frac{\bar{c}_{A1}}{\bar{c}_{Ain}}$$

$$= \frac{\alpha K_2 \cosh\alpha + (T_2 s + 1)\sinh\alpha}{\left\{\alpha^2 K_1 K_2 + (T_1 s + 1)(T_2 s + 1)\right\}\sinh\alpha + \left\{\alpha K_1 (T_2 s + 1) + \alpha K_2 (T_1 s + 1)\right\}\cosh\alpha}$$

Dividing top and bottom by sinhα

$$G(s) = \frac{1 + T_2 s + \alpha K_2 \coth\alpha}{\alpha^2 K_1 K_2 + (T_1 s + 1)(T_2 s + 1) + \left\{\alpha K_1 (T_2 s + 1) + \alpha K_2 (T_1 s + 1)\right\}\coth\alpha}$$

$$\coth\alpha = \frac{1}{\alpha} + \frac{\alpha}{3} - \frac{\alpha^3}{45} + \ldots$$

$$= \frac{1 + T_2 s + \alpha K_2 \left(\frac{1}{\alpha} + \frac{\alpha}{3} - \frac{\alpha^3}{45}\right)}{\alpha^2 K_1 K_2 + T_1 T_2 s^2 + (T_1 + T_2)s + 1 + \left\{(\alpha K_1 T_2 + \alpha K_2 T_1)s + \alpha K_1 + \alpha K_2\right\}\left\{\frac{1}{\alpha} + \frac{\alpha}{3} - \frac{\alpha^3}{45}\right\}}$$

$$= \frac{1 + T_2 s + K_2 + \frac{\alpha^2 K_2}{3} \ldots}{\left[\alpha^2 K_1 K_2 + T_1 T_2 s^2 + (T_1 + T_2)s + 1 + \frac{1}{\alpha}\alpha\left\{(K_1 T_2 + K_2 T_1)s + K_1 + K_2\right\} + \frac{\alpha^2}{3}\left\{(K_1 T_2 + K_2 T_1)s + K_1 + K_2\right\} + \ldots\ldots\right]}$$

$$= \frac{1 + K_2 + \left(T_2 + \frac{K_2 K_3}{3}\right)s}{\left[K_1 K_2 K_3 s + T_1 T_2 s^2 + (T_1 + T_2)s + 1 + (K_1 T_2 + K_2 T_1)s + K_1 + K_2 + \frac{K_3}{3}(K_1 + K_2)s + \frac{K_3}{3}(K_1 T_2 + K_2 T_1)s^2\right]}$$

$$= \frac{1 + K_2 + \left(T_2 + \frac{K_2 K_3}{3}\right)s}{\left[(1 + K_1 + K_2) + \left\{K_1 K_2 K_3 + T_1 + T_2 + K_1 T_2 + K_2 T_1 + \frac{K_3}{3}(K_1 + K_2)\right\}s + \left\{T_1 T_2 + \frac{K_3}{3}(K_2 T_1 + K_1 T_2)\right\}s^2\right]}$$

Let $1 + K_2 = a_1$

$$T_2 + \frac{K_2 K_3}{3} = a_2$$

$$1 + K_1 + K_2 = a_3$$

$$K_1 K_2 K_3 + T_1 + T_2 + K_1 T_2 + K_2 T_1 + \frac{K_3}{3}(K_1 + K_2) = a_4$$

$$T_1 T_2 + \frac{K_3}{3}(K_2 T_1 + K_1 T_2) = a_5$$

So,

$$G(s) = \frac{a_1 + a_2 s}{a_3 + a_4 s + a_5 s^2} = \frac{1}{(a_3 + a_4 s + a_5 s^2)(a_1 + a_2 s)^{-1}}$$

Now,

$$(a + b)^{-1} = \frac{1}{a} - \frac{b}{a^2} + \frac{b^2}{a^3} - \frac{b^3}{a^4} + \ldots$$

i.e.,

$$(a_1 + a_2 s)^{-1} = \frac{1}{a_1} - \frac{a_2 s}{a_1^2} + \ldots$$

$$G(s) = \frac{1}{(a_3 + a_4 s + a_5 s^2)\left(\frac{1}{a_1} - \frac{a_2 s}{a_1^2}\right)}$$

$$= \frac{1}{\frac{1}{a_1}(a_3 + a_4 s + a_5 s^2) - \frac{a_2 s}{a_1^2}(a_3 + a_4 s + a_5 s^2)}$$

$$= \frac{1}{\frac{a_3}{a_1} + \frac{a_4}{a_1} s + \frac{a_5}{a_1} s^2 - \frac{a_2 a_3}{a_1^2} s - \frac{a_2 a_4}{a_1^2} s^2 - \frac{a_2 a_5}{a_1^2} s^3}$$

$$= \frac{1}{\alpha_0 + \alpha_1 s + \alpha_2 s^2 + \ldots.}$$

$$\frac{a_3}{a_1} = \frac{1 + K_1 + K_2}{1 + K_2} = \alpha_0 \text{ (zeroth moment)}$$

$$\frac{a_4}{a_1}s = \frac{1}{1+K_2}\left[K_1K_2K_3 + T_1(1+K_2) + T_2(1+K_1) + \frac{K_3}{3}(K_1+K_2)\right]s$$

$$\frac{a_2a_3}{a_1^2}s = \frac{1}{(1+K_2)^2}\left[\left(\frac{3T_2 + K_2K_3}{3}\right)\left\{1+K_1+K_2\right\}\right]s$$

$$\left(\frac{a_4}{a_1} - \frac{a_2a_3}{a_1^2}\right)s = \frac{K_1K_2K_3}{1+K_2} + T_1 + \frac{T_2(1+K_1)}{1+K_2} + \frac{K_3(K_1+K_2)}{3(1+K_2)}$$

$$- \frac{3T_2(1+K_1+K_2)}{3(1+K_2)^2} - \frac{K_2K_3(1+K_1+K_2)}{3(1+K_2)^2}$$

$$= \frac{\left[3K_1K_2K_3(1+K_2) + 3T_1(1+K_2)^2 + 3T_2(1+K_1)(1+K_2)\right.}{\left. + K_3(K_1+K_2)(1+K_2) - 3T_2(1+K_1+K_2) - K_2K_3(1+K_1+K_2)\right]}{3(1+K_2)^2}$$

$$= \frac{\left[3K_1K_2K_3 + 3K_1K_2^2K_3 + 3T_1(1+K_2)^2 + 3T_2(1+K_1+K_2+K_1K_2)\right.}{\left. + K_3(K_1+K_2+K_1K_2+K_2^2) - 3T_2(1+K_1+K_2) - K_2K_3(1+K_1+K_2)\right]}{3(1+K_2)^2}$$

$$= \frac{\left[3K_1K_2K_3 + 3K_1K_2^2K_3 + 3T_1(1+K_2)^2 + 3T_2(1+K_1+K_2) + 3T_2K_1K_2 + K_1K_3\right.}{\left. + K_2K_3 + K_2^2K_3 + K_1K_2K_3 - 3T_2(1+K_1+K_2) - K_2K_3 - K_1K_2K_3 - K_2^2K_3\right]}{3(1+K_2)^2}$$

$$= \frac{3K_1K_2K_3(1+K_2) + 3T_1(1+K_2)^2 + 3T_2K_1K_2 + K_1K_3}{3(1+K_2)^2}$$

$$= \frac{3K_1K_2K_3(1+K_2) + 3T_1(1+K_2)^2 + K_1(3T_2K_2 + K_3)}{3(1+K_2)^2} = \alpha_1$$

Now,

$$\frac{\alpha_1}{\alpha_0} = \frac{3K_1K_2K_3(1 + K_2) + 3T_1(1 + K_2)^2 + K_1(3T_2K_2 + K_3)}{3(1 + K_2)^2} \times \frac{(1 + K_2)}{(1 + K_1 + K_2)}$$

$$= \frac{3K_1K_2K_3(1 + K_2) + 3T_1(1 + K_2)^2 + K_1(3T_2K_2 + K_3)}{3(1 + K_1 + K_2)(1 + K_2)}$$

$$= \frac{K_1K_2K_3}{1 + K_1 + K_2} + \frac{T_1(1 + K_2)}{1 + K_1 + K_2} + \frac{K_1(3T_2K_2 + K_3)}{3(1 + K_1 + K_2)(1 + K_2)}$$

R.H.S. transfer function can be written as

$$G(s) = \frac{\alpha K_2}{\left[\left\{\alpha^2K_1K_2 + (T_1s + 1)(T_2s + 1)\right\}\sinh\alpha + \left\{\alpha K_1(T_2s + 1) + \alpha K_2(T_1s + 1)\right\}\cosh\alpha\right.}$$

$$\left.\begin{aligned}\sinh\alpha &= \alpha + \frac{\alpha^3}{6} - \frac{\alpha^5}{120} = \alpha + \frac{\alpha^3}{6}\\ \cosh\alpha &= 1 + \frac{\alpha^2}{2} - \frac{\alpha^4}{24} = \alpha + \frac{\alpha^2}{2}\end{aligned}\right\} \text{ for small values of } \alpha$$

$$= \frac{\alpha K_2}{\left[\left\{\alpha^2K_1K_2 + T_1T_2s^2 + (T_1 + T_2)s + 1\right\}\left\{\alpha + \frac{\alpha^3}{6}\right\}\right.}$$
$$\left. + \left\{\alpha K_1T_2s + \alpha K_1 + \alpha K_2 + \alpha K_2T_1s\right\}\left\{\alpha + \frac{\alpha^2}{2}\right\}\right]$$

$$= \frac{\alpha K_2}{\alpha\left[\alpha^2K_1K_2 + T_1T_2s^2 + (T_1 + T_2)s + 1 + \frac{\alpha^2}{6}\left\{\alpha^2K_1K_2 + T_1T_2s^2 + (T_1 + T_2)s\right.\right.}$$
$$\left.\left. + 1\right\} + (K_1T_2 + K_2T_1)s + K_1 + K_2 + \frac{\alpha^2}{2}\left\{(K_1T_2 + K_2T_1)s + K_1 + K_2\right\}\right]$$

$$= \frac{1}{\frac{1}{K_2}\left[K_1K_2K_3s + (T_1 + T_2)s + 1 + \frac{K_3 s}{6} + (K_1T_2 + K_2T_1)s + K_1 + K_2 + \frac{K_3}{2}(K_1 + K_2)s\right]}$$

$$s^0 = \frac{1 + K_1 + K_2}{K_2} = \alpha_0$$

$$s^1 = \frac{1}{K_2}\left[K_1K_2K_3 + T_1 + T_2 + \frac{K_3}{6} + K_1T_2 + K_2T_1 + \frac{K_3}{2}(K_1 + K_2)\right]$$

$$= \frac{1}{6K_2}\left[6K_1K_2K_3 + 6T_1(1 + K_2) + 6T_2(1 + K_1) + 3K_3(K_1 + K_2) + K_3\right]$$

$$= \frac{1}{6K_2}\left[6K_1K_2K_3 + 6T_1(1 + K_2) + 6T_2(1 + K_1) + \left\{3(K_1 + K_2) + 1\right\}K_3\right]$$

$$= \alpha_1$$

$$\therefore \text{1st moment} = \frac{\alpha_1}{\alpha_0}$$

$$= \frac{1}{6K_2}\left[6K_1K_2K_3 + 6T_1(1 + K_2) + 6T_2(1 + K_1) + \left\{3(K_1 + K_2) + 1\right\}K_3\right] \times \frac{K_2}{1 + K_1 + K_2}$$

$$= \frac{6K_1K_2K_3 + 6T_1(1 + K_2) + 6T_2(1 + K_1) + \left\{3(K_1 + K_2) + 1\right\}K_3}{6(1 + K_1 + K_2)}$$

APPENDIX - 3

Numerical solution of isobaric diffusion using Crank-Nicolson technique.

Wicke-Kallenbach type diffusion test cell used (see figure 1).

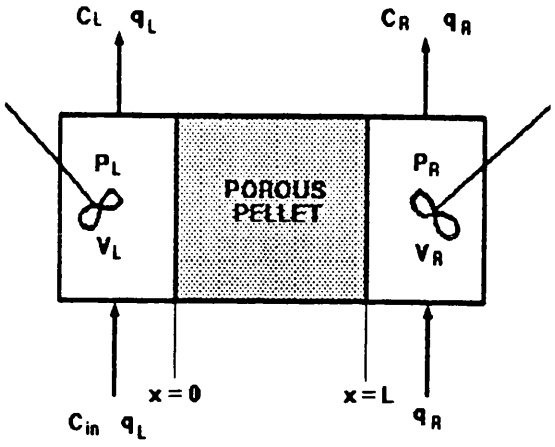

Figure 1

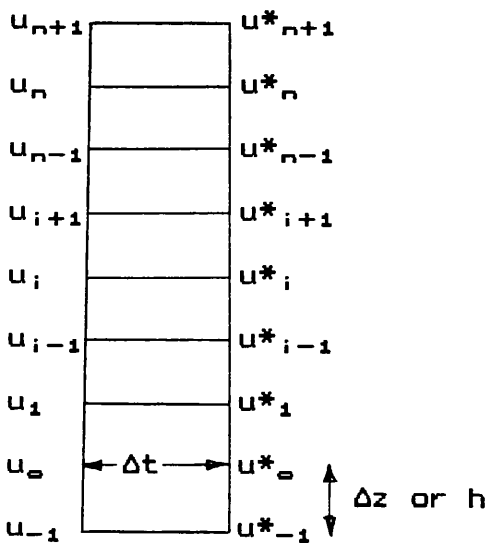

Figure 2

$$q_L C_{in} - q_L C_L + AD_e \left(\frac{\partial C_L}{\partial x} \right)\Bigg|_{x=0} = V_L \frac{dC_L}{dt} \qquad \text{Let } C_L = u;$$

or,

$$\frac{du}{dt} = \frac{q_L C_{in}}{V_L} - \frac{q_L u}{V_L} + \frac{AD_e}{V_L} \left(\frac{\partial u}{dx} \right)\Bigg|_{x=0} \qquad \text{Let } z = \frac{x}{L} \therefore x = zL$$

or,

$$\frac{du}{dt} = \frac{q_L C_{in}}{V_L} - \frac{q_L u}{V_L} + \frac{AD_e}{LV_L} \left(\frac{\partial u}{dz} \right)\Bigg|_{z=0}$$

Writing in Crank-Nicolson finite difference form (see figure 2)

$$\frac{u_0^* - u_0}{\Delta t} = \frac{q_L C_{in}}{V_L} - \frac{q_L}{V_L}\left(\frac{u_0 + u_0^*}{2h}\right)$$

$$+ \frac{1}{2}\frac{AD_e}{LV_L}\left\{\frac{u_1 - \underline{u}_{-1}}{2h} + \frac{u_1^* - \underline{u}_{-1}^*}{2h}\right\}$$

or,

$$u_0^* - u_0 = \frac{q_L \Delta t C_{in}}{V_L} - \frac{\Delta t q_L}{V_L}\left(\frac{u_0 + u_0^*}{2}\right)$$

$$+ \frac{1}{4}\frac{AD_e \Delta t}{LV_L h}\left(u_1 - \underline{u}_{-1} + u_1^* - \underline{u}_{-1}^*\right)$$

Let

$$A_1 = \frac{q_L \Delta t C_{in}}{V_L}; \quad A_2 = \frac{q_L \Delta t}{2V_L} \text{ and } A_3 = \frac{AD_e \Delta t}{4LV_L h}$$

Hence

$$u_0^* - u_0 = A_1 - A_2 u_0 + A_3\left(u_1 + u_1^*\right) - A_3\left(\underline{u}_{-1} + \underline{u}_{-1}^*\right) - A_2 u_0^*$$

or,

$$\left(\underline{u}_{-1} + \underline{u}_{-1}^*\right) = \frac{A_1}{A_3} + \left(\frac{1 - A_2}{A_3}\right)u_0 - \left(\frac{1 + A_2}{A_3}\right)u_0^* + u_1 + u_1^* \quad \ldots\ldots(1)$$

Consider the pellet equation: $\frac{\partial u}{\partial t} = \frac{D_e}{\varepsilon}\frac{\partial^2 u}{\partial x^2} = \frac{D_e}{\varepsilon L^2}\frac{\partial^2 u}{\partial z^2}$

Writing in Crank-Nicolson numerical form at the ith point (Figure 2)

$$\frac{u_i^* - u_i}{\Delta t} = \frac{1}{2}\frac{D_e}{\varepsilon L^2}\left\{\frac{u_{i-1} - 2u_i + u_{i+1}}{h^2} + \frac{u_{i-1}^* - 2u_i^* + u_{i+1}^*}{h^2}\right\}$$

or,

$$u_i^* - u_i = \frac{1}{2}\frac{D_e \Delta t}{\varepsilon L^2 h^2}\left\{u_{i-1} - 2u_i + u_{i+1} + u_{i-1}^* - 2u_i^* + u_{i+1}^*\right\}$$

Let $\frac{1}{2}\frac{D_e \Delta t}{\varepsilon L^2 h^2} = A_4$

i.e., $u_i^* - u_i = A_4\left(u_{i-1} + u_{i-1}^*\right) + A_4\left(u_{i+1}^* + u_{i+1} - 2u_i^* - 2u_i\right) \quad \ldots\ldots(2)$

Substituting i = 0 in equation (2), we have,

$$u_0^* - u_0 = A_4\left(\underline{u}_{-1} + \underline{u}_{-1}^*\right) + A_4\left(u_1^* + u_1 - 2u_0^* - 2u_0\right)$$

or,

$$\left(\underline{u}_{-1} + \underline{u}^*_{-1}\right) = \frac{u^*_0 - u_0}{A_4} - \left(u^*_1 + u_1 - 2u^*_0 - 2u_0\right) \ldots\ldots\ldots\ldots(3)$$

From (2) and (3) eliminating $u_{-1} + u^*_{-1}$, we have

$$\frac{A_1}{A_3} + \left(\frac{1 - A_2}{A_3}\right)u_0 - \left(\frac{1 + A_2}{A_3}\right)u^*_0 + u_1 + u^*_1 = \frac{u^*_0 - u_0}{A_4} - \left(u^*_1 + u_1 - 2u^*_0 - 2u_0\right)$$

or,

$$2u^*_1 - \left(2 + \frac{1 + A_2}{A_3} + \frac{1}{A_4}\right)u^*_0 = \left(2 - \frac{1 - A_2}{A_3} - \frac{1}{A_4}\right)u_0 - 2u_1 - \frac{A_1}{A_3} \ldots\ldots(4)$$

equation (2) can be rearranged as -

$$\left(1 + 2A_4\right)u^*_i - A_4\left(u^*_{i+1} + u^*_{i-1}\right) = \left(1 - 2A_4\right)u_i + A_4\left(u_{i+1} + u_{i-1}\right) \ldots\ldots\ldots(5)$$

RHS chamber equation:-

$$-q_R C_R - AD_e\left(\frac{\partial C_R}{\partial x}\right)\Bigg|_{x = L} = V_R \frac{dC_R}{dt}$$

or,

$$\frac{-q_R}{V_R}u_n - \frac{AD_e}{V_R L}\left(\frac{\partial u_n}{\partial z}\right)\Bigg|_{z = 1} = \frac{du_n}{dt}$$

Writing in Crank-Nicolson numerical form -

$$\frac{u^*_n - u_n}{\Delta t} = -\frac{q_R}{V_R}\left(\frac{u_n + u^*_n}{2}\right) - \frac{1}{2}\frac{AD_e}{LV_R}\left(\frac{u_{n+1} - u_{n-1}}{2h} + \frac{u^*_{n+1} - u^*_{n-1}}{2h}\right)$$

or,

$$u^*_n - u_n = -\frac{q_R \Delta t}{V_R}\left(\frac{u_n + u^*_n}{2}\right) - \frac{AD_e \Delta t}{4V_R Lh}\left(u_{n+1} - u_{n-1} + u^*_{n+1} - u^*_{n-1}\right)$$

Let $A_5 = \dfrac{q_R \Delta t}{2V_R}$ and $A_6 = \dfrac{AD_e \Delta t}{4V_R Lh}$

or,

$$u^*_n - u_n = -A_5 u_n - A_6\left(u_{n+1} + u^*_{n+1}\right) + A_6\left(u_{n-1} + u^*_{n-1}\right) - A_5 u^*_n$$

or,

$$u_{n+1} + u^*_{n+1} = \left(u_{n-1} + u^*_{n-1}\right) - \frac{u^*_n - u_n}{A_6} - \frac{A_5}{A_6} u_n - \frac{A_5}{A_6} u^*_n \ldots\ldots(6)$$

From equation (2) replacing i by n we have

$$u^*_n - u_n = A_4\left(u_{n-1} + u^*_{n-1}\right) + A_4\left(u^*_{n+1} + u_{n+1} - 2u^*_n - 2u_n\right)$$

or,

$$u^*_{n+1} + u_{n+1} = 2\left(u^*_n + u_n\right) + \frac{u^*_n}{A_4} - \frac{u_n}{A_4} - u_{n-1} - u^*_{n-1} \ldots\ldots\ldots(7)$$

From equations (6) and (7) we have

$$-\frac{A_5}{A_6} u^*_n + u_{n-1} + u^*_{n-1} - \frac{u^*_n}{A_6} + \frac{u_n}{A_6} - \frac{A_5}{A_6} u_n$$

$$= 2u^*_n - 2u_n + \frac{u^*_n}{A_4} - \frac{u_n}{A_4} - u_{n-1} - u^*_{n-1}$$

or,

$$2u^*_{n-1} - \left(\frac{A_5}{A_6} + 2 + \frac{1}{A_4} + \frac{1}{A_6}\right) u^*_n = \left(2 - \frac{1}{A_4} - \frac{1}{A_6} + \frac{A_5}{A_6}\right) u_n - 2u_{n-1} \ldots\ldots(8)$$

APPENDIX - 4

Numerical solution of non-isobaric diffusion using Crank-Nicolson technique Wicke-Kallenbach diffusion test cell used (see Appendix 1).

Balance on A

$$\frac{\partial}{\partial x}\left\{D_{Ae}\frac{\partial}{\partial x}\left(P_T x_A\right)\right\} + B_0\frac{\partial}{\partial x}\left\{\frac{P_T x_A}{\mu_m}\frac{\partial P_T}{\partial x}\right\} = \varepsilon\frac{\partial}{\partial t}\left(P_T x_A\right)$$

Let $z = \frac{x}{L}$; $P = \frac{P_T}{P_1}$ and then

$$\frac{P_1}{L^2}\frac{\partial}{\partial z}\left\{D_{Ae}\frac{\partial}{\partial z}\left(Px_A\right)\right\} + \frac{B_0 P_1^2}{L^2}\frac{\partial}{\partial z}\left\{\frac{Px_A}{\mu_m}\frac{\partial P}{\partial z}\right\} = \varepsilon P_1\frac{\partial}{\partial t}\left(Px_A\right)$$

or,

$$\frac{P_1}{L^2\varepsilon P_1}\frac{\partial}{\partial z}\left\{D_{Ae}\frac{\partial}{\partial z}\left(Px_A\right)\right\} + \frac{B_0 P_1^2}{L^2\varepsilon P_1}\frac{\partial}{\partial z}\left\{\frac{Px_A}{\mu_m}\frac{\partial P}{\partial z}\right\} = \frac{\partial}{\partial t}\left(Px_A\right)$$

or,

$$\frac{1}{\varepsilon L^2}\frac{\partial}{\partial z}\left\{D_{Ae}\frac{\partial}{\partial z}\left(Px_A\right)\right\} + \frac{B_0 P_1}{\varepsilon L^2}\frac{\partial}{\partial z}\left\{\frac{Px_A}{\mu_m}\frac{\partial P}{\partial x}\right\} = \frac{\partial}{\partial t}\left(Px_A\right)$$

Let $A_1 = \frac{1}{\varepsilon L^2}$; $A_2 = \frac{B_0 P_1}{\varepsilon L^2}$; $Px_A = u$; $Px_B = v$ $\therefore$ $P = u + v$

Therefore the final equation becomes

$$A_1\frac{\partial}{\partial z}\left(D_{Ae}\frac{\partial u}{\partial z}\right) + A_2\frac{\partial}{\partial z}\left(\frac{u}{\mu_m}\frac{\partial}{\partial z}(u + v)\right) = \frac{\partial u}{\partial t} \quad \ldots\ldots \qquad (1)$$

Balance on B

$$\frac{\partial}{\partial x}\left\{D_{Be}\frac{\partial}{\partial x}\left(P_T x_B\right)\right\} + B_0\frac{\partial}{\partial x}\left\{\frac{P_T x_B}{\mu_m}\frac{\partial P_T}{\partial x}\right\} = \varepsilon\frac{\partial}{\partial t}\left(P_T x_B\right)$$

This can be rearranged as above to obtain

$$A_1 \frac{\partial}{\partial z}\left(D_{Be}\frac{\partial v}{\partial z}\right) + A_2 \frac{\partial}{\partial z}\left(\frac{v}{\mu_m}\frac{\partial}{\partial z}(u+v)\right) = \frac{\partial v}{\partial t} \ldots\ldots \quad (2)$$

L.H.S. Chamber Balance

$$q_{1in}P_T x_{Ain} - q_{1out}P_T x_A + AD_{Ae}\frac{\partial}{\partial x}(P_T x_A) + \frac{AB_0 P_T x_A}{\mu_m}\frac{\partial P_T}{\partial x} = V_1 \frac{d}{dt}(P_T x_A)$$

or,

$$q_{1in}x_{Ain}PP_1 - q_{1out}x_A PP_1 + \frac{AD_{Ae}P_1}{L}\frac{\partial}{\partial z}(Px_A) + \frac{AB_0 P_1^2 Px_A}{L\mu_m}\frac{\partial P}{\partial z} = V_1 P_1 \frac{d}{dt}(P_T x_A)$$

or,

$$\frac{q_{1in}x_{Ain}PP_1}{V_1P_1} - \frac{q_{1out}P_1 Px_A}{V_1P_1} + \frac{AD_{Ae}P_1}{LV_1P_1}\frac{\partial}{\partial z}(Px_A) + \frac{AB_0P_1^2Px_A}{L\mu_m V_1P_1}\frac{\partial P}{\partial z} = \frac{d}{dt}(Px_A)$$

Let $\frac{q_{1in}x_{Ain}P}{V_1P_1} = A_5$; $\frac{q_{1out}}{V_1} = A_6$; $\frac{A}{LV_1} = A_7$ and $A_8 = \frac{AB_0P_1}{LV_1}$

The final equation becomes

$$A_5 - A_6 u + A_7 D_{Ae}\frac{\partial u}{\partial z}\Big|_{z=0} + \frac{A_8}{\mu_m}u\frac{\partial}{\partial z}(u+v)\Big|_{z=0} = \frac{du}{dt} \ldots\ldots \quad (3)$$

R.H.S. Chamber Balance

$$-q_{2out}P_T x_A - AD_{Ae}\frac{\partial}{\partial x}(P_T x_A) - \frac{AB_0P_T x_A}{\mu_m}\frac{\partial P_T}{\partial x} = V_2\frac{d}{dt}(P_T x_A)$$

or,

$$\frac{-q_{2out}P_1 Px_A}{V_2} - \frac{AD_{Ae}P_1}{LV_2}\frac{\partial}{\partial z}(Px_A) - \frac{AB_0P_1^2Px_A}{LV_2\mu_m}\frac{\partial P}{\partial z} = P_1\frac{d}{dt}(Px_A)$$

Let $B_9 = \frac{q_{2out}}{V_2}$; $B_{10} = \frac{A}{LV_2}$; $B_{11} = \frac{AB_0P_1}{LV_2}$

Hence the final equation becomes

$$-B_9 u - B_{10}D_{Ae}\frac{\partial u}{\partial z}\Big|_{z=1} - B_{11}\frac{u}{\mu_m}\frac{\partial}{\partial z}(u+v)\Big|_{z=1} = \frac{du}{dt} \ldots\ldots \quad (4)$$

If the viscosity term is independent of composition, the four equations to solve become

$$A_1 \frac{\partial}{\partial z}\left(D_{Ae}\frac{\partial u}{\partial z}\right) + \frac{A_2}{\mu_m}\frac{\partial}{\partial z}\left(u\frac{\partial}{\partial z}(u+v)\right) = \frac{\partial u}{\partial t} \quad \ldots\ldots (5)$$

$$A_1 \frac{\partial}{\partial z}\left(D_{Be}\frac{\partial v}{\partial z}\right) + \frac{A_2}{\mu_m}\frac{\partial}{\partial z}\left(v\frac{\partial}{\partial z}(u+v)\right) = \frac{\partial v}{\partial t} \quad \ldots\ldots (6)$$

$$A_5 - A_6 u + A_7 D_{Ae}\frac{\partial u}{\partial z}\Big|_{z=0} + \frac{A_8}{\mu_m} u\frac{\partial}{\partial z}(u+v)\Big|_{z=0} = \frac{du}{dt} \quad ..(7)$$

$$-B_9 u - B_{10} D_{Ae}\frac{\partial u}{\partial z}\Big|_{z=1} - B_{11}\frac{u}{\mu_m}\frac{\partial}{\partial z}(u+v)\Big|_{z=1} = \frac{du}{dt} \quad \ldots (8)$$

Now $$D_{Ae} = \frac{D_{ABe}D_{KAe}}{(1-\alpha_{AB}x_A)D_{KAe} + D_{ABe}} = \frac{D_{ABe}D_{KAe}}{D_{ABe} + D_{KAe} - \alpha_{AB}x_A D_{KAe}}$$

$$= \frac{1}{\frac{D_{ABe}+D_{KAe}}{D_{ABe}D_{KAe}} - \frac{\alpha_{AB}D_{KAe}}{D_{ABe}D_{KAe}}x_A}$$

Let $TM_1 = \frac{D_{ABe}+D_{KAe}}{D_{ABe}D_{KAe}}$, $TM_2 = \frac{\alpha_{AB}}{D_{ABe}}$

$$\therefore D_{Ae} = \frac{1}{TM_1 - TM_2 x_A} = (TM_1 - TM_2 x_A)^{-1}$$

Now $$(a-b)^{-1} = \frac{1}{a} + \frac{b}{a^2} - \frac{b^2}{a^3} + \frac{b^3}{a^4} - \ldots = \frac{1}{TM_1} + \frac{TM_2 x_A}{TM_1^2}$$

Let $m_1 = 1/TM_1$; $m_2 = \frac{TM_2}{TM_1^2}$

$$\therefore D_{Ae} = m_1 + m_2 x_A = m_1 + \frac{m_2 u}{u+v}; \text{ and}$$

$$D_{Be} = \frac{D_{ABe}D_{KBe}}{D_{ABe} + D_{KBe} - \alpha_{BA}D_{KBe}(1-x_A)} = \frac{D_{ABe}D_{KBe}}{D_{ABe} + D_{KBe} - \alpha_{BA}D_{KBe} + \alpha_{BA}D_{KBe}x_A}$$

Let $TM_3 = \frac{D_{ABe} + D_{KBe} - \alpha_{BA}D_{KBe}}{D_{ABe}D_{KBe}}$; $TM_4 = \frac{\alpha_{BA}D_{KBe}}{D_{ABe}D_{KBe}}$

$$\therefore D_{Be} = \frac{1}{TM_3 + TM_4 x_A} = \left(TM_3 + TM_4 x_A\right)^{-1} = \frac{1}{TM_3} - \frac{TM_4}{TM_3^2} x_A$$

Let $m_3 = \frac{1}{TM_3}$; $m_4 = \frac{TM_4}{TM_3^2}$ $\therefore D_{Be} = m_3 - m_4 \frac{u}{u + v}$.

Hence we can define now

$$D^*_{Ai} = m_1 + \frac{m_2 u^*_i}{u^*_i + v^*_i}; \quad D^*_{Ai+1} = m_1 + \frac{m_2 u^*_{i+1}}{u^*_{i+1} + v^*_{i+1}}$$

$$D_{Ai} = m_1 + \frac{m_2 u_i}{u_i + v_i}; \quad D_{Ai+1} = m_1 + \frac{m_2 u_{i+1}}{u_{i+1} + v_{i+1}}$$

$$D_{Ai-1} = m_1 + \frac{m_2 u_{i-1}}{u_{i-1} + v_{i-1}}; \quad D^*_{Ai-1} = m_1 + \frac{m_2 u^*_{i-1}}{u^*_{i-1} + v^*_{i-1}}$$

$$D^*_{Bi} = m_3 - \frac{m_4 u^*_i}{u^*_i + v^*_i}; \quad D^*_{Bi+1} = m_3 - \frac{m_4 u^*_{i+1}}{u^*_{i+1} + v^*_{i+1}}$$

$$D_{Bi} = m_3 - \frac{m_4 u_i}{u_i + v_i}; \quad D_{Bi+1} = m_3 - \frac{m_4 u_{i+1}}{u_{i+1} + v_{i+1}}$$

$$D_{Bi-1} = m_3 - \frac{m_4 u_{i-1}}{u_{i-1} + v_{i-1}}; \quad D^*_{Bi-1} = m_3 - \frac{m_4 u^*_{i-1}}{u^*_{i-1} + v^*_{i-1}}$$

$$D_{A0} = D_A\Big|_{z=0} = m_1 + \frac{m_2 u_0}{u_0 + v_0}; \quad D^*_A\Big|_{z=0} = m_1 + \frac{m_2 u^*_0}{u^*_0 + v^*_0} = D^*_{A0}$$

$$D_{B0} = D_B\Big|_{z=0} = m_3 - \frac{m_4 u_0}{u_0 + v_0}; \quad D^*_B\Big|_{z=0} = m_3 - \frac{m_4 u^*_0}{u^*_0 + v^*_0} = D^*_{B0}$$

$$D_{An} = D_A\Big|_{z=1} = m_1 + \frac{m_2 u_n}{u_n + v_n}; \quad D^*_A\Big|_{z=1} = m_1 + \frac{m_2 u^*_n}{u^*_n + v^*_n} = D^*_{An}$$

$$D_{Bn} = D_B\Big|_{z=1} = m_3 - \frac{m_4 u_n}{u_n + v_n}; \quad D^*_B\Big|_{z=1} = m_3 - \frac{m_4 u^*_n}{u^*_n + v^*_n} = D^*_{Bn}$$

Equation (5) can now be written in Crank-Nicolson finite difference form as

$$\frac{1}{2}A_1\frac{\partial}{\partial z}\left(D_A^*\frac{\partial u}{\partial z}\right) + \frac{1}{2}A_1\frac{\partial}{\partial z}\left(D_A\frac{\partial u}{\partial z}\right) + \frac{1}{2}\frac{A_2}{\mu_m}\frac{\partial}{\partial z}\left\{u^*\frac{\partial}{\partial z}(u+v)^*\right\}$$

$$+ \frac{1}{2}\frac{A_2}{\mu_m}\frac{\partial}{\partial z}\left\{u\frac{\partial}{\partial z}(u+v)\right\} = \frac{\partial u}{\partial t}$$

or,

$$\frac{1}{2}A_1\frac{1}{h}\left(\frac{D^*_{Ai+1}+D^*_{Ai}}{2}\right)\left(\frac{u^*_{i+1}-u^*_i}{h}\right) - \frac{1}{2}\frac{A_1}{h}\left(\frac{D^*_{Ai}+D^*_{Ai-1}}{2}\right)\left(u^*_i-u^*_{i-1}\right)$$

$$+ \frac{1}{2}A_1\frac{1}{h}\left(\frac{D_{Ai+1}+D_{Ai}}{2}\right)\left(\frac{u_{i+1}-u_i}{h}\right) - \frac{1}{2}\frac{A_1}{h}\left(\frac{D_{Ai}+D_{Ai-1}}{2}\right)\left(u_i-u_{i-1}\right)$$

$$+ \frac{1}{2}\frac{A_2}{\mu_m}\frac{1}{h}\left(\frac{U^*_{i+1}+U^*_i}{2}\right)\left(\frac{u^*_{i+1}-u^*_i+v^*_{i+1}-v^*_i}{h}\right)$$

$$- \frac{1}{2}\frac{A_2}{\mu_m}\frac{1}{h}\left(\frac{u^*_i+u^*_{i-1}}{2}\right)\left(u^*_i-u^*_{i-1}+v^*_i-v^*_{i-1}\right)$$

$$+ \frac{1}{2}\frac{A_2}{\mu_m}\frac{1}{h}\left(\frac{u_{i+1}+u_i}{2}\right)\left(u_{i+1}-u_i+v_{i+1}-v_i\right)$$

$$- \frac{1}{2}\frac{A_2}{\mu_m}\frac{1}{h}\left(\frac{u_i+u_{i-1}}{2}\right)\left(u_i-u_{i-1}+v_i-v_{i-1}\right) = \frac{u^*_i-u_i}{\Delta t}.$$

Let $\frac{A_1\Delta t}{4h^2} = c_1$ and $\frac{A_2\Delta t}{4h^2\mu_m} = c_2$

Hence the final equation becomes

$$c_1\left(D^*_{Ai+1}+D^*_{Ai}\right)\left(u^*_{i+1}-u^*_i\right) - c_1\left(D^*_{Ai}+D^*_{Ai-1}\right)\left(u^*_i-u^*_{i-1}\right)$$

$$+ c_1\left(D_{Ai+1}+D_{Ai}\right)\left(u_{i+1}-u_i\right) - c_1\left(D_{Ai}+D_{Ai-1}\right)\left(u_i-u_{i-1}\right)$$

$$+ c_2\left(u^*_{i+1}+u^*_i\right)\left(u^*_{i+1}-u^*_i+v^*_{i+1}-v^*_i\right) - c_2\left(u^*_i+u^*_{i-1}\right)\left(u^*_i-u^*_{i-1}+v^*_i-v^*_{i-1}\right)$$

$$+ c_2(u_{i+1} + u_i)(u_{i+1} - u_i + v_{i+1} - v_i) - c_2(u_i + u_{i-1})(u_i - u_{i-1} + v_i - v_{i-1})$$

$$- u_i^* + u_i = 0 \qquad (9)$$

Equation (6) can now be written in Crank-Nicolson finite difference form as

$$\frac{1}{2}A_1\frac{\partial}{\partial z}\left(D_B^*\frac{\partial v}{\partial z}\right) + \frac{1}{2}A_1\frac{\partial}{\partial z}\left(D_B\frac{\partial v}{\partial z}\right) + \frac{1}{2}\frac{A_2}{\mu_m}\frac{\partial}{\partial z}\left\{v^*\frac{\partial}{\partial z}(u + v)\right\}$$

$$+ \frac{1}{2}\frac{A_2}{\mu_m}\frac{\partial}{\partial z}\left\{v\frac{\partial}{\partial z}(u + v)\right\} = \frac{\partial v}{\partial t}$$

or,

$$\frac{1}{2}A_1\frac{1}{h}\left(\frac{D_{Bi+1}^* + D_{Bi}^*}{2}\right)\left(\frac{v_{i+1}^* - v_i^*}{h}\right) - \frac{1}{2}\frac{A_1}{h}\left(\frac{D_{Bi}^* + D_{Bi-1}^*}{2}\right)\left(\frac{v_i^* - v_{i-1}^*}{h}\right)$$

$$+ \frac{1}{2}\frac{A_2}{\mu_m}\frac{1}{h}\left(\frac{v_{i+1}^* + v_i^*}{2}\right)\left(\frac{u_{i+1}^* - u_i^* + v_{i+1}^* - v_i^*}{h}\right)$$

$$- \frac{1}{2}\frac{A_2}{\mu_m}\frac{1}{h}\left(\frac{v_i^* + v_{i-1}^*}{2}\right)\left(\frac{u_i^* - u_{i-1}^* + v_i^* - v_{i-1}^*}{h}\right)$$

$$+ \frac{1}{2}A_1\frac{1}{h}\left(\frac{D_{Bi+1} + D_{Bi}}{2}\right)\left(\frac{v_{i+1} - v_i}{h}\right) - \frac{1}{2}\frac{A_1}{h}\left(\frac{D_{Bi} + D_{Bi-1}}{2}\right)\left(\frac{v_i - v_{i-1}}{h}\right)$$

$$+ \frac{1}{2}\frac{A_2}{\mu_m}\frac{1}{h}\left(\frac{v_{i+1} + v_i}{2}\right)\left(\frac{u_{i+1} - u_i + v_{i+1} - v_i}{h}\right)$$

$$- \frac{1}{2}\frac{A_2}{\mu_m}\frac{1}{h}\left(\frac{v_i + v_{i-1}}{2}\right)\left(\frac{u_i - u_{i-1} + v_i - v_{i-1}}{h}\right) = \frac{v_i^* - v_i}{\Delta t}.$$

or,

$$c_1(D_{Bi+1}^* + D_{Bi}^*)(v_{i+1}^* - v_i^*) - c_1(D_{Bi}^* + D_{Bi-1}^*)(v_i^* - v_{i-1}^*)$$

$$+ c_1(D_{Bi+1} + D_{Bi})(v_{i+1} - v_i) - c_1(D_{Bi} + D_{Bi-1})(v_i - v_{i-1})$$

$$+ c_2(v_{i+1}^* + v_i^*)(u_{i+1}^* - u_i^* + v_{i+1}^* - v_i^*) - c_2(v_i^* + v_{i-1}^*)(u_i^* - u_{i-1}^* + v_i^* - v_{i-1}^*)$$

$$+ c_2(v_{i+1} + v_i)(u_{i+1} - u_i + v_{i+1} - v_i) - c_2(v_i + v_{i-1})(u_i - u_{i-1} + v_i - v_{i-1})$$

$$- v_i^* + v_i = 0 \qquad (10)$$

Equation (7) becomes

$$A_5 - \frac{1}{2}A_6 u + \frac{1}{2}A_7 D_{Ae}\frac{\partial u}{\partial z}\bigg|_{z=0} + \frac{1}{2}\frac{A_8}{\mu_m}u\frac{\partial}{\partial z}(u+v)\bigg|_{z=0}$$

$$- \frac{1}{2}A_6 u^* + \frac{1}{2}A_7 D^*_{Ae}\frac{\partial u^*}{\partial z}\bigg|_{z=0} + \frac{1}{2}\frac{A_8}{\mu_m}u^*\frac{\partial}{\partial z}(u+v)^*\bigg|_{z=0} = \frac{du}{dt}$$

or,

$$A_5 - \frac{1}{2}A_6(u_0 + u_0^*) + \frac{1}{2}A_7 D_{A0}\left(\frac{u_1 - \underline{u}_1}{2h}\right) + \frac{1}{2}A_7 D^*_{A0}\left(\frac{u_1^* - \underline{u}_1^*}{2h}\right)$$

$$+ \frac{1}{2}\frac{A_8}{\mu_m}u_0\left(\frac{u_1 - \underline{u}_1 + v_1 - \underline{v}_1}{2h}\right) + \frac{1}{2}\frac{A_8}{\mu_m}u_0^*\left(\frac{u_1^* - \underline{u}_1^* + v_1^* - \underline{v}_1^*}{2h}\right)$$

$$= \frac{u_0^* - u_0}{\Delta t}.$$

Let $A_9 = A_5\Delta t$; $A_{10} = \frac{A_6\Delta t}{2}$; $A_{11} = \frac{A_7\Delta t}{4h}$; $A_{12} = \frac{A_8\Delta t}{4h\mu_m}$.

Hence the final equation becomes

$$A_9 - A_{10}(u_0 + u_0^*) + A_{11}D_{A0}(u_1 - \underline{u}_1) + A_{11}D^*_{A0}(u_1^* - \underline{u}_1^*) + A_{12}u_0(u_1 - \underline{u}_1 + v_1 - \underline{v}_1)$$

$$+ A_{12}u_0^*(u_1^* - \underline{u}_1^* + v_1^* - \underline{v}_1^*) - u_0^* + u_0 = 0 \qquad (11)$$

Equation (8) becomes

$$-\frac{1}{2}B_9 u - \frac{1}{2}B_9 u^* - \frac{1}{2}B_{10}D_{Ae}\frac{\partial u}{\partial z}\bigg|_{z=1} - \frac{1}{2}B_{10}D^*_{Ae}\frac{\partial u^*}{\partial z}\bigg|_{z=1}$$

$$- \frac{1}{2}\frac{B_{11}}{\mu_m}u\frac{\partial}{\partial z}(u+v)\bigg|_{z=1} - \frac{1}{2}\frac{B_{11}}{\mu_m}u^*\frac{\partial}{\partial z}(u+v)^*\bigg|_{z=1} = \frac{du}{dt}$$

or,

$$-\frac{1}{2}B_9\left(u_n + u_n^*\right) - \frac{1}{2}B_{10}D_{An}\left(\frac{u_{n+1} - u_{n-1}}{2h}\right) - \frac{1}{2}B_{10}D_{An}^*\left(\frac{u_{n+1}^* - u_{n-1}^*}{2h}\right)$$

$$-\frac{1}{2}\frac{B_{11}}{\mu_m}u_n\left(\frac{u_{n+1} - u_{n-1} + v_{n+1} - v_{n-1}}{2h}\right)$$

$$-\frac{1}{2}\frac{B_{11}}{\mu_m}u_n^*\left(\frac{u_{n+1}^* - u_{n-1}^* + v_{n+1}^* - v_{n-1}^*}{2h}\right) = \frac{u_n^* - u_n}{\Delta t}.$$

Let $B_{12} = = \frac{B_9\Delta t}{2}$; $B_{13} = \frac{B_{10}\Delta t}{4h}$; $B_{14} = \frac{B_{11}\Delta t}{4h\mu_m}$.

Hence the final equation becomes

$$-B_{12}\left(u_n + u_n^*\right) - B_{13}D_{An}\left(u_{n+1} - u_{n-1}\right) - B_{13}D_{An}^*\left(u_{n+1}^* - u_{n-1}^*\right)$$

$$-B_{14}u_n\left(u_{n+1} - u_{n-1} + v_{n+1} - v_{n-1}\right) - B_{14}u_n^*\left(u_{n+1}^* - u_{n-1}^* + v_{n+1}^* - v_{n-1}^*\right)$$

$$-u_n^* + u_n = 0 \qquad (12)$$

APPENDIX - 5

Derivation of steady state diffusivity using a Wicke-Kallenbach type diffusion cell (see figure)

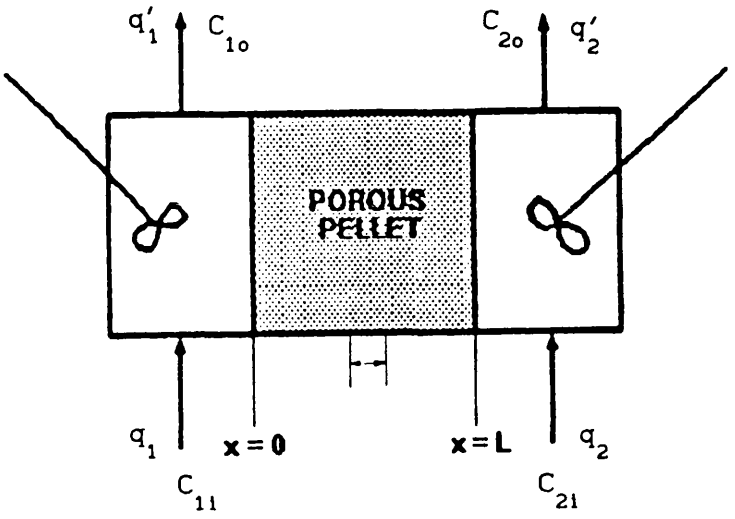

Suppose a step change in concentration of unit magnitude is made in the inlet flow stream q_1. This will result in left or right hand katharometer voltage readings of C_{1i} or C_{2i} respectively. The outlet concentrations C_{1o} and C_{2o} are then given by the following expressions

$$C_{1o} = \frac{C_{1o}}{C_{1i}} \text{ and } C_{2o} = \frac{C_{2o}}{C_{2i}}$$

(A) Cylindrical pellet, L.H.S. step

Mass balance equations are:

L.H.S.
$$q_1 - q_1' \frac{C_{1o}}{C_{11}} - \frac{DA}{L}\left(\frac{C_{1o}}{C_{11}} - \frac{C_{2o}}{C_{21}}\right) = 0..... \quad (1)$$

R.H.S.
$$0 - q_2' \frac{C_{2o}}{C_{21}} + \frac{DA}{L}\left(\frac{C_{1o}}{C_{11}} - \frac{C_{2o}}{C_{21}}\right) = 0..... \quad (2)$$

Assume $q_1 = q_1'$ and $q_2 = q_2'$

From (2) we have,

$$\frac{C_{2o}}{C_{21}} = \frac{DA/L \quad \frac{C_{1o}}{C_{11}}}{\left(q_2 + \frac{DA}{L}\right)} ..... \quad (3)$$

Putting (3) in (1) we have

$$q_1 - q_1 \frac{C_{1o}}{C_{11}} - \frac{DA}{L}\frac{C_{1o}}{C_{11}} + \frac{DA}{L}\left(\frac{DA/L \quad \frac{C_{1o}}{C_{11}}}{q_2 + \frac{DA}{L}}\right) = 0..... \quad (4a)$$

Solving for D the following equation can be obtained:

$$D = \frac{q_2\left(\frac{C_{1o}}{C_{11}} - 1\right)}{\left(1 - \frac{C_{1o}}{C_{11}} - \frac{q_2}{q_1}\frac{C_{1o}}{C_{11}}\right)} \times \frac{L}{\pi R^2}$$

Multiplying both top and bottom by $\frac{C_{11}}{C_{1o}}$ and rearranging, the final form becomes

$$D = D_L = \frac{q_2\left(\frac{C_{11}}{C_{1o}} - 1\right)}{\left(1 + \frac{q_2}{q_1} - \frac{C_{11}}{C_{1o}}\right)} \times \frac{L}{\pi R^2} ..... \quad (4b)$$

The overall mass balance is

$$q_1 - q_1 \frac{C_{1o}}{C_{11}} - q_2 \frac{C_{2o}}{C_{21}} = 0.$$

or,

$$\frac{C_{1o}}{C_{1i}} = 1 - \frac{q_2}{q_1}\frac{C_{2o}}{C_{2i}} \quad \ldots\ldots\ldots\ldots\ldots \quad (5)$$

Putting (5) in (2) we have

$$-q_2\frac{C_{2o}}{C_{2i}} + \frac{DA}{L}\left[1 - \frac{q_2}{q_1}\frac{C_{2o}}{C_{2i}} - \frac{C_{2o}}{C_{2i}}\right] = 0.$$

Solving for D we have the final form as

$$D = D_R = \frac{q_2}{\left[\frac{C_{2i}}{C_{2o}} - \frac{q_2}{q_1} - 1\right]} \times \frac{L}{\pi R^2} \quad \ldots\ldots\ldots \quad (6)$$

(B) Cylindrical pellet, step on R.H.S.

Mass balance equations are:

L.H.S.
$$-q_1'\frac{C_{1o}}{C_{1i}} - \frac{DA}{L}\left[\frac{C_{1o}}{C_{1i}} - \frac{C_{2o}}{C_{2i}}\right] = 0 \ldots\ldots\ldots\ldots \quad (7)$$

R.H.S.
$$q_2 - q_2'\frac{C_{2o}}{C_{2i}} + \frac{DA}{L}\left[\frac{C_{1o}}{C_{1i}} - \frac{C_{2o}}{C_{2i}}\right] = 0 \ldots\ldots \quad (8)$$

From (7) we have

$$\frac{C_{1o}}{C_{1i}} = \left[\frac{DA/L \quad \frac{C_{2o}}{C_{2i}}}{q_1 + \frac{DA}{L}}\right] \quad \ldots\ldots\ldots\ldots\ldots \quad (9)$$

Substituting (9) in (8) we have,

$$q_2 - q_2\frac{C_{2o}}{C_{2i}} + \frac{DA}{L}\left\{\frac{DA/L \quad \frac{C_{2o}}{C_{2i}}}{q_1 + \frac{DA}{L}} - \frac{C_{2o}}{C_{2i}}\right\} = 0$$

Now solving for D we have the final expression as

$$D = D_R = \frac{q_1\left[\frac{C_{2i}}{C_{2o}}\right]}{\left[1 + \frac{q_1}{q_2} - \frac{C_{2i}}{C_{2o}}\right]} \times \frac{L}{\pi R^2} \quad \ldots\ldots\ldots \quad (10)$$

Again the overall mass balance is

$$- q_1 \frac{C_{1o}}{C_{11}} + q_2 \qquad - q_2 \frac{C_{2o}}{C_{21}} = 0$$

or,

$$\frac{C_{2o}}{C_{21}} = 1 - \frac{q_1}{q_2} \frac{C_{1o}}{C_{11}} \ldots\ldots\ldots\ldots\ldots\ldots \quad (11)$$

Putting (11) in (7) we have

$$D = D_L = \frac{q_1}{\left(\frac{C_{11}}{C_{1o}} - 1 - \frac{q_1}{q_2} \right)} \times \frac{L}{\pi R^2} \ldots\ldots\ldots\ldots \quad (12)$$

APPENDIX - 6

Sample calculation for prediction of the tortuosity factor

Sample no S-1/7

$$D_{KAe} = 19400 \frac{\varepsilon^2_{micro}}{\tau_m S_{gm} \rho_p} (T/ M_A)^{0.5} \quad \text{(Satterfield, 1970)}$$

Determination of ε_{micro}

For 10 pellets:

Average mass per pellet, M = 0.1400 g

Average length per pellet, L = 0.3386 cm

Average radius per pellet, r = 0.2782 cm

Thus volume of pellet/g = $(\pi r^2 L/ M)$

$$= \frac{\pi \times (0.2782)^2 \times 0.3386}{0.14}$$

$$= \underline{0.5879 \text{ ml/g}}$$

Therefore solid volume + macro pore volume + micro pore volume + meso pore volume = 0.5879 ml/g.

From table 6.2 of Chapter 6,

Micro pore volume = 0.2856 - 0.0351 = 0.2505 ml/g (from 168 A radius and below).

Macro pore volume = 0.0031 ml/g (from 18455 A radius and above).

Hence macroporosity, ε_{macro} = 0.0031/0.5879 = 0.0053

and microporosity, ε_{micro} = 0.2505/0.5879 = 0.4261

Determination of ρ_p

Volume of pellet/g = 0.5879 ml/g

Hence ρ_p = 1/ 0.5879 = 1.7011 g/ml

Determination of S_{gm}

Again from table 6.2, the following table can be obtained:

Pore size (A)	Volume (ml/g)	Average Pore size x 10^8 (cm)	Difference in volume (ml/g)	Surface area x 10^{-4} (cm^2/g)
168	0.0351	138.0	0.0466	6.75
108	0.0817	90.0	0.1005	22.33
72	0.1822	63.0	0.0663	21.05
54	0.2485	48.5	0.0175	7.22
43	0.2660	39.5	0.0068	3.44
36	0.2728	33.5	0.0042	2.51
31	0.2770	29.0	0.0026	1.79
27	0.2796	25.5	0.0021	1.65
24	0.2817	23.0	0.0016	1.39
22	0.2833	21.0	0.0012	1.14
20	0.2845	19.0	0.0011	1.16
18	0.2856	-	-	-

NB Average pore size = (168 + 108)/2 = 138 x 10^{-8} cm

Difference in volume = 0.0817 - 0.0351 = 0.0466 ml/g

$\pi r^2 L = 0.0466$

$L = 0.0466/(\pi r^2)$

Hence surface area = $2\pi rL = 2\pi r \times \frac{0.0466}{\pi r^2}$

$$= \frac{0.0932}{r}$$

$$= \frac{0.0932}{138 \times 10^{-8}}$$

$$= 6.75 \times 10^4 \text{ cm}^2/\text{g}$$

Hence S_{gm} = sum of all the surface area = 70.43 x 10^4 cm^2/g.

Now $$D_{KAe} = \frac{19400 \times (0.4261)^2}{\tau_m \times 70.43 \times 10^4 \times 1.7011} \times (300/\ 4.0026)^{0.5}$$

If $D_{KAe} = 0.018$, then $\tau_m = 0.0255/0.018 = 1.41$

From equation 1.1 of Chapter 1,

$$\tau_m = 1/\ \varepsilon_{micro} = 1/\ 0.4261 = 2.35$$

$$D_{ABe} = D_{AB} \frac{\varepsilon_{macro}}{\tau} = \frac{0.7079 \times 0.0053}{\tau}$$

If $D_{ABe} = 0.025$, then $$\tau = \frac{0.7079 \times 0.0053}{0.025}$$

$$= 0.15$$

Using equation 1.1, $\tau = 1/\varepsilon_{macro} = 1/0.0053 = 188.7$

APPENDIX - 7

Constants of regression analysis

For each sample $D_e = a_o + a_1\epsilon + a_2\epsilon^2$

Size < 50 μm A	a_o	a_1	a_2
Sample 1	3.43×10^{-2}	5.2×10^{-1}	-2.5×10^{-1}
Sample 2	-3.34×10^{-2}	7.4×10^{-1}	-5.0×10^{-1}
Size 50-100 μm B			
Sample 1	6.8×10^{-2}	2.0×10^{-1}	4.24×10^{-13}
Sample 2	5.8×10^{-2}	2.0×10^{-1}	4.38×10^{-13}
Size 150-200 μm C			
Sample 1	3.8×10^{-2}	2.0×10^{-1}	4.38×10^{-13}
Sample 2	4.8×10^{-2}	2.0×10^{-1}	4.38×10^{-13}
Size 150-200 μm D			
Sample 1	1.01×10^{-1}	-2.0×10^{-2}	2.5×10^{-1}
Sample 2	4.8×10^{-2}	2.0×10^{-1}	4.38×10^{-13}

APPENDIX - 8

Sample calculation for the determination of permeability

(A) BP carbon system (sample C2, 150 - 200 μm dia particles)

Pellet permeability by the integral method

$$B_0 = \frac{2\,\mu RT\,\rho L q_p}{A(P_1^2 - P_2^2)}$$

μ_{N_2} at 300 K = 1.8×10^{-5} Ns/ m^2
R = 8.314 J/ (mol K)
T = 300 K
ρ_{N_2} at 300 K = 4.063×10^{-2} k mol/ m^3
L = 0.018 m
q_p = 0.22 cm^3/ s = 2.2×10^{-7} m^3/s
A = 2.545×10^{-4} m^2
P_1= 524 mV = 1.0399×10^5 N/ m^2
P_2= 517 mV = 1.0395×10^5 N/ m^2

$P_1^2 - P_2^2 = 7.322 \times 10^6$ N^2/ m^4

$$B_o = \frac{2 \times 1.8 \times 10^{-5} \times 8.314 \times 300 \times 4.063 \times 10^{-2} \times 0.018 \times 2.2 \times 10^{-7} \times 1000}{2.545 \times 10^{-4} \times 7.322 \times 10^6}$$

$= \underline{7.75} \times \underline{10}^{-12}\ \underline{m}^2$

Pellet permeability by the differential method

From equation 2.7 of chapter 2, we have,

$$\frac{dq_p}{d(\Delta P)} = -\frac{B_o PA}{\mu RT\rho L}$$

or, $-B_o$ = (slope of figure 7.2, Chapter 7) x $\frac{\mu RT\rho L}{PA}$

Slope of figure 7.2 at $\Delta P = 0 = -0.029\ cm^3/(s\ mV)$

$$= -5.78 \times 10^{-9}\ m^5/(Ns)$$

$A = 2.545 \times 10^{-4}\ m^2$

$P = 387$ mV above atmospheric pressure $= 1.033 \times 10^5\ N/m^2$

μ_{N_2} at 300 K $= 1.8 \times 10^{-5}\ Ns/m^2$

$T = 300$ K

ρ_{N_2} = at 300 K $= 4.063 \times 10^{-2}$ k mol$/m^3$

$$B_o = \frac{5.78\times10^{-9}\times1.8\times10^{-5}\times8.314\times300\times1000\times4.063\times10^{-2}\times0.018}{1.033\times10^{5}\times2.545\times10^{-5}}$$

$$= 7.18 \times 10^{-12}\ m^2$$

(B) Determination of pellet permeability of ICI sample using integral method

Sample no S-20/5

$$B_o = \frac{2\mu RT\ \rho L q_p}{A(P_1^2 - P_2^2)}$$

μ_{N_2} at 300 K $= 1.8 \times 10^{-5}\ Ns/m^2$

$R = 8.314$ J/(mol K)

$T = 300$ K

ρ_{N_2} at 300 K $= 4.063 \times 10^{-2}$ k mol$/m^3$

$L = 0.3256\ cm = 3.256 \times 10^{-3}\ m$

$q_p = 2.64 \times 10^{-3}\ cm^3/s = 2.64 \times 10^{-9}\ m^3/s$

$A = 2.36 \times 10^{-5}\ m^2$

$P_1 = 1757\ mV = 1.1237 \times 10^5\ N/m^2$

$P_2 = 6\ mV = 1.0137 \times 10^5\ N/m^2$

$P_1^2 - P_2^2 = 2.352 \times 10^9\ N^2/m^4$

$$B_o = \frac{2\times1.8\times10^{-5}\times8.314\times300\times4.063\times10^{-2}\times3.256\times10^{-3}\times2.64\times10^{-9}}{2.36\times10^{-5}\times2.352\times10^{9}}$$

$$= \underline{5.65}\ \underline{\times}\ \underline{10}^{-16}\ \underline{m}^2$$

APPENDIX - 9

Sample calculation for the determination of tortuosity factor as appearing in table 6.1 of Chapter 6.

Sample no S-1

$$D_K = 9700\ r_e (T/M)^{0.5}$$

Where $r_e = \frac{2V_g}{S_g} = \frac{2\varepsilon}{S_g \rho_p}$

ε = porosity = 0.549
S_g = surface area = 115.6 m^2/g
ρ_p = Bulk or pellet density = 1.02 g/cm^3

$$r_e = \frac{2 \times 0.549}{115.6 \times 10^4 \times 1.02} = 93.12 \times 10^{-8}\ cm$$

Hence for pure helium, the Knudsen diffusivity is

$$D_K = 9700 \times 93.12 \times 10^{-8} \times (300/4.0026)^{0.5}$$
$$= \underline{0.078}\ \underline{cm^2/s}$$

From the Bosanquet extrapolation formula and assuming that the tortuosity factor τ will be same for both bulk and Knudsen diffusion, we can write

$$D_e = \frac{D_{AB} D_{KA} \tau^2}{(D_{AB} + D_{KA})\tau} = \frac{0.078 \times 0.7079 \times \tau}{(0.078 + 0.7079)}$$

or, $$\tau = \frac{1}{25.926 \times D_e}$$

Now if D_e = 0.014 (average experimental result for sample S-1), then

$$\tau = \frac{1}{25.926 \times .014} = \underline{2.76}$$

APPENDIX - 10

Program "ICIDWF2" for diffusivity measurement

```
10    PRINTER IS 701
11    DIM Dd(1:500)
20    COM /Path/ @Disco
30    COM /Arrays/ B(1:2,1:50),C(1:3,1:500),A1(1:4,1:500)
35    COM /Variables/ Ss,Ss1,Q1,Qr,C10,Cr0,F,G
40    INPUT "FILENAME",F$
50    ASSIGN @Disco TO F$
60    CALL Digitise2(F$,Dd(*))
70    CALL Steady
80    CALL Steady2
90    CALL Mass_bal
100   CALL Ss_dif
101   ON KEY 0 LABEL "YES" GOTO 107
102   ON KEY 1 LABEL " NO" GOTO 124
103   DISP "Do you wish printout of concentration"
104   GOTO 104
105   PRINTER IS 701
107   PRINT F$
108   PRINT
110 ! PRINT "  LHS CONC ="
111   PRINT
112!  FOR I=1 TO 500
113 ! PRINT USING "#,10(M4D,3X)":C(2,I)
114 ! NEXT I
115   PRINT
116   PRINT
118   PRINT " RHS CONC="
119   PRINT
120   FOR I=1 TO 500
121   PRINT USING "#,10(M4D,3X)":C(3,I)
122   NEXT I
123   PRINT
124   OFF KEY
125   DISP ""
126   INPUT "IS RUN WORTH SAVING ?",E$
127   IF E$="NO" THEN 130
128   PROTECT F$,"PA"
129   DISP "File is now protected "
130   PRINTER IS 1
131   WAIT 2
132   END
133   SUB Digitise2(F$,Dd(*))
134   COM /Path/ @Disco
140   COM /Arrays/ B(*),C(*),A1(*)
150   COM /Variables/ Ss,Ss1,Q1,Qr,C10,Cr0,F,G
170   SEND 7;CMD "?U&" DATA "HE1J" CMD "5F"
180   FOR I=1 TO 50
190   ENTER 706 USING "#,W":B(1,I)
200   SEND 7;CMD "U&" DATA "2" CMD "5F"
210   ENTER 706 USING "#,W":B(2,I)
```

Program "ICIDWF2" continued

```
220   SEND 7;CMD "U&" DATA "1"
230   NEXT I
240   BEEP
250   SEND 7;CMD "?U&" DATA "HC1K" CMD "5F"
260   FOR I=1 TO 500
270   ENTER 706 USING "#,W";C(2,I)
275   SEND 7;CMD "U&" DATA "2" CMD "5F"
280   ENTER 706 USING "#,W";Dummy
285   SEND 7;CMD "U&" DATA "1" CMD "5F"
290   ENTER 706 USING "#,W";A1(1,I)
295   SEND 7;CMD "U&" DATA "2" CMD "5F"
300   ENTER 706 USING "#,W";Dummy
305   SEND 7;CMD "U&" DATA "1" CMD "5F"
310   ENTER 706 USING "#,W";A1(2,I)
320   SEND 7;CMD "U&" DATA "2" CMD "5F"
330   ENTER 706 USING "#,W";C(3,I)
340   SEND 7;CMD "U&" DATA "1" CMD "5F"
341   ENTER 706 USING "#,W";A1(3,I)
342   SEND 7;CMD "U&" DATA "2" CMD "5F"
343   ENTER 706 USING "#,W";Dummy
344   SEND 7;CMD "U&" DATA "1" CMD "5F"
345   ENTER 706 USING "#,W";A1(4,I)
346   SEND 7;CMD "U&" DATA "2" CMD "5F"
347   ENTER 706 USING "#,W";Dummy
348   SEND 7;CMD "U&" DATA "1" CMD "5F"
350   NEXT I
351   SEND 7;CMD "U&" DATA "H"
360   FOR I=1 TO 500
361   Dd(I)=C(2,I)
370   C(1,I)=(I-1)/10
380   DISP C(1,I)
390   NEXT I
400   OUTPUT @Disco;B(*),C(*)
410   GINIT
420   GRAPHICS ON
430   WINDOW 0,50,0,1023
440   AXES 100,100,0,0
450   MOVE 0,0
460   FOR I=1 TO 500
470   DRAW C(1,I),C(2,I)
480   NEXT I
481   MOVE C(1,1)+1/20,C(3,1)
490   FOR I=1 TO 500
500   DRAW C(1,I)+1/20,C(3,I)
510   NEXT I
520   INPUT "QLHS & QRHS",Ql,Qr
530   INPUT "AMP1",P1
540   F=P1/10
541   INPUT "AMP2",P3
542   G=P3/100
543   INPUT "APPLIED SIG",S
544   INPUT "DVM",D1
570   INPUT "ROT2 & ROT5",R2,R5
580   OUTPUT @Disco;Ql,Qr,Amp,S,D1,R2,R5
```

Program "ICIDWF2" continued

```
590    PRINT USING "3/"
600    PRINTER IS 701
660    PRINT F$
670    PRINT "Q(LHS)=",Q1,"CUBIC CM"
680    PRINT "Q(RHS)=",Qr,"CUBIC CM"
690 !  PRINT "RADIUS=",Rd,"CM"
691 !  PRINT "LENGTH=",L,"CM"
700    SUBEND
710    SUB Steady
720    PRINTER IS 701
730    COM /Path/ @Disco
740    COM /Arrays/ B(*),C(*),A1(*)
750    COM /Variables/ Ss,Ss1,Q1,Qr,C10,Cr0,F,G
760    ALLOCATE A(1:1000)
770    Base=0
780    FOR I=1 TO 50
790    Base=Base+B(1,I)
800    NEXT I
810    Base=Base/50
820    PRINT "AVERAGE BASE VALUE ON LHS =",Base
830    FOR I=1 TO 500
840    C(2,I)=C(2,I)-Base
850    NEXT I
860    N=10
870    Kk=5
880    Sum=0
890    I=1
900    FOR J=1 TO N
910    Sum=Sum+C(2,J)
920    NEXT J
930    A(I)=Sum/N
940    FOR I=2 TO 500-N
950    Dum=I
960    Sum=Sum+C(2,I+N-1)-C(2,I-1)
970    A(I)=Sum/N
980    IF I>Kk THEN
990    IF A(I)<50 THEN 1060
1000   FOR K=Kk TO 1 STEP -1
1010   IF ABS(A(I)-A(I-K))>1.E-3*ABS(A(I)) THEN 1060
1020   NEXT K
1030   GOSUB Printout
1040   GOTO 1080
1050   END IF
1060   NEXT I
1070   PRINT "NO STEADY STATE"
1080   Sum=0
1090   FOR J=500 TO 501-N STEP -1
1100   Sum=Sum+C(2,J)
1110   NEXT J
```

Program "ICIDWF2" continued

```
1120  A(1)=Sum/N
1130  FOR I=2 TO 500-N
1140  Dum1=I
1150  Sum=Sum+C(2,502-I-N)-C(2,502-I)
1160  A(I)=Sum/N
1170  IF I>Kk THEN
1180  IF A(I)<10 THEN 1250
1190  FOR K=Kk TO 1 STEP -1
1200  IF ABS(A(I)-A(I-K))>1.E-3*ABS(A(I)) THEN 1250
1210  NEXT K
1220  GOSUB Printout
1230  GOTO 1270
1240  END IF
1250  NEXT I
1260  PRINT "NO STEADY STATE"
1261  L=0
1270  FOR I=Dum TO 500-Dum1
1280  L=L+C(2,I)
1290  NEXT I
1300  Ss=L/(501-Dum1-Dum)*10
1310  PRINT USING "22A,5D.2D":"FINAL SS VALUE ON LHS=",Ss
1320  GOTO End
1330 Printout: !
1340           PRINT "STEADY STATE =":A(I)
1350    RETURN
1360 End:    !
1370         SUBEND
1380  SUB Steady2
1390  COM /Path/ @Disc
1400  COM /Arrays/ B(*),C(*),A1(*)
1410  COM /Variables/ Ss,Ss1,Q1,Qr,C10,Cr0,F,G
1420  ALLOCATE A(1:1000)
1430  Base=0
1440  FOR I=1 TO 50
1450  Base=Base+B(2,I)
1460  NEXT I
1470  Base=Base/50
1480  PRINT "AVERAGE BASE VALUE ON RHS= ",Base
1490  FOR I=1 TO 500
1500  C(3,I)=C(3,I)-Base
1510  NEXT I
1520  N=10
1530  Kk=5
1540  Sum1=0
1550  I=1
1560  FOR J=1 TO N
1570  Sum1=Sum1+C(3,J)
1580  NEXT J
1590  A(I)=Sum1/N
1600  FOR I=2 TO 500-N
1610  Dum=I
1620  Sum1=Sum1+C(3,I+N-1)-C(3,I-1)
1630  A(I)=Sum1/N
1640  IF I>Kk THEN
```

Program "ICIDWF2" continued

```
1650  IF A(I)<50 THEN 1720
1660  FOR K=Kk TO 1 STEP -1
1670  IF ABS(A(I)-A(I-K))>1.E-3*ABS(A(I)) THEN 1720
1680  NEXT K
1690  GOSUB Printout
1700  GOTO 1740
1710  END IF
1720  NEXT I
1730  PRINT "NO STEADY STATE"
1740  Sum1=0
1750  FOR J=500 TO 501-N STEP -1
1760  Sum1=Sum1+C(3,J)
1770  NEXT J
1780  A(1)=Sum1/N
1790  FOR I=2 TO 500-N
1800  Dum1=I
1810  Sum1=Sum1+C(3,502-I-N)-C(3,502-I)
1820  A(I)=Sum1/N
1830  IF I>Kk THEN
1840  IF A(I)<10 THEN 1910
1850  FOR K=Kk TO 1 STEP -1
1860  IF ABS(A(I)-A(I-K))>1.E-3*ABS(A(I)) THEN 1910
1870  NEXT K
1880  GOSUB Printout
1890  GOTO 1930
1900  END IF
1910  NEXT I
1920  PRINT "NO STEADY STATE"
1921  L=0
1930  FOR I=Dum TO 500-Dum1
1940  L=L+C(3,I)
1950  NEXT I
1960  Ss1=L/(501-Dum1-Dum)
1970  PRINT USING "22A,3D.2D";"FINAL SS VALUE ON RHS=",Ss1
1980  GOTO End
1990 Printout: !
2000           PRINT "STEADY STATE =";A(I)
2010    RETURN
2020 End:   !
2030        SUBEND
2031        PRINT
2040  SUB Mass_bal
2050  COM /Path/ @Disco
2060  COM /Arrays/ B(*),C(*),A1(*)
2070  COM /Variables/ Ss,Ss1,Q1,Qr,C10,Cr0,F,G
2080  COM /Text/ E$[5]
```

Program "ICIDWF2" continued

```
2105  REM:4 VOLTS LINEAR CALIBRATION
2106  C10=(100/2.933)*(205.267-8.5*Q1)*F
2107  Cr0=(100/2.933)*(210.741-10.557*Qr)*G
2108  PRINT
2113  PRINT USING "22A,5D.2D":"C0_VALUE (LHS)=",C10," mV"
2120  PRINT USING "22A,5D.2D":"C0_VALUE (RHS)=",Cr0," mV"
2130  INPUT "IS STEP ON LHS ?",E$
2140  IF E$="NO" THEN GOTO 2170
2150  Mb=Ss/C10+((Qr/Q1)*(Ss1/Cr0))
2160  GOTO 2180
2170  Mb=Ss1/Cr0+(Q1/Qr)*(Ss/C10)
2180  PRINTER IS 701
2190  Mb=-(1-Mb)*100
2200  PRINT USING "29A,M5D.2D,2X,A":"MASS BALANCE CLOSES TO WITHIN",Mb,"%"
2210  PRINTER IS 1
2220  SUBEND
2230  SUB Ss_dif
2240  COM /Path/ @Disco
2250  COM /Arrays/ B(*),C(*),A1(*)
2260  COM /Variables/ Ss,Ss1,Q1,Qr,C10,Cr0,F,G
2270  COM /Text/ E$
2280  DEG
2290  PRINTER IS 701
2300  Rd=.2746
2301  L=.243
2302  E=.554
2310  Dif=.7079
2330  PRINT USING "17A,D.3D,2X,2A":"RADIUS OF PELLET=",Rd,"CM"
2340  PRINT USING "8A,2D.D,2X,A":"VOIDAGE=",E*100
2350  PRINT USING "29A,D.4D":"BINARY DIFFUSIVITY OF N2/He=",Dif
2400  IF E$="NO" THEN 2440
2410  D1=(Qr*(C10/Ss-1))*L/((PI*Rd*Rd)*(Qr/Q1+1-C10/Ss))
2420  Dr=(L*Qr)/(PI*Rd*Rd*(Cr0/Ss1-1-Qr/Q1))
2430  GOTO 2460
2440  Dr=Q1*(Cr0/Ss1-1)*L/((Q1/Qr+1-Cr0/Ss1)*PI*Rd*Rd)
2450  D1=L*Q1/(PI*Rd*Rd*(C10/Ss-1-Q1/Qr))
2460  PRINT USING "45A,MD.5D,10A":"EFFECTIVE DIFFUSIVITY CALCULATED FROM LHS=",D
1," Sq.cm/sec"
2470  PRINT USING "45A,MD.5D,10A":"EFFECTIVE DIFFUSIVITY CALCULATED FROM RHS=",D
r," Sq.cm/sec"
2480  PRINT USING "28A,M5D.2D,A":"DIFFERENCE BETWEEN LHS & RHS=",(D1-Dr)/D1*100,
"%"
2490  Dav=(Dr+D1)/2
2500  PRINT USING "11A,4D.3D":"TORTUOSITY=",(E*Dif)/Dav
2501  PRINT USING "5/"
2510  SUBEND
```

REFERENCES

Abramowitz M.A., Stegun I.A.(1970), Handbook of mathematical functions, Dover, 55.

Allawi Z.M, Gunn D.J.(1987), AIChE J, 33, No 5, 766.

Al-Rqobah H.A., Kam E.K.T., Hughes R. (1988), Chem Eng Res Des, 66, 275.

Asaeda M., Yoneda, S., Toei R.(1974a), J Chem Eng Japan, 7, No 2, 93.

Asaeda M., Nakano M., Toei R.(1974b), J Chem Eng Japan, 7, No 3, 173.

Asaeda M., Toei, R.(1979), J Chem Eng Japan, 12, No 3, 214.

Asaeda M., et al(1981), J chem Eng Japan, 14, No 2, 129.

Balder J.R., Petersen E.E.(1968a), J Catal, 11, 195-201.

Balder J.R, Petersen E.E.(1968b), J Catal, 11, 202-210.

Berzelius J.(1936), Jahrestbericht, 15, 236.

Bhowmik S.B., Waldram S.P.(1989), BP Contract (No C514) Research Report.

Bhowmik S.B., Waldram S.P., McMurray R., Tennison R.(1990), Proceedings of COPS II Conference, 6 - 9 May, 1990, Elsevier, in press.

Bird R.B., Stewart W.E., Lightfoot E.N.(1960), Transport Phenomena, John Wiley & Sons, 19-26.

Bower P.E, Dudukovic M.P., Mills P.L., Waldram S.P.(1984), IChemE Symp Series, No 87, 9-16.

Burghardt A., Smith J.M.(1979), Chem Eng Sci, 34, 67.

Carneiro F.L.L.B, Barcellos A.(1953), RILEM Bulletin 13, 7.

Cochren W.G., Cox G.M.(1957), Experimental designs, John Wiley & Sons, 2nd ed., 148-153.

Cox D.R.(1958), Planning of experiments, John Wiley & Sons, 91-113.

Crank J.(1975), The Mathematics of Diffusion, 2nd ed., Oxford University Press.

Cresswell D.L., Orr N.H.(1982), Residence time distribution theory in chemical engineering, Eds Patho A., Noble R.D., Verlag Chemie.

Cresswell D.L.(1985), Applied Catal, 15, 103.

Cunningham R.E., Williams R.J.J.(1980), Diffusion in Gases and Porous Media, Plenum Press, 234-246.

Cussler E.L.(1984), Diffusion:Mass transfer in fluid system, Cambridge University Press, 1-21.

Damkohler G.(1937), Der Chemie Ingenieur, III, Pt.1, Academische Verlagsgesellschaft M.B.H., Leipzig.

Das M.N, Giri N.C.(1979), Design and Analysis of Experiments, Wiley Eastern Ltd., 78-97.

Davies O.L.(1954), The design and analysis of industrial experiments, Oliver and Boyd, 247-253.

Davis B.R., Scott D.S.(1965), AIChE Meeting, Philadelphia.

Dubinin M.(1960), Chem Rev, 60, 235.

Duckworth W.E.(1968), Statistical Techniques in Technological Research, Methuen & Co Ltd., 60-112.

Dullien F.A.L., Vatra V.K.(1969), Flow through porous media symp, Washington D.C., June 9-11.

Eberly P.E. Jr.(1969), Ind Eng Chem Fundam, 8, 25.

Emmett P.H.(1948), Advances in Catalysis, Academic Press, 1, 65.

Evans R.B., Watson G.M., Mason E.A.(1961), J Chem Physics, 35, No 6, 2076.

Fell J.T., Newton J.M.(1970), J Pharm Sci, 59, No 5, 688-691.

Fick A.(1855), Phil Mag, 10, 30.

Finlayson B.A.(1980), Non-linear Analysis in Chemical Engineering, McGraw-Hill.

Foscolo P.U., Gibilaro L.G., Waldram S.P.(1983), Chem Eng Sci, 38, 1251.

Gibilaro L.G., Waldram S.P.(1981), J catal, 67, 392-401.

Graham T.(1829), Quart J Sci, 2, 74.

Gregg S.J., Sing K.S.W.(1967), Adsorption, surface area and porosity, Academic Press, 1-32.

Hashimoto N., Smith J.M.(1973), Ind Eng Chem Fundam, 12, No 3, 353.

Hawtin P., Gibson J.A.(1966), Caron 4, 501.

Hawtin P., Gibson J.A., Murdoch R., Lewis J.B.(1964a), Carbon 2, 299.

Hawtin P., Murdoch R.(1964b), Chem Eng Sci, 19, 819.

Hegedus L.L., et al (1987), Catalyst design progress and perspectives, John Wiley & Sons, 1-20.

Henry P., et al(1961), AIChE J, 7, 10.

Hirschfelder J.O., et al(1954), Molecular Theory of Gases and Liquids, Wiley.

Hoogschagen J.(1955), Ind Eng Chem 47, No 5, 906.

ICI catalyst manual for LT shift catalysts.

Jenson V.G., Jeffreys G.V.(1977), Mathematical methods in chemical engineering, 2nd ed., Academic press.

Jackson R.(1977), Transport in porous catalysts, Elsevier, 14-24.

Johnson M.F.L., Stewart W.E.(1965), J Catal, 4, 248.

Kennerley J.W., Newton J.M., Stanley P.(1979), Actapharmaceutica, APV-information Sdienst, Supplement 7.

Leach B.E.(1983), Applied Industrial Catalysis, 2, Academic Press, 1-25.

Ibid (1984), Applied Industrial Catalysis, 3, Academic Press, 23.

Masamune S., Smith J.M.(1962), AIChE J, 8, 217.

Mason E.A., et al(1967), J Chem Physics, 46, 3199.

Mason E.A., Malinauskas A.P.(1983), Gas transport in porous media:The dusty gas model, Elsevier.

Mason E.A., Evans R.B.(1969), J Chem Education, 46, 358.

Maxted B.E.(1933), Catalysis and its Industrial Applications, J&A Churchill, 14-15.

McGreavy C., Asaeda M., Personal communication, Unpublished manuscript.

McGreavy C., Siddique M.A.(1980), Chem Eng Sci, 35, 3.

Mukhlyonov I.P.(1976), Catalyst Technology, Mir Publishers, 330-341.

Mukhlyonov I.P., Kuznetsov D., Averbukh A., Tumerkina E., Furmer I.(1974), Chemical Technology, Mir Publishers, 298-338.

Newton J.M., Ingham S., Onabaji O.O.(1970), Acta pharm Technol, 32(2), 61-62.

Operator's Manual, Accupyc 1330 (1989), Micromeritics Instrument Corporation.

Operator's Manual, Autopore II 9220(1987), Micromeritics Instrument Corporation.

Otani M., Smith J.M.(1966), J Catal, 5, 332.

Park S.H., Kim Y.J.(1984a), Chem Eng Sci, 39, No 3, 523.

Ibid (1984b), Chem Eng Sci, 39, No 3, 533.

Perry R.H.(1986), Chemical Engineers Handbook, 6th ed., 5-56.

Petrini G., Schneider P.(1984), Chem Eng Sci, 39, No 4, 637.

Pitt K.G., Newton J.M.(1988), J Material Sci, 23, 2723.

Pollard W.G., Present R.D.(1948), Physical Rev, 73, 762.

Rothfeld L.B.(1963), AIChE J, 9, No 1, 19.

Rudnick W.C., Hunter A.R., Holden F.C.(1963), Mater Res Stand, 1, 283.

Ryan D., Carbonell R.G., Whitaker S.(1980), Chem Eng Sci, 35, 10.

Satterfield C.N.(1970), Mass Transfer in Heterogeneous Catalysis, MIT Press, 12, 25-33, 41.

Ibid (1980), Heterogeneous Catalysis in Practice, McGraw-Hill, 68-82, 99-118.

Schneider P., Smith J.M.(1968), AIChE J, 14, 886.

Scott D.S., Cox K.H.(1960), J Chim Phys, 57, 1010.

Scott D.S., Dullien F.A.L.(1962), AIChE J, 8, No 1, 113.

Sing K.S.W, et al (1985), Pure and Applied Chem, 57, No 4, 603-619.

Smith G.D.(1985), Numerical solutions of partial differential equations: finite difference methods, 3rd ed., Clarendon press.

Smith J.M.(1970), Chemical Engineering Kinetics, 2nd ed, McGraw-Hill, 294-323, 480.

Stanley P., Newton J.M.(1977), J Powd Bulk Solids Tech 1, 13-19.

Steisel N., Butt J.B.(1967), Chem Eng Sci, 22, 469.

Stone M.(1985), European Chemical News, Specialty Chemical Supplement.

Thiele E.W.(1939), Ind Eng Chem, 31, 916.

Toei R., et al(1973), J Chem Eng Sci, 6, 50.

Twigg M.V.(1989), Catalyst Handbook, 2nd ed, Wolfe, 48-56, 440.

Vuuren D.S.(1980), "Review of experimental methods for determining effective diffusivities in catalyst pellets" CSIR Report CENG 319.

Wagner C.(1943), Z. Physikal. Chem. Adt. A 193, 1.

Wakao N., Smith J.M.(1962), Chem Eng Sci, 17, 825.

Wakao N., Smith J.M.(1964), I & EC Fundam, 3, 123.

Wakao N., Nardse Y.(1974), Chem Eng Sci, 29, 1304.

Wakao N., Kimura H., Shibata M.(1969), J Chem Eng Japan, 2, 51.

Waldram S.P.(1983), The Chemical Engineer, No 394, 28.

Waldram S.P.(1976), Ph D Thesis, University College London.

Waldram S.P.(1985a), Non-ideal flow in chemical reactors, 23, Chapter 6, Comprehensive Chemical Kinetics, Ed C.H. Bamford et al, Elsevier.

Waldram S.P., Bower P.E.(1985b), J Catal, 94, 303.

Waldram S.P., Bhowmik S.B., Chinchen G.C.(1990), Manufacturing Chemist, in press.

Weast R.C.(1978), Handbook of Chemistry and Physics, CRC press.

Weisz P.B., Prater C.D.(1954), Advances in Catalysis, 6, Academic Press, 144-189.

Westerterp K.R., Van Swaaij W.P.M., Beenackers A.A.C.M.(1984), Chemical Reactor Design and Operation, John wiley & Sons, 2nd ed., 1.

Wheeler A.(1951), Advances in Catalysis, 3, Academic Press, 250-275.

Wicke E., Kallenbach R.(1941), Kolloid Z., 97, 135.

Youngquist G.R.(1970), Ind Eng Chem, 62, No 8, 52.

Zel'dowitsch Y.B.(1934), Acta Physicochimica USSR, 10, 583.